Alma Mater Studiorum – Università di Bologna

DOTTORATO DI RICERCA IN

Scienze Farmacologiche e Tossicologiche,
dello Sviluppo e del Movimento Umano

Ciclo XXXI

Settore Concorsuale: 05/G1

Settore Scientifico Disciplinare: BIO/14

Neuroprotective effects of coumarins in neurodegenerative disease models

Presentata da: Letizia Pruccoli

Coordinatore Dottorato

Prof.ssa Patrizia Hrelia

Supervisore

Prof. Andrea Tarozzi

Esame finale anno 2019

ABSTRACT

Coumarins are a large group of phenolic compounds firstly found in the Tonka bean called *coumarou* and known to show an extensive range of biological activities including neuroprotective activities. Both natural coumarins and its synthetic analogues represent promising scaffolds for the design and development of novel polyfunctional drugs for the treatment and/or prevention of chronic neurodegenerative disorders including Alzheimer's (AD), Parkinson's and Huntington's (HD) diseases. Currently, there are no therapies that meaningfully control or prevent the development of neurodegenerative disorders. All the available therapeutic agents aim to treat the symptoms only. In this context, the aim of our research was to evaluate the potential antioxidant and neuroprotective effects of various natural coumarins such as esculetin (ESC), scopoletin (SCOP), fraxetin (FRAX) and daphnetin (DAPH) in several experimental models of AD and HD. In particular, we used: i) human neuronal SH-SY5Y cells treated with *tert*-butyl hydroperoxide (*t*-BuOOH) and amyloid-β (Aβ) protein oligomers, a specific neurotoxin for AD; ii) an inducible cell model (PC12 HD-Q74) and a transgenic *Drosophila melanogaster* model (HTT93Q, pan-neuronal expression), both of which express mutant huntingtin (HTT) exon 1 fragments, a typical feature of HD.

Initially, we evaluated the coumarins ESC, SCOP, FRAX and DAPH in AD experimental models. Among the studied coumarins, ESC showed the best profile of biological activities in SH-SY5Y cells. ESC exerted the ability to prevent or counteract the oxidative stress elicited by *t*-BuOOH in SH-SY5Y cells. The peroxide *t*-BuOOH mimics the membrane peroxidation induced by Aβ oligomers. Further, the treatment of

SH-SY5Y cells with ESC effectively increased intracellular glutathione (GSH) levels and activated the translocation of Nrf2 into nucleus via Erk and Akt/GSK3β signalling pathways. Similar treatment also showed the ability of ESC to prevent both the oxidative damage and necrosis induced by Aβ oligomers in SH-SY5Y cells. In order to evaluate the role of GSH, Erk and Akt kinases in ESC neuroprotection we used the respective inhibitors buthionine sulfoximine, PD98059 and LY294002. The addition of the inhibitors markedly abrogated the neuroprotective effects of ESC against the necrosis induced by Aβ oligomers in SH-SY5Y cells. Finally, ESC counteracted the early and late neurotoxic events, in terms of formazan exocytosis and necrosis, respectively, evoked by Aβ oligomers. Our results encourage further research in AD animal models to better investigate the potential therapeutic profile of ESC as a neuroprotective agent.

Subsequently, we evaluated the coumarin ESC in HD experimental models. The treatment with ESC partially counteracted the aggregation of mutant HTT protein in PC12 HD-Q74 cells induced by doxycycline. The same treatment with ESC ameliorated the cell proliferation and counteracted the necrosis elicited by HTT74Q expression in PC12 HD-Q74 cells. Further, ESC showed to counteract the oxidative stress as well as to increase the intracellular GSH levels and restore the nuclear Nrf2 levels in induced PC12 HD-Q74 cells. ESC also ameliorated the mitochondrial dysfunction observed in induced PC12 HD-Q74 cells. In addition, we found that ESC significantly decreased photoreceptor neurodegeneration in HTT93Q flies and enhanced in a dose-dependent manner the emergence of adult HD flies from the pupal case. We also recorded that ESC feeding improved the shortening of median life span in HD flies. Our results show

that ESC ameliorated different disease-related neurodegeneration parameters in both PC12 HD-Q74 and *Drosophila* models suggesting its potential development as a novel neuroprotective agent for the treatment of HD.

TABLE OF CONTENTS

Background

1. Coumarins

Coumarins are a group of natural compounds widely distributed in the plant kingdom, that consists of a fused benzene and α-pyrone ring as basic parent scaffold. Coumarins are initially found in tonka bean (*Dipteryx odorata* Wild) in 1820 [1]. Currently, more than 1300 coumarins have been identified in natural sources particularly from the families Rutaceae, Umbelliferae, Clusiaceae, Caprifoliaceae, Oleaceae and Apiaceae [2]. Some plants like *Fructus cnidii*, *Fructus psoraleae*, *Angelica pubescentis*, Radix *Angelica dahurica*, *Peucedanum praeruptorum* Dunn, *Cortex fraxini* are very rich in coumarins [3]. Further, the coumarins are found in green tea and other plants such as chicory. Although distributed throughout all parts of the plant, the coumarins occur at the highest levels in the fruits and seeds followed by the roots, leaves and latex. They are also isolated at high levels in some essential oils such as cassia oil, cinnamon bark oil and lavender oil. Environmental conditions and seasonal changes could influence the incidence of coumarins in varied parts of the plant. The function of coumarins is not clear, although suggestions include plant growth regulators, bacteriostats and fungistats. Coumarins are divided into simple coumarins, furanocoumarins, pyranocoumarins and other coumarins based on the substituent location and chemical structure. These compounds are characterized by low weight, easy synthesis and high bioavailability. Recently, they have become important lead compounds in drug research development thanks to their pharmacological activities [4]. Coumarins exhibit a wide spectrum of pharmacological activities including anti-inflammatory, antioxidant, anti-adipogenic, anticancer, antiviral, anticoagulant and neuroprotective properties (Fig. 1). The

relationship between their pharmacological effects and chemical structures represents the basis for the design and development of novel therapeutic drugs [5].

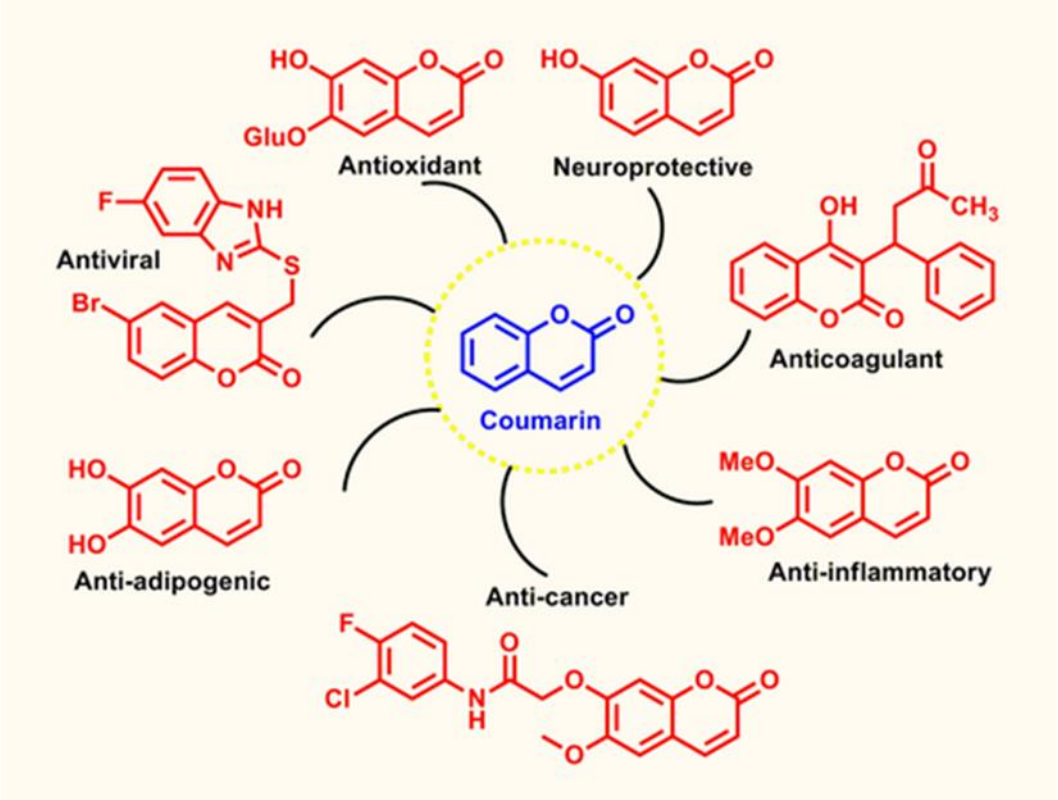

Figure 1. Pharmacological activities of coumarins (from Jameel *et al.*, *Coumarin: a privileged scaffold for the design and development of antineurodegenerative agents*, Chem. Biol. Drug Des. 87 (2016) 21-38).

2. Coumarins and evidences of neuroprotection

During the last years, the scientific research has focused on coumarins and its analogues as possible multi-target drugs for the treatment of neurodegenerative disorders including Alzheimer's (AD), Parkinson's (PD) and Huntington's diseases (HD). Several studies reported the evidence that the neuronal death in AD, PD and HD is associated with glutamate excitotoxicity [6]. Thus, glutamate-induced toxicity has become a pharmacological target for neurodegenerative diseases treatment. In this regard, some dihydropyranocoumarins demonstrated notable protective activity against the neurotoxicity induced by glutamate. In particular, six dihydropyranocoumarin analogues including decursin and decursinol showed to markedly enhance the viability of rat cortical cells treated with a toxic concentration of glutamate [7]. MAO-A and MAO-B oxidize neurotransmitters via oxidative deamination which is important for maintaining the normal neuronal homeostasis. MAO inhibitors are used for the treatment of neurodegenerative disorders, especially PD. Several studies identified new compounds derived by incorporating basic coumarin moiety as significant MAO inhibitors [8]. In particular, four coumarin derivatives, praeruptorin A, xanthotoxin, psoralen and bergapten exert *in vitro* MAO inhibitory effect with micromolar activities [9]. N-methyl-D-aspartate receptors are known to be implicated in different neurodegenerative diseases. A recent study reported a selective coumarin-based analogue, 6-bromocoumarin-3-carboxylic acid, that is able to modulate NMDA receptors function [10]. Neurotrophic factors such as brain-derived neurotrophic factor (BDNF) and nerve growth factor (NGF) are also considerably involved in the pathogenesis of neurodegenerative disorders [11]. BDNF, largely present in hippocampus, cortex and basal forebrain, is found to be linked with many neurological

disorders [12]. Neurotrophins are lower proteins that regulate neuron survival, neurite outgrowth and neural stem cell differentiation [13]. Daphnetin has shown to increase neurite outgrowth and neuronal survival in the primary cultured rat cortical neurons probably by raising BDNF expression [14]. Chronic inflammation process in the central nervous system is related to the neuronal cell death occurring in neurodegenerative disorders [15]. Activated microglia that secretes trypsinogen is one of the prime participants in the enhancement of neuroinflammation [16]. Numerous coumarins including esculetin, scopoletin, marmin, umbelliferone and visnadine exhibit excellent anti-inflammatory effects. Another derivate of coumarins, imperatorin, also shows extremely good anti-inflammatory activity *in vitro* and *in vivo*. This compound eliminates oedema fluid and protein from injured tissue via phagocyte stimulation [17]. Further, imperatorin blocks the protein expression of inducible nitric oxide synthase and cyclooxygenase-2 enzyme. The reduction in acetylcholine is believed to play an important role in the cognitive impairment associated with AD [18]. Accordingly, increasing the levels in acetylcholine has been regarded as one of the most promising approach for the symptomatic treatment of AD [19]. Different coumarin analogues have also shown to exhibit potent AChE inhibition. Specifically, the natural coumarin ensaculin, having benzopyranone scaffold, with piperazine substitution is under clinical analysis for its potential against AD. The coumarin ensaculin improved learning and memory in animal models and is well tolerated in daily doses up to 200 mg and with inferior target organ toxicity. This compound effects neurotransmitter systems and exhibits significant neurotrophic and neuroprotective characteristics [20]. Among the natural coumarins, decursinol, mesuagenin B, scopoletin, scopoletin glucoside, (R)-(+)-6’-hydroxy-7’-methoxybergamottin and (R)-(+)-6’7’-dihydroxybergamottin were

shown to possess effective anti-AChE activity, followed by bergapten, 4-methylumbelliferone, feronielloside, marmesin and columbianetin [21–23]. Scopoletin has been shown to potentiate long-term potentiation (LTP) in rat hippocampal slices [24]. It improved LTP in CA1 region of hippocampus and enhanced cognitive properties in cholinergically impaired mice via NMDA dependent pathway. Moreover, it is known to exert anti-inflammatory, antiproliferative and MAO inhibitory activity along with radical scavenging and antioxidant properties [25–28].

However, there are no current studies that evaluate the potential ability of the natural coumarins to prevent or counteract the pathogenetic events occurring in the onset and progression of AD and HD.

Chapter I

1. Introduction

1.1 Alzheimer's disease

Alzheimer's disease (AD) is a progressive neurodegenerative disease characterized by neuronal cell death that impairs memory and learning function. AD is the most common form of dementia in elderly and according to the World Alzheimer Report 2018, there are currently about 46 million people suffering with AD worldwide [29]. Brains of AD patients exhibit cortical atrophy resulting from a massive loss of neurons and synapses. Pathogenesis of AD is characterized by extracellular deposits of amyloid-β peptide and intracellular neurofibrillary tangles in the brain. AD is classified into preclinical, mild, moderate and late stage depending on the degree of cognitive impairments. The initial symptoms are usually mild confusion, amnesia and personality change. These symptoms are followed by impairment in problem solving, judgment, executive functioning, lack of motivation and disorganization. Neuropsychiatric symptoms such as apathy, disinhibition, agitation and psychosis are also common [30]. Until now only five drugs have been approved by the Food and Drug Administration to treat AD. These approved drugs including cholinesterase inhibitors, N-methyl-D-aspartate (NMDA) receptor antagonist or their combination provide only temporary and incomplete symptomatic relief accompanied by severe side effects. The marginal benefits were unable to treat or slow the progression of AD. Thus, the development of novel pharmacological strategies for the treatment of AD has become an urgent need. AD is a multifactorial disease that involves many factors. The multiple mechanisms related to

AD are still unclear and many hypotheses have been done in order to identify possible pharmacological target to develop novel therapeutic compounds for the treatment of AD [31].

1.2 Aβ cascade hypothesis

Extracellular deposits of amyloid-β peptide usually named senile plaques represent a hallmark of AD. Amyloid-β (Aβ) peptide have long been viewed as a potential therapeutic target for AD during the past twenty years [32]. Aβ plaques emerge roughly 15 years before the symptoms of AD appear and once AD develops the cognitive decline caused by neuronal damage cannot be reversed. Thus, prevention of Aβ accumulation is considered an important part of preventing AD [33]. Aβ peptide is generated after enzymatic cleavage by β- and γ-secretases of the Amyloid Precursor Protein (APP), a type-1 trans-membrane protein expressed in various tissues, especially in the central nervous system. The most direct strategy in anti-Aβ therapy is to reduce Aβ production by targeting β- and γ-secretases [34].

1.3 Tau hypothesis

Neurofibrillary tangles composed of tau protein represent an intracellular hallmark of AD. Tau is one of the microtubule-associated proteins that regulate the stability of tubulin assemblies and are located mainly in axons. In pathological conditions, tau aggregation impairs axons of neurons and causes subsequent neurodegeneration. After numerous failures of Aβ-targeting drugs for AD, more interests are turning to explore the therapeutic potential of targeting tau [35]. Normally, tau undergoes many

modifications, including phosphorylation, arginine mono-methylation, lysine acetylation, lysine mono-methylation, lysine demethylation, lysine and serine ubiquitylation. In AD brains, tau is accumulated in a hyperphosphorylated state in the pathological inclusions. Tau hyperphosphorylation leads to major aggregation, reduces its affinity for microtubules and influences neuronal plasticity. Consequently, strategies to target tau involve blocking of tau aggregation, stabilizing microtubules and manipulating kinases and phosphatases that are responsible of tau modifications.

1.4 Inflammation hypothesis

Reactive gliosis and neuroinflammation are also considered hallmarks of AD. Emerging genetic and transcriptomic studies consider central the role of microglia-related pathways in AD risk and pathogenesis [36–40]. Microglia dysfunction in pruning and in regulating plasticity is regarded as an early prime cause in AD evolution. Further, reactive microglia and astrocytes can surround amyloid plaques and secrete numerous pro-inflammatory cytokines. The recent advances in understanding the mechanisms that underline microglia dysfunction in pruning, regulating plasticity and neurogenesis are opening up to new opportunities for AD pharmacological interventions. Targeting these aberrant microglia functions and thereby restore physiological homeostasis may represent novel possibilities for AD therapy [41].

1.5 Cholinergic hypothesis

The cholinergic hypothesis suggests that AD is caused by a deficiency in the brain levels of the cerebral neurotransmitter acetylcholine (Ach), which is hydrolysed by

acetylcholinesterase (AChE) and butyrylcholinesterase (BChE). Ach is an important neurotransmitter used by cholinergic neurons that is involved in critical physiological processes including attention, learning, memory, stress response and sensory information. Cholinergic neurons damage is considered a critical pathological event which correlates with the cognitive impairment observed in AD. Further, the BChE activity is increased by 40-70% during the progression of AD. Cholinesterase inhibitors represent currently the most available clinical treatment for AD patients [42,43].

1.6 Oxidative stress hypothesis

Oxidative stress due to an imbalance between oxidants and antioxidants species is considered to play a crucial role in the pathogenesis of AD. Neurons in the brain are more easily exposed to excessive ROS generation and oxidative damage because of their high oxygen consumption and energy production. About 20% of all oxygen and 25% of all glucose are used for cerebral functions [44]. The vulnerability of neurons to the oxidative damage include also the presence of redox active metals promoting ROS formation, high content of polyunsaturated fatty acids that are more sensitive to oxidation and modest levels of antioxidant enzymes [45]. Mitochondrial dysfunction and enhanced apoptosis accompanied by a poor antioxidant status are considered the mechanisms for AD pathogenesis. Several studies underlined the role of superoxide anion, hydroxyl radical, hydrogen peroxide and nitric oxide in the oxidative stress mediated neurodegeneration in AD. Microglia activation due to neuronal lesions generates excessive superoxide radicals. The low rate of brain regeneration and insufficient antioxidant potential in the brain lead to oxidative damage. Further, mitochondrial autophagy serves as a major source of ROS production [46]. Recent

studies reported also that the oxidative stress defence mechanisms are compromised in AD brain. Specifically, post mortem analysis of the human brains as well as *in vivo* analysis revealed decreased glutathione (GSH) levels and increased glutathione disulphide (GSSG) amount in the brain regions affected by AD pathology, such as frontal cortex and hippocampus. In addition to the altered GSH/GSSG balance, a decreased activity of GSH reductase, GSH peroxidase and GSH S-transferase has been detected. The activity of other important antioxidant enzymes, superoxide dismutase and catalase, has been reported to be reduced in AD patients [47]. In addition, reduced levels of thioredoxin, a potent ROS scavenger, as well as reduced transcription of detoxifying genes and diminished expression of antioxidant enzymes have been observed in amygdala and hippocampus. These data are in line with the decreased levels of nuclear factor (erythroid-derived 2)-like 2 (Nrf2) observed in the nucleus of hippocampal neurons in human AD brains [48–50]. Accumulation of amyloid-β peptide can also induce oxidative stress in the brain of AD patients by enhancing lipid peroxidation. Several studies explored iron accumulation in the brain of AD patients and found that it is capable of generating hydroxyl radical through the Fenton reaction. Amyloid-β peptide could elevate oxidative stress by binding with iron. Also, the accumulation of copper in amyloid plaques represents a well-established event in AD pathogenesis. Copper can be coordinated to amyloid-β peptide and the resulting complex could be directly involved in reactive oxygen species (ROS) production. The neuronal death occurs due to ROS mediated changes in the neuronal lipid molecules, which includes alterations in the membrane, fluidity, rigidity, permeability, and transport [51]. Finally, it has been noticed that mitochondrial damage in AD could lead to excessive generation of ROS and lowered ATP production [52,53]. Several evidences

indicate that oxidative stress and impaired oxidative stress defence represent the main early causes of neurodegeneration in AD. Thus, the development of novel AD therapies targeting oxidant/antioxidant imbalance could be a promising pharmacological strategy.

In this context, the aim of our research was to investigate the potential neuroprotective effects of the natural coumarins esculetin, scopoletin, fraxetin and daphnetin in *in vitro* models of AD. We used human neuronal SH-SY5Y cells treated with *t*-BuOOH and Aβ oligomers, a specific neurotoxin for AD. Cells were incubated with the studied coumarins before and during the treatment with *t*-BuOOH or Aβ oligomers to evaluate the capacity of coumarins to prevent and counteract, respectively, the pathogenic events occurring in AD. Several neurodegeneration parameters including oxidative damage and neuronal death, were assessed in order to investigate the neuroprotective activities of the studied coumarins.

2. Materials and methods

2.1 Coumarins

The phenolic coumarins esculetin (ESC, purity: 98%), scopoletin (SCOP, purity: ≥99%), fraxetin (FRAX, purity: ≥98%) and daphnetin (DAPH, purity: ≥97%) were purchased from Sigma-Aldrich (St. Louis, MO, USA) (Fig. 2). The powder was dissolved in dimethyl sulfoxide (DMSO) to obtain a 40 mM stock solution. Stock solutions were then aliquoted and stored frozen at -20°C. At the time of use, stock solutions were diluted directly in cell culture medium or in Hanks' balanced salt solution (HBSS) to achieve the desired concentrations.

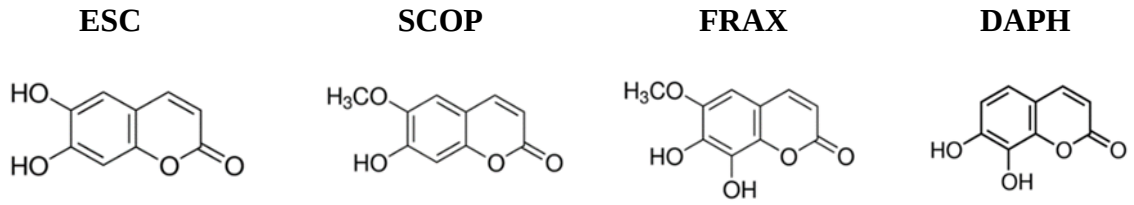

Figure 2. Chemical structure of coumarins.

2.2 Cell culture

Human neuronal (SH-SY5Y) cells were purchased from Lombardy and Emilia Romagna Experimental Zootechnic Institute (Italy). SH-SY5Y cells were routinely grown in Dulbecco's modified Eagle's Medium (DMEM) supplemented with 10% fetal bovine serum, 2 mM L-glutamine, 50 U/mL penicillin and 50 μg/mL streptomycin at 37°C in a humidified incubator with 5% CO_2.

2.3 Amyloid-β peptide

The human amyloid-β (1-42) peptide was purchased from AnaSpec (Fremont, CA, USA). Peptides were first dissolved in hexafluoroisopropanol 1 mg/mL, sonicated, incubated at room temperature for 24 hours and lyophilized. The resulting unaggregated amyloid-β ($A\beta_{1-42}$) peptide film was dissolved in DMSO to obtain a 1 mM stock solution. Stock solution was then aliquoted and stored at -20°C until use. The $A\beta_{1-42}$ peptide aggregation to oligomeric form was prepared by dilute stock solution in DMEM and store the diluted solution at -20°C for 24 hours. The morphology of oligomeric $A\beta_{1-42}$ forms obtained was checked using the transmission electron microscopy.

2.4 Determination of neuronal viability

The neuronal viability was assessed using the tetrazolium salt colorimetric assay. To establish the range of concentrations not associated with neurotoxicity, SH-SY5Y cells were seeded in a 96 well plate at 2×10^4 cells/well, incubated for 24 hours and subsequently treated with various concentrations of coumarins [2.5 – 80 µM] for 24 hours at 37°C in 5% CO_2. The cell viability, in terms of mitochondrial metabolic function, was evaluated by the reduction of 3-(4,5-dimethyl-2-thiazolyl)-2,5-diphenyl-2H-tetrazolium bromide (MTT) to its insoluble formazan. Briefly, the treatment was replaced with MTT in HBSS [0.5 mg/mL] for 2 h at 37°C in 5% CO_2. After washing with HBSS, formazan crystals were dissolved in isopropanol. The amount of formazan was measured (570 nm, reference filter 690 nm) using a multilabel plate reader (VICTOR™ X3, PerkinElmer, Waltham, MA, USA). The quantity of formazan was directly proportional to the number of living cells (Fig. 3). The neurotoxicity is

expressed as percentages of neuronal viability with control (untreated cells) taken as 100 % viability.

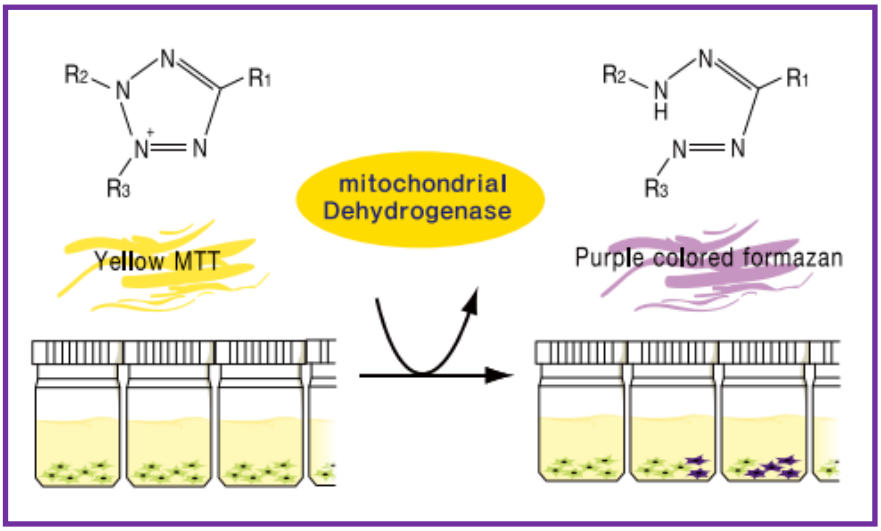

Figure 3. Reduction of yellow MTT to blue insoluble formazan by mitochondrial Dehydrogenase.

2.5 Determination of intrinsic antioxidant activity

The intrinsic antioxidant activity of the studied coumarins was determined using both 2,2-diphenyl-1-picrylhydrazyl (DPPH) and 2,2′-Azino-bis (3-ethylbenzothiazoline-6-sulfonic acid) diammonium salt (ABTS) radicals. Briefly, 150 µL of 100 µM DPPH in ethanol was added to 50 µL of coumarins at different concentrations [2.5 – 40 µM] in a 96 well plate. The absorbance of the reaction solution was measured at 490 nm on a VICTOR™ X3 multilabel plate reader after 30 min. Data are expressed as optical density of DPPH solution in absence or presence of coumarins. The intrinsic antioxidant activity of coumarins was also determined by using the ABTS radical-scavenging assay.

Briefly, ABTS radical was generated by mixing a 2 mM ABTS solution with 7 mM potassium persulfate ($K_2S_2O_8$) and incubating the obtained solution in the dark for 24 hours at room temperature. Before use, ABTS solution was diluted (1–25 mL of phosphate buffered saline) to obtain an absorbance value of 0.70 ± 0.02 at 734 nm. Upon addition of 1 mL of the diluted ABTS solution to 10 µL of coumarins at different concentrations [2.5 – 40 µM], the absorbance at 734 nm was recorded after 1 min. The final total antioxidant activity (TAA) of coumarins was calculated by comparing ABTS decolorization with that of trolox, a water-soluble analog of vitamin E. Data are expressed as millimole of trolox equivalent antioxidant activity per millilitre of sample (mmolTE/mL).

2.6 Determination of direct and indirect antioxidant activity

The intracellular ROS formation was evaluated in SH-SY5Y cells by using the fluorescent probe 2',7'-Dichlorodihydrofluorescein diacetate (DCFH-DA) (Fig. 4). Briefly, SH-SY5Y cells were seeded in a 96 well plate at 3×10^4 and 2×10^4 cells/well to evaluate direct and indirect antioxidant activity, respectively. Plates were incubated for 24 hours at 37°C in 5% CO_2. Subsequently SH-SY5Y cells were incubated for 2 and 24 hours with various concentrations of ESC, SCOP, FRAX and DAPH [2.5 – 20 µM]. At the end of incubation, the treatment was removed and 100 µL of the fluorescent probe DCFH-DA [10 µg/mL] was added to each well. After 30 min of incubation at room temperature, DCFH-DA solution was replaced with a solution of *tert*-Butyl hydroperoxide (*t*-BuOOH) [200 µM] for 30 min. The reactive oxygen species (ROS) formation was measured (excitation at 485 nm and emission at 535 nm) using a

VICTOR™ X3 multilabel plate reader. The values are expressed as fold increases in ROS formation induced by *t*-BuOOH.

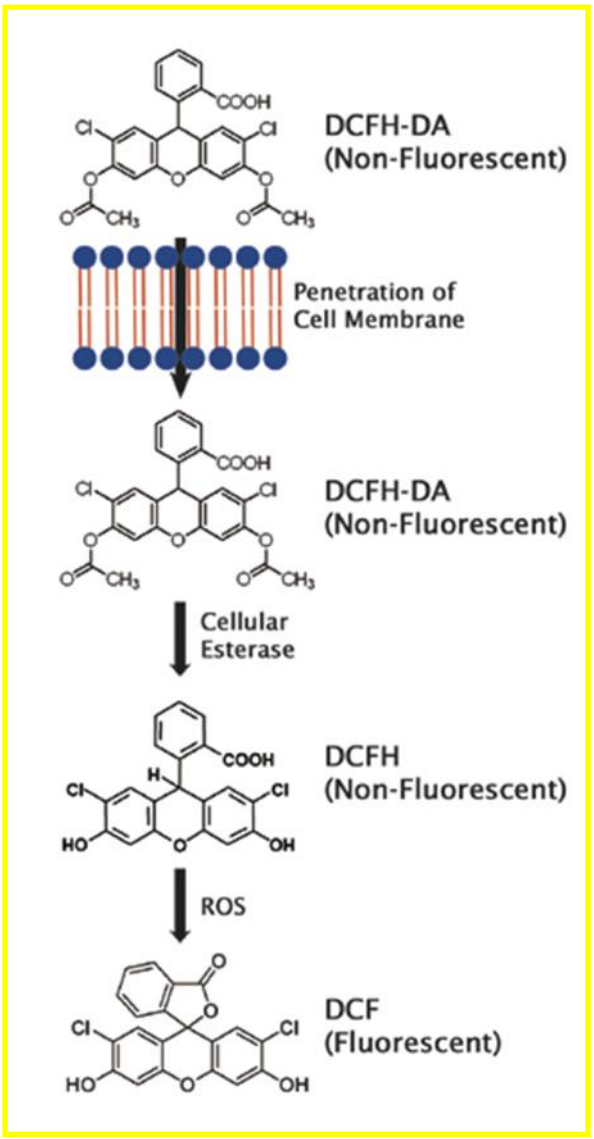

Figure 4. Oxidation of DCFH to DCF in the presence of intracellular ROS.

2.7 Determination of antioxidant coumarins in membrane and cytosolic fractions

The cellular uptake was determined indirectly by using ABTS assay. This experimental approach allowed us to determine the cellular uptake of antioxidant molecules and their ability to counteract free radicals at different subcellular levels. SH-SY5Y cells were seeded in 60 mm dishes at 2×10^6 cells/plate and incubated for 24 hours at 37°C in 5% CO_2. Subsequently, SH-SY5Y cells were incubated for 2 hours with ESC and DAPH [20 µM]. At the end of incubation, SH-SY5Y cells were washed 3 times with cold phosphate buffered saline (PBS) and removed from dish by gently scraping with cell lifter. Then cells were collected in 1 mL of PBS and centrifugated for 10 min at 10000 rpm at 4°C. The supernatant was removed and cells were washed with 1 mL of PBS. This was repeated a further 2 times and the pellet was finally reconstituted in 600 µL of lysis buffer containing Triton X-100 0.05%. Cells were then homogenized and allowed to stand at 4°C for 30 min. Cytosolic fraction was obtained by centrifugation at 14000 rpm for 15 min at 4°C. The remaining pellet was solubilized in 400 µL of lysis buffer containing Triton X-100 1% to obtain the membrane fraction. Cytosolic and membrane fractions were stored at -20°C. Small amounts were removed for the determination of the protein concentration using the Bradford method. The antioxidant activity of coumarins was then measured on cytosolic and membrane fractions using ABTS assay. The final total antioxidant activity (TAA) of cytosol and membrane fractions were calculated by comparing ABTS decolorization with that of trolox. Data are expressed as micromole of trolox equivalent antioxidant activity per milligram of protein (µmolTE/mg protein).

2.8 Determination of intracellular glutathione levels

The intracellular glutathione (GSH) levels were evaluated in SH-SY5Y cells by using the fluorescent probe monochlorobimane (MCB) (Fig. 5). SH-SY5Y cells were seeded in a black 96 well plate at 2×10^4 cells/well and incubated for 24 hours at 37°C in 5% CO_2. Subsequently, SH-SY5Y cells were incubated for 24 hours with various concentrations of ESC and DAPH [20 µM]. At the end of incubation, the treatment was removed and 100 µL of the fluorescent probe MCB [50 µM] was added to each well. After 30 min of incubation at 37°C, GSH levels were measured (excitation at 355 nm and emission at 460 nm) using a VICTOR™ X3 multilabel plate reader. The values are expressed as fold increases.

To determine GSH levels after different treatment-time with ESC, SH-SY5Y cells were seeded in 60 mm dishes at 2×10^6 cells/dish and incubated for 24 h at 37°C in 5% CO_2. Subsequently, SH-SY5Y cells were incubated for 1, 2, 3, 6, 12 and 24 hours with ESC [20 µM]. At the end of incubation, SH-SY5Y cells were trypsinized and counted to obtain 5×10^5 cells/mL suspension from each dish. Then 100 µL of the cell suspension and 100 µL of MCB [100 µM] were added to a black 96 well plate. After 30 min of incubation at 37°C, GSH levels were measured (excitation at 355 nm and emission at 460 nm) using a VICTOR™ X3 multilabel plate reader. The values are expressed as fold increases.

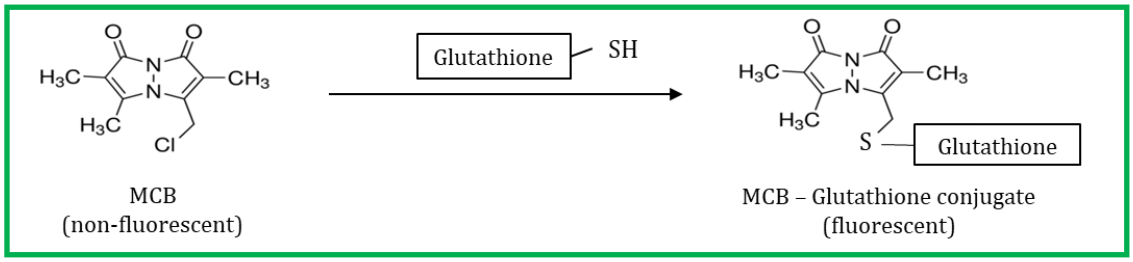

Figure 5. Intracellular conjugation of MCB probe with GSH.

2.9 Nuclear extraction and determination of Nrf2 nuclear levels

SH-SY5Y cells were seeded in 60 mm dishes at 2×10^6 cells/plate and incubated for 24 hours at 37°C in 5% CO_2. Subsequently, SH-SY5Y cells were incubated for 1 and 3 hours with ESC [20 µM]. At the end of incubation, nuclear extraction and determination of Nrf2 nuclear levels were performed using the Nuclear Extract Kit (Active Motif, Carlsbad, CA, USA) and western blotting, respectively.

The nuclear extracts (50 µg per sample) were separated by SDS-polyacrylamyde gels and were transferred onto nitrocellulose membranes, which were probed with primary Nrf2 antibody (Santa Cruz Biotechnology, Dallas, TX, USA) and secondary antibody. ECL reagents (Pierce, Rockford, IL, USA) were utilized to detect targeted bands. The same membranes were stripped and reprobed with β-actin antibody (Sigma Aldrich). Data were analysed by densitometry, using Quantity One software (Bio-Rad, Hercules, CA, USA). Values are expressed as fold increases versus respective contralateral intact site.

2.10 Determination of Erk, Akt, GSK3β protein phosphorylation

Phospho-Erk (p-Erk), Phospho-Akt (p-Akt), Phospho-GSK3β (p-GSK3β), Erk, Akt and GSK3β antibodies were purchased from Cell Signaling Technology (Danvers, MA, USA). The phosphorylation of Erk, Akt and GSK3β kinases was evaluated by using western blotting method (Fig. 6-7). SH-SY5Y cells were seeded in 60 mm dishes at 2×10^6 cells/dish and incubated for 24 hours at 37°C in 5% CO_2. Subsequently, SH-SY5Y cells were incubated for 15, 30, 60 and 120 minutes with ESC [20 µM]. At the end of incubation, SH-SY5Y cells were trypsinized and cellular pellet was resuspended in complete lysis buffer containing leupeptin 2 µg/mL and PMSF 100 µg/mL. We determined the protein concentration of the samples by using Bradford method. The protein lysates (30 µg per sample) were separated by SDS-polyacrylamide gels and were transferred onto nitrocellulose membranes, which were probed with primary phosphorylated antibody p-Erk, p-Akt and p-GSK3β, and then with secondary antibodies. ECL reagents (Pierce, Rockford, IL, USA) were utilized to detect targeted bands. The same membranes were stripped and reprobed with Erk, Akt and GSK3β antibodies. Data were analysed by densitometry, using Quantity One software (Bio-Rad). Values are expressed as relative protein expression (phosphorylated form/total protein expression).

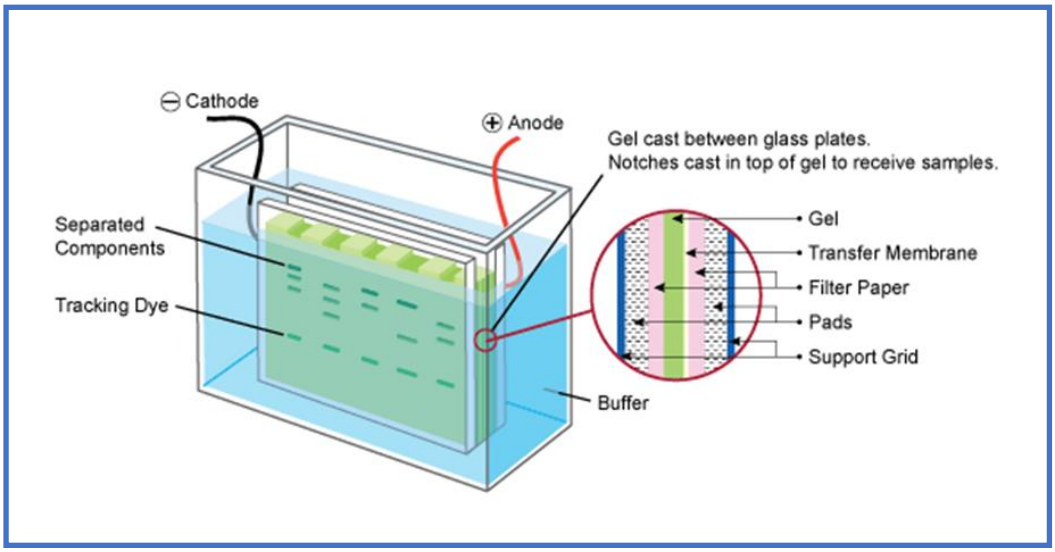

Figure 6. Illustration of western blotting setup.

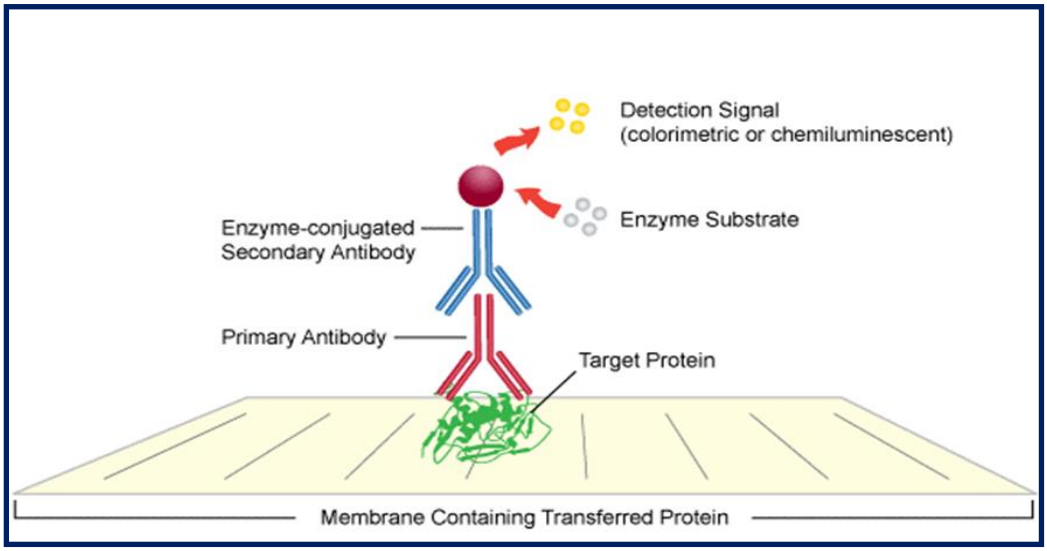

Figure 7. Detection in western blotting.

2.11 Determination of MTT formazan exocytosis

The neuroprotective activity of ESC against $A\beta_{1-42}$ oligomers was evaluated in SH-SY5Y cells using MTT formazan exocytosis assay (Fig. 8). This method takes advantage of the unique ability of $A\beta_{1-42}$ oligomers ($OA\beta_{1-42}$) to rapidly induce the exocytosis of formazan formed by MTT reduction. Briefly, SH-SY5Y cells were seeded in a 96 well plate at 3×10^4 cells/well and incubated for 24 h at 37°C in 5% CO_2. Subsequently, SH-SY5Y cells were incubated with ESC [20 µM] and $A\beta_{1-42}$ oligomers [10 µM] for 4 hours. At the end of incubation, the treatment was replaced with MTT in HBSS [0.5 mg/mL] for 1 hour at 37°C in 5% CO_2. For sequential solubilization of formazan, intracellular MTT granules were first solubilized by 1% Tween 20 at 37°C for 10 minutes with shaking. Solubilized formazan in the supernatant was transferred to a new plate as the Tween 20-soluble MTT (TS-MTT). The remaining cell surface needle-like crystals were solubilized with 100% isopropanol as the Tween 20-insoluble MTT (TI-MTT). Absorbance values at 570 nm were determined for each fraction using 690 nm as the reference wavelength. Values are expressed as percentages with control (untreated cells) set at 100 %.

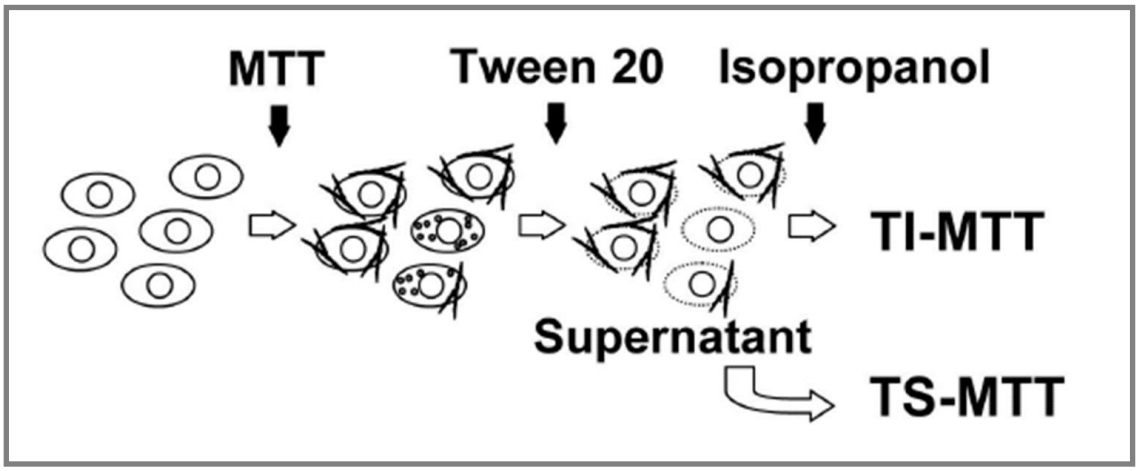

Figure 8. Sequential solubilization of intracellular MTT and exocytosed MTT. The intracellular granules of formazan are completely solubilized by Tween 20 as the TS-MTT while cell surface crystals are dissolved by isopropanol as the TI-MTT.

2.12 Determination of ROS formation induced by $A\beta_{1-42}$ oligomers

The neuroprotective activity of ESC against $A\beta_{1-42}$ oligomers - induced ROS formation was evaluated in SH-SY5Y cells using the fluorescent probe dihydroethidium (DHE) (Sigma Aldrich). DHE freely permeates cell membranes and is useful for the detection of ROS generation directly in living cells. DHE exhibits blue-fluorescence in the cytosol until it is oxidized by ROS to form ethidium, which then intercalates into DNA and stains the nucleus of living cells a bright fluorescent red (excitation at 535 nm and emission at 610 nm). Briefly, SH-SY5Y cells were seeded in a 96-well plate at 5×10^3 cells/well and incubated for 24 hours at 37°C in 5% CO_2. Subsequently SH-SY5Y cells were incubated for 24 hours with ESC [20 µM] and then for 3 hours with $A\beta_{1-42}$ oligomers. At the end of incubation, the treatment was removed and 100 µL of the fluorescent probe DHE were added to each well. ROS formation was evaluated using an inverted fluorescent microscope (Eclipse Ti-E, Nikon Instruments S.p.a, Firenze, Italy). Data are expressed as arbitrary units of fluorescence (AUF).

2.13 Determination of necrosis induced by $A\beta_{1-42}$ oligomers

To evaluate the ability of ESC to both counteract and prevent the necrosis evoked by $A\beta_{1-42}$ oligomers, SH-SY5Y cells were seeded in a 96-well plate at 5×10^3 cells/well and incubated for 24 hours at 37°C in 5% CO_2. Subsequently, SH-SY5Y cells were

incubated for 24 hours with ESC [20 µM] and $A\beta_{1-42}$ oligomers [10 µM]. While to determine the capacity of ESC to prevent the necrosis induced by $A\beta_{1-42}$ oligomers, SH-SY5Y cells were incubated for 24 hours with ESC [20 µM] and then 24 hours with $A\beta_{1-42}$ oligomers [10 µM]. At the end of incubation, the necrosis was determined using the fluorescent probe propidium iodide (PI) [25 µg/mL] (Sigma Aldrich). PI is not permeant to living cells, for this reason it is commonly used to detect dead cells in a population. PI binds to DNA by intercalating between the bases. Data are expressed as percentages of necrotic cells. Under the same experimental conditions, the neuroprotective effects of ESC were evaluated in the presence of DL-Buthionine-(S,R)-sulfoximine (BSO) [400 µM], PD98059 [5 µM] and LY294002 [10 µM] (Alexis Biochemicals, San Diego, CA, USA).

2.14 Statistical analysis

Data are reported as mean ± SD. Statistical analysis was performed using one-way ANOVA with Dunnett or Bonferroni post hoc test and Pearson's correlation coefficient for relations among variables. Differences were considered significant at $p < 0.05$. Analyses were performed using PRISM 5 software (GraphPad Software, La Jolla, CA, USA).

3. Results

3.1 Neurotoxicity of coumarins in SH-SY5Y cells

In the first part of the experiments, we determined the neurotoxicity of coumarins in SH-SY5Y cells. After 24 hours of treatment with different concentrations of ESC, SCOP, FRAX and DAPH [2.5 - 80 µM], the neuronal viability was measured using MTT assay. As reported in figure 9, the treatment with concentrations up to 20 µM did not affect neuronal viability. Therefore, we selected the range of 2.5 - 20 µM for all the following experiments.

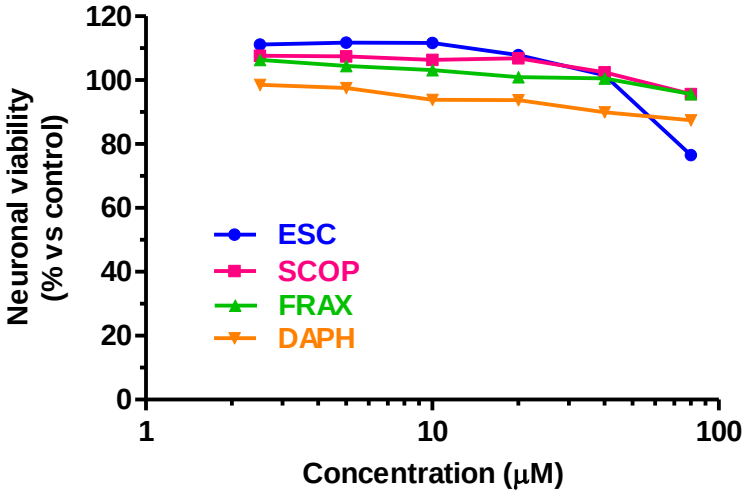

Figure 9. Neurotoxicity of ESC, SCOP, FRAX and DAPH in SH-SY5Y cells. SH-SY5Y cells were incubated for 24 hours with different concentrations of coumarins [2.5 - 80 µM]. At the end of incubation, the neuronal viability was measured using MTT assay as described in the materials and methods section. MTT values are expressed as percentages of neuronal viability with control (untreated cells) taken as 100 % viability. Data are reported as mean ± SD of at least three independent experiments.

3.2 Antioxidant activity of coumarins against *t*-BuOOH – induced ROS formation

The intrinsic antioxidant activity of coumarins was evaluated using the DPPH and ABTS assays. Coumarins showed to neutralize both the DPPH and ABTS radicals according to the following order of strength ESC>DAPH>FRAX>SCOP (data not shown). Then, we evaluated the ability of coumarins to counteract the ROS formation induced by *t*-BuOOH. SH-SY5Y cells were incubated for 2 hours with various concentrations of coumarins [2.5 – 20 μM] and then treated with *t*-BuOOH [200 μM] for 30 minutes. At the end of incubation, the ROS formation was determined using the fluorescent probe DCFH-DA. The treatment with 10 and 20 μM of ESC, FRAX and DAPH counteracted significantly the ROS formation induced by *t*-BuOOH, while we did not observe antioxidant activity with SCOP (Fig. 10A). The correlation between ROS formation and total antioxidant capacity is shown in figure 10B. We can observe a significant correlation for ESC ($R^2 = 0.8257$), FRAX ($R^2 = 0.9272$) and DAPH ($R^2 = 0.7796$) but no correlation is found for SCOP.

(A)

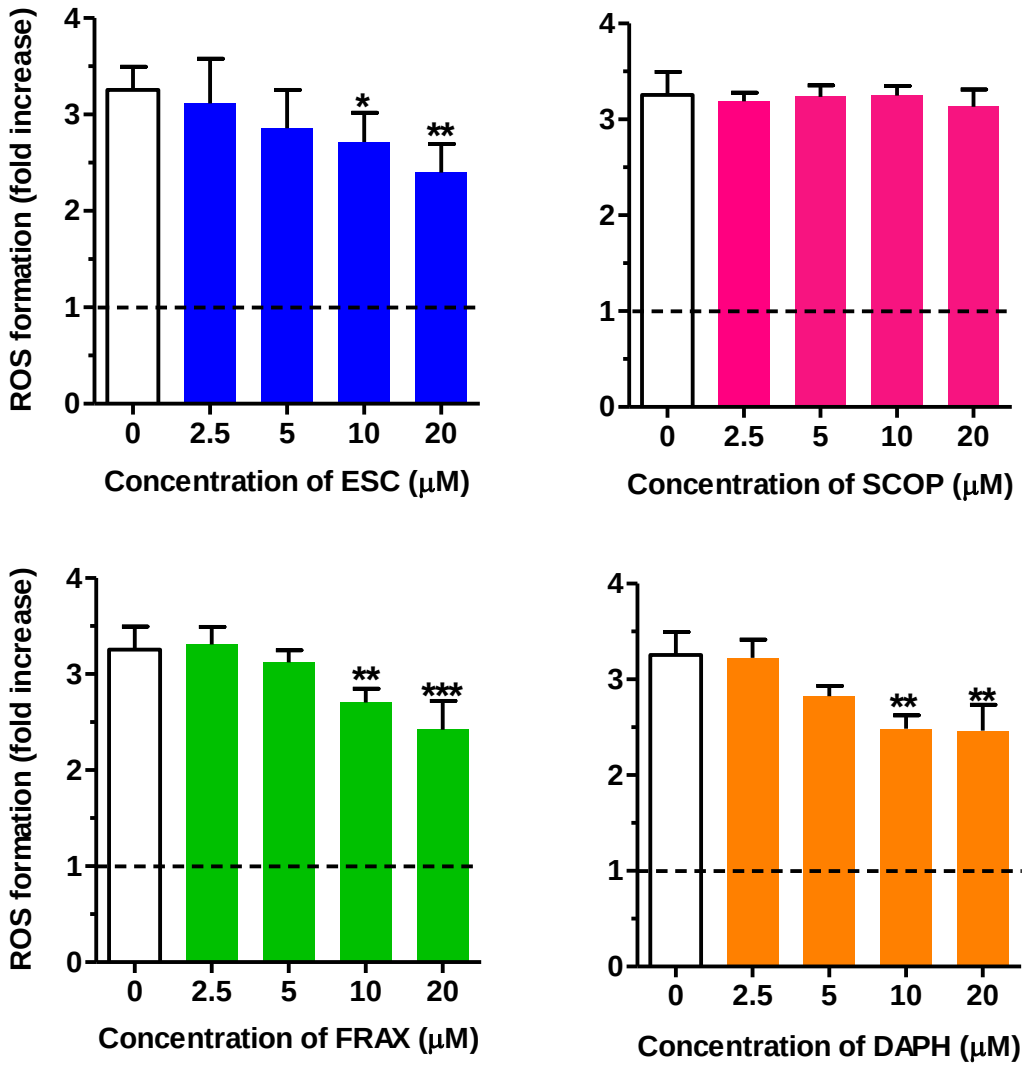
ROS formation (fold increase)
Concentration of ESC (μM)
Concentration of SCOP (μM)
Concentration of FRAX (μM)
Concentration of DAPH (μM)
0
2.5
5
10
20
*
**
***

(B)

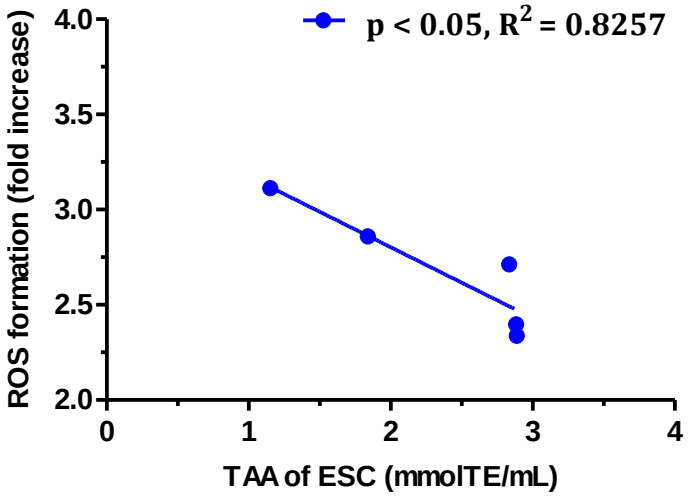
p < 0.05, R2 = 0.8257
ROS formation (fold increase)
TAA of ESC (mmolTE/mL)

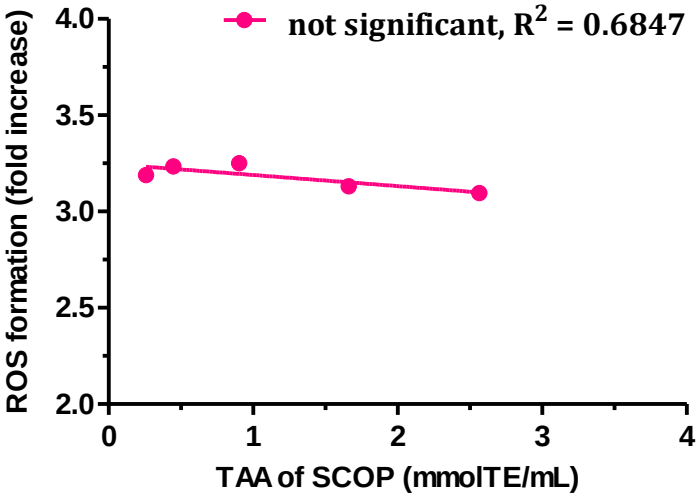
not significant, R2 = 0.6847
ROS formation (fold increase)
4.0
3.5
3.0
2.5
2.0
0
1
2
3
4
TAA of SCOP (mmolTE/mL)

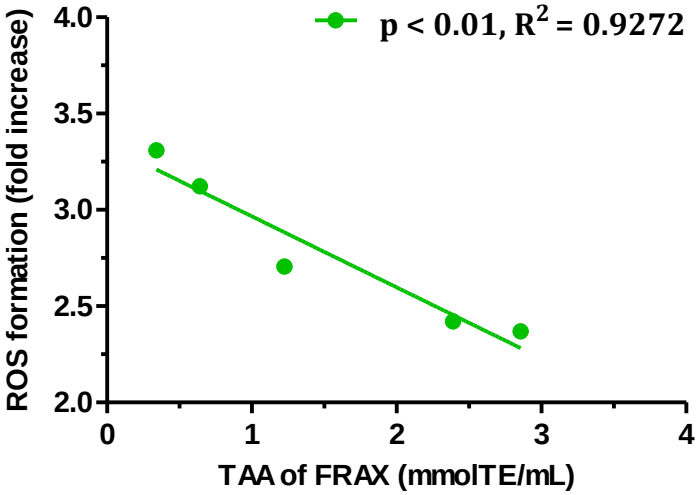
p < 0.01, R2 = 0.9272
ROS formation (fold increase)
4.0
3.5
3.0
2.5
2.0
0
1
2
3
4
TAA of FRAX (mmolTE/mL)

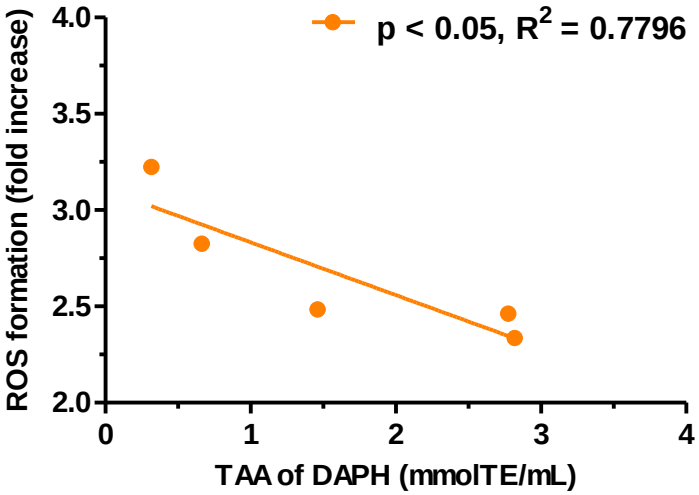
p < 0.05, R2 = 0.7796
ROS formation (fold increase)
4.0
3.5
3.0
2.5
2.0
0
1
2
3
4
TAA of DAPH (mmolTE/mL)

Figure 10. ESC, FRAX and DAPH, but not SCOP, counteract *t*-BuOOH – induced ROS formation in SH-SY5Y cells. (A) Cells were incubated for 2 hours with various concentrations of coumarins [2.5 – 20 μM] and then treated with *t*-BuOOH [200 μM] for 30 minutes. At the end of incubation, ROS formation was determined using the fluorescent probe DCFH-DA as described in the materials and methods section. Values are expressed as fold increases in ROS formation induced by *t*-BuOOH. Data are reported as mean ± SD of at least three independent experiments (*$p<0.05$, **$p<0.01$, ***$p<0.001$ versus cells treated with *t*-BuOOH at one-way ANOVA with Dunnett post hoc test). (B) Correlation between the ability of coumarins to counteract the ROS formation induced by *t*-BuOOH and their total antioxidant capacity (TAA). TAA is expressed as mmol of trolox equivalent antioxidant activity per mL of sample (mmolTE/mL).

Then, we evaluated the ability of coumarins to prevent the ROS formation induced by *t*-BuOOH. SH-SY5Y cells were incubated for 24 hours with various concentrations of coumarins [2.5 – 20 μM] and then treated with *t*-BuOOH [200 μM] for 30 minutes. At the end of incubation, the ROS formation was determined using the fluorescent probe DCFH-DA. The treatment with 20 μM of ESC and DAPH showed to prevent significantly the ROS formation induced by *t*-BuOOH (Fig. 11).

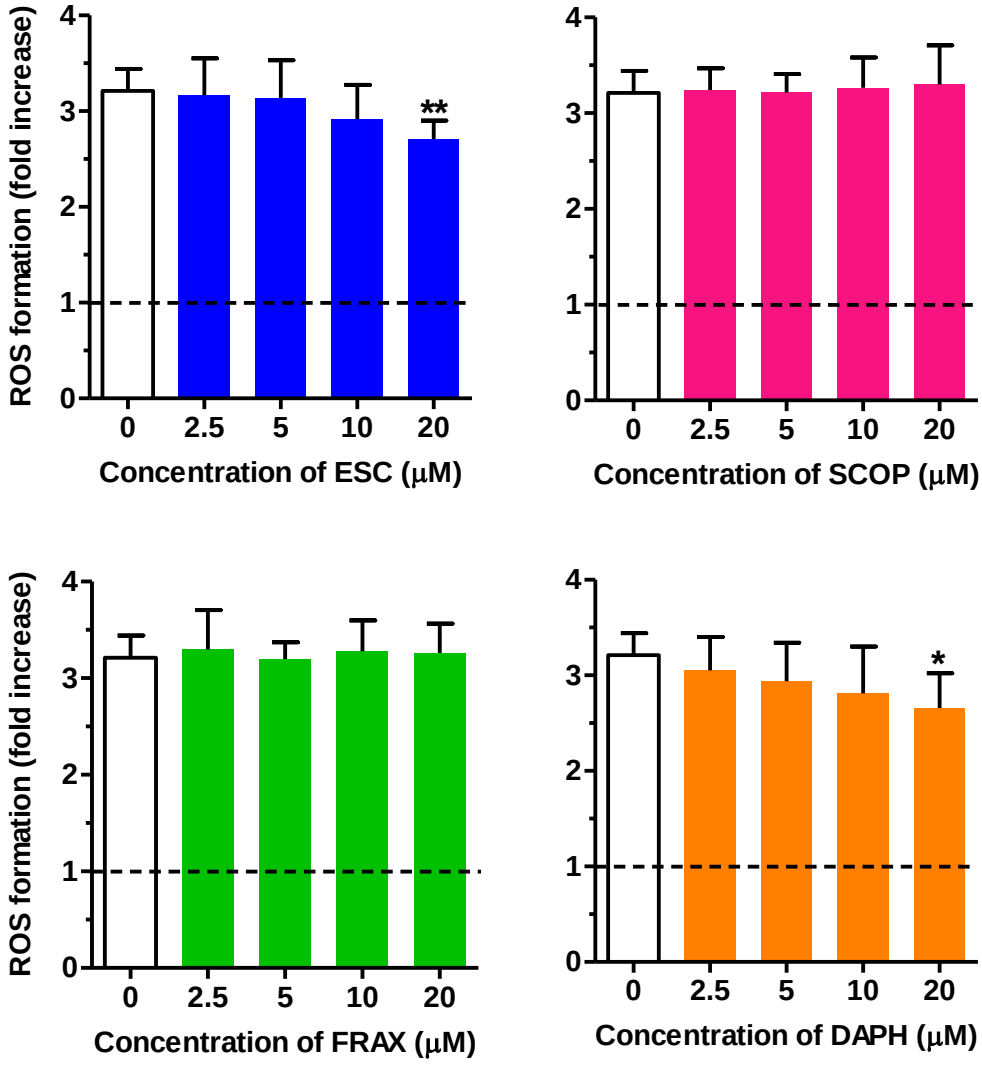

Figure 11. ESC and DAPH prevent *t*-BuOOH – induced ROS formation in SH-SY5Y cells. Cells were incubated 24 hours with various concentrations of coumarins [2.5 – 20 µM] and then treated with *t*-BuOOH [200 µM] for 30 minutes. At the end of incubation, ROS formation was determined using the fluorescent probe DCFH-DA as described in the materials and methods section. Values are expressed as fold increases in ROS formation induced by *t*-BuOOH. Data are reported as mean ± SD of at least three independent experiments (*$p<0.05$ and **$p<0.01$ versus cells treated with *t*-BuOOH at one-way ANOVA with Dunnett post hoc test).

The coumarins ESC and DAPH showed the ability to both counteract and prevent the ROS formation induced by *t*-BuOOH. To investigate the molecular mechanisms involved in the indirect antioxidant activities we evaluated the cellular uptake of ESC and DAPH in SH-SY5Y cells. Cells were incubated for 2 hours with ESC and DAPH [20 µM]. At the end of incubation, cytosolic and membrane fractions were separated and submitted to the ABTS assay. As shown in figure 12, both the coumarins ESC and DAPH enhanced in a significant manner the total antioxidant activity (TAA) of SH-SY5Y cells cytosol. While we did not record antioxidant activity in membrane fraction (data not shown). These results suggest the ability of ESC and DAPH to cross the cell membrane and enter the cells.

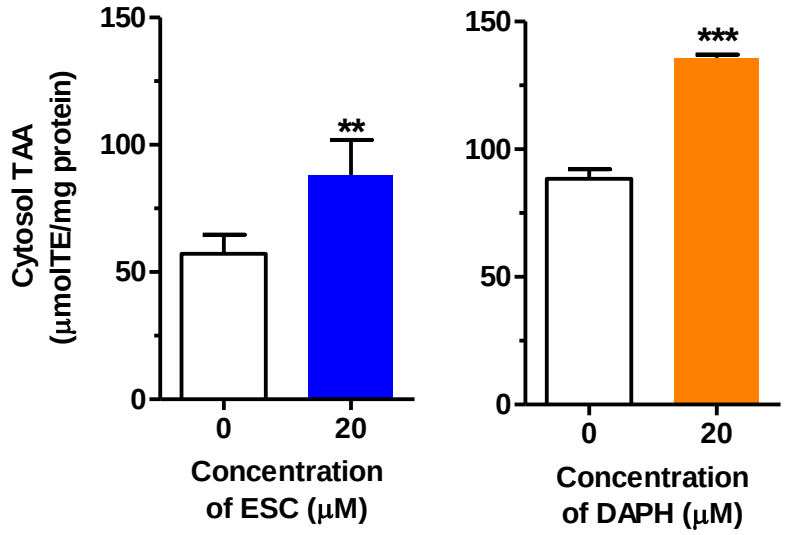

Figure 12. ESC and DAPH enhance the total antioxidant activity (TAA) of SH-SY5Y cells cytosol. Cells were incubated for 2 hours with ESC and DAPH [20 µM]. At the end of incubation, cytosolic fraction was separated and submitted to the ABTS assay as described in the materials and methods section. TAA of the cytosol fraction is expressed as µmol of trolox equivalent antioxidant activity per mg of protein (µmolTE/mg protein). Data are reported as mean ± SD of at least three independent

experiments (**p<0.01 and ***p<0.001 versus untreated cells at one-way ANOVA with Dunnett post hoc test).

3.3 Effects of ESC and DAPH on neuronal antioxidant response

The coumarins ESC and DAPH showed the ability to enter the cells. Thus, we decided to further investigate the cytoprotective effects of the coumarins ESC and DAPH evaluating their potential ability to increase GSH and Nrf2 levels in SH-SY5Y cells. Cells were incubated for 24 hours with ESC and DAPH [20 µM]. At the end of incubation, the intracellular GSH levels were determined using the fluorescent probe MCB. The treatment with 20 µM of ESC showed to increase in a significant manner GSH levels in SH-SY5Y cells. After the same treatment, DAPH did not show effects on GSH levels (Fig. 13A). In parallel, the treatment with ESC [20 µM] at different times (1, 2, 3, 6, 12 and 24 hours) registered to decrease GSH levels after short times of treatment and increase significantly GSH levels after long times of treatment (Fig. 13B).

(A)

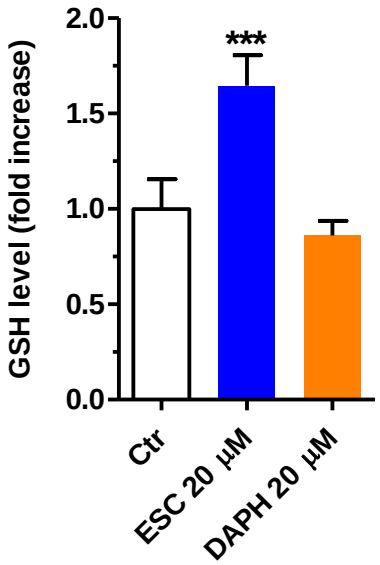

(B)

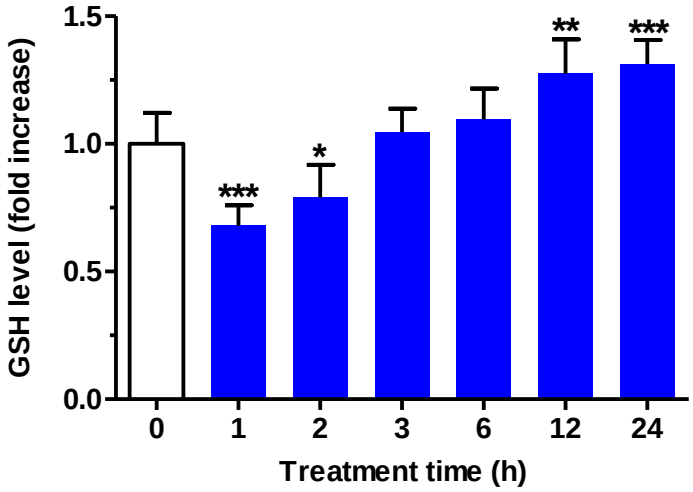

Figure 13. ESC, but not DAPH, increases GSH levels in SH-SY5Y cells. (A) Cells were incubated for 24 hours with ESC and DAPH [20 µM]. (B) Cells were incubated with ESC [20 µM] for different times. At the end of incubation, GSH levels were measured using the fluorescent probe MCB as described in the materials and methods section. GSH levels are expressed as fold increases. Data are reported as mean ± SD of at least three independent experiments (*p<0.05, **p<0.01 and ***p<0.001 versus untreated cells at one-way ANOVA with Dunnett post hoc test).

Subsequently, we investigated the ability of the coumarins ESC and DAPH to activate the nuclear transcription factor Nrf2. Among the endogenous defence systems, Nrf2 regulates the transcription of several detoxifying and antioxidant genes by binding to antioxidant response elements (AREs). Under quiescent conditions, Nrf2 is suppressed by the negative regulator Kelch-like ECH-associated protein 1 (Keap1). Under stimulation, Nrf2 escapes Keap1-mediated repression, translocates into the nucleus and subsequently binds to AREs in the promoter regions of its target genes activating their transcription. Nrf2 targets include genes that encode detoxification, antioxidant and

anti-inflammatory proteins. The activation of Nrf2 also leads to the upregulation of proteins involved in the synthesis of GSH, the main intracellular antioxidant. SH-SY5Y cells were incubated with ESC and DAPH [20 µM] for 1 and 3 hours. At the end of incubation, the expression of nuclear Nrf2 was detected by western blotting. We registered a translocation of Nrf2 after 1 hour of treatment with ESC in SH-SY5Y cells. In the same experimental conditions, the treatment with DAPH did not show the ability to activate nuclear Nrf2 (Fig. 14).

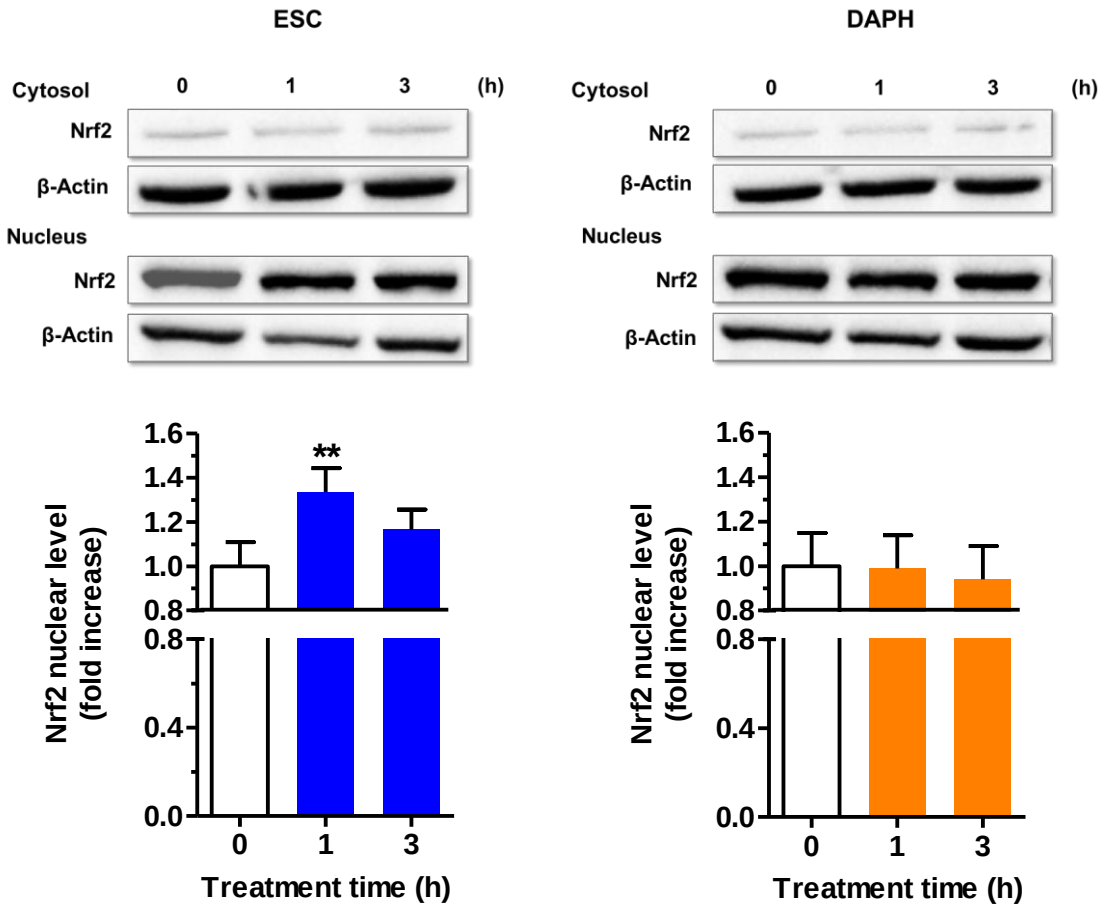

Figure 14. ESC, but not DAPH, activates the translocation of Nrf2 into nucleus in SH-SY5Y cells. Cells were incubated with either ESC and DAPH [20 µM] for 1 and 3 hours. At the end of incubation, Nrf2 nuclear levels were analysed by western blotting as previously described in the materials and methods section. Nrf2 levels are expressed

as fold increases. Data are reported as mean ± SD of at least three independent experiments (**p<0.01 versus untreated cells at one-way ANOVA with Dunnett post hoc test).

3.4 Effects of ESC on survival kinases pathways

Then we focused on the ability of ESC to activate Erk, Akt and GSK3β kinases to underline the possible molecular mechanisms by which ESC exerts cytoprotective effects in SH-SY5Y cells. The studied kinases are known to regulate diverse cellular processes including cell survival and activation of Nrf2. Akt also controls the glycogen synthesis through phosphorylation and inactivation of GSK3β. The phosphorylation of Erk, Akt and GSK3β kinases was determined after different times of incubation (15, 30, 60 and 120 minutes) with ESC [20 μM] by western blotting. The treatment of 15 and 30 minutes with ESC decreased the phosphorylation of Erk kinase while the treatment of 120 minutes with ESC increased the phosphorylation of Erk kinase (Fig. 15A). In parallel, after 120 minutes of treatment with ESC, we registered an increase of the Akt kinase phosphorylation (Fig. 15B). Further, the same treatment showed to induce the phosphorylation of GSK3β at Ser9, the inactive form (Fig. 15C).

(A)

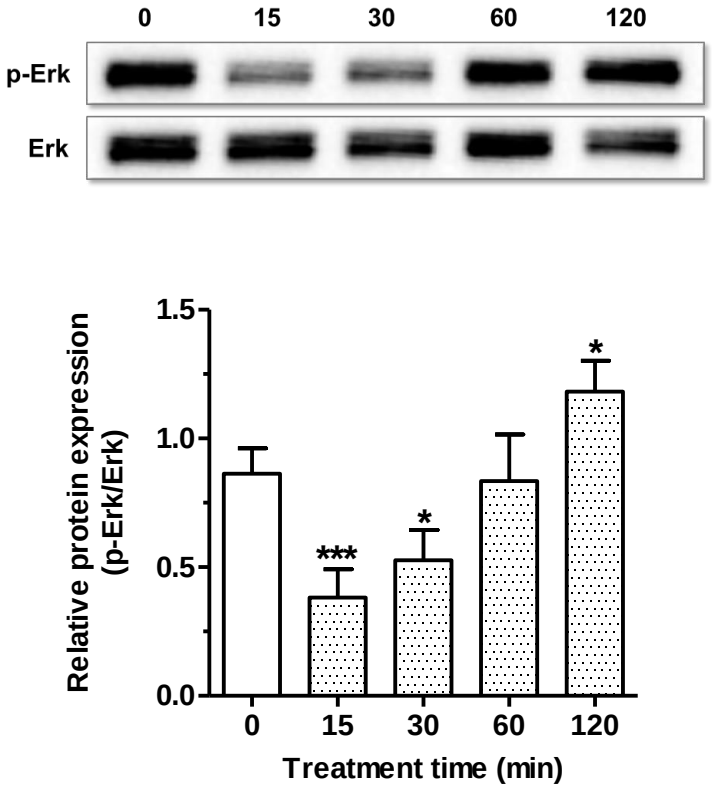
0
15
30
60
120
(min)
p-Erk
Erk
Relative protein expression (p-Erk/Erk)
1.5
1.0
0.5
0.0
***
*
*
0
15
30
60
120
Treatment time (min)

(B)

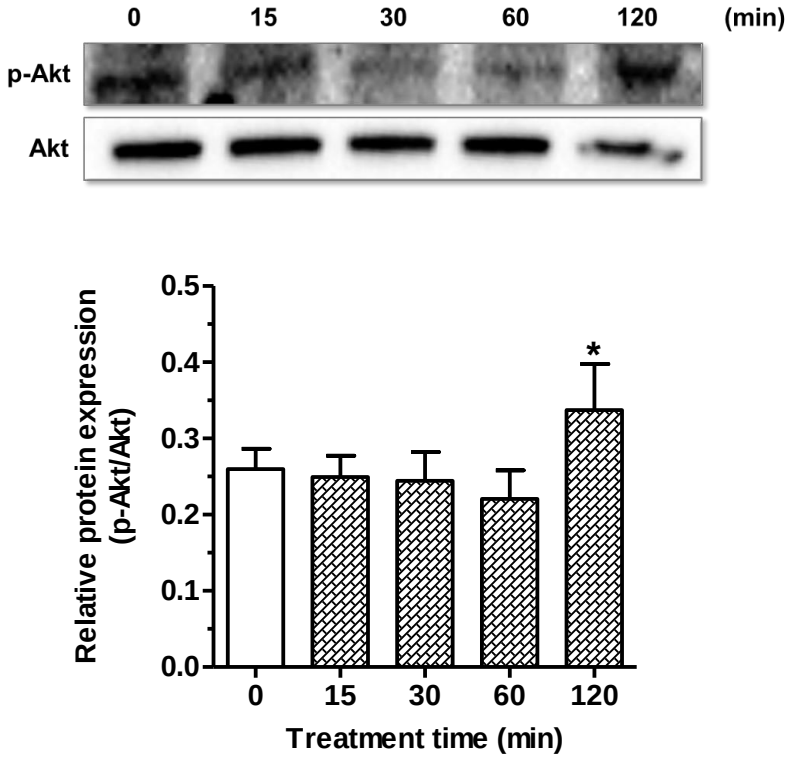
0
15
30
60
120
(min)
p-Akt
Akt
Relative protein expression (p-Akt/Akt)
0.5
0.4
0.3
0.2
0.1
0.0
*
0
15
30
60
120
Treatment time (min)

(C)

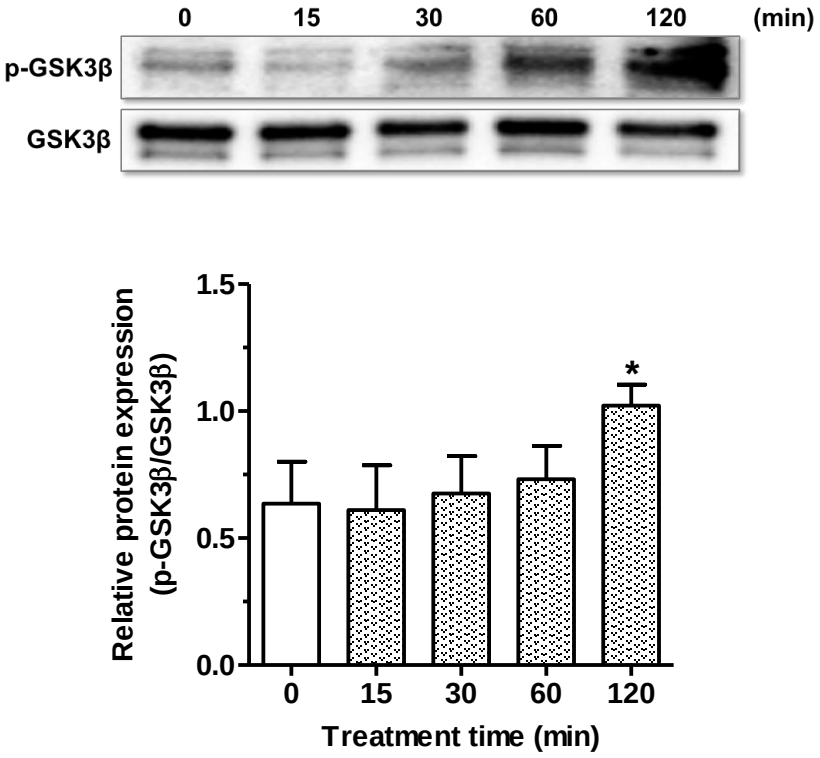

Figure 15. Effects of ESC on the phosphorylation of Erk, Akt and GSK3β kinases in SH-SY5Y cells. Cells were incubated with ESC [20 µM] for different times. At the end of incubation, the phosphorylated Erk (A), Akt (B) and GSK3β (C) kinases levels were measured by western blotting as previously described in the materials and methods section. Protein levels are reported as relative protein expression (phosphorylated form/total protein expression). Data are reported as mean ± SD of at least three independent experiments (*p<0.05 and ***p<0.001 versus untreated cells at one-way ANOVA with Dunnett post hoc test).

3.5 Neuroprotective effects of ESC against $A\beta_{1-42}$ oligomers - induced toxicity

We evaluated the ability of ESC to counteract the early and late neurotoxic events induced by $A\beta_{1-42}$ oligomers ($OA\beta_{1-42}$), in terms of formazan exocytosis and necrosis respectively. SH-SY5Y cells were incubated with ESC [20 µM] and $A\beta_{1-42}$ oligomers

[10 µM] for 4 hours. At the end of incubation, the ability of ESC to counteract the early phase of $A\beta_{1-42}$ oligomers - induced toxicity was measured by MTT formazan exocytosis assay. As shown in figure 16A-B, both the decrease of intracellular formazan and the increase of extracellular formazan were significantly counteracted by 4 hours of treatment with ESC. These results suggest a steric interaction between $OA\beta_{1-42}$ and ESC. In parallel, SH-SY5Y cells were treated with ESC [20 µM] and $OA\beta_{1-42}$ [10 µM] for 24 hours. At the end of treatment, the necrosis was measured using the fluorescent probe PI. The treatment with ESC showed to decrease in a significant manner the necrosis evoked by $OA\beta_{1-42}$ (Fig. 17A-B).

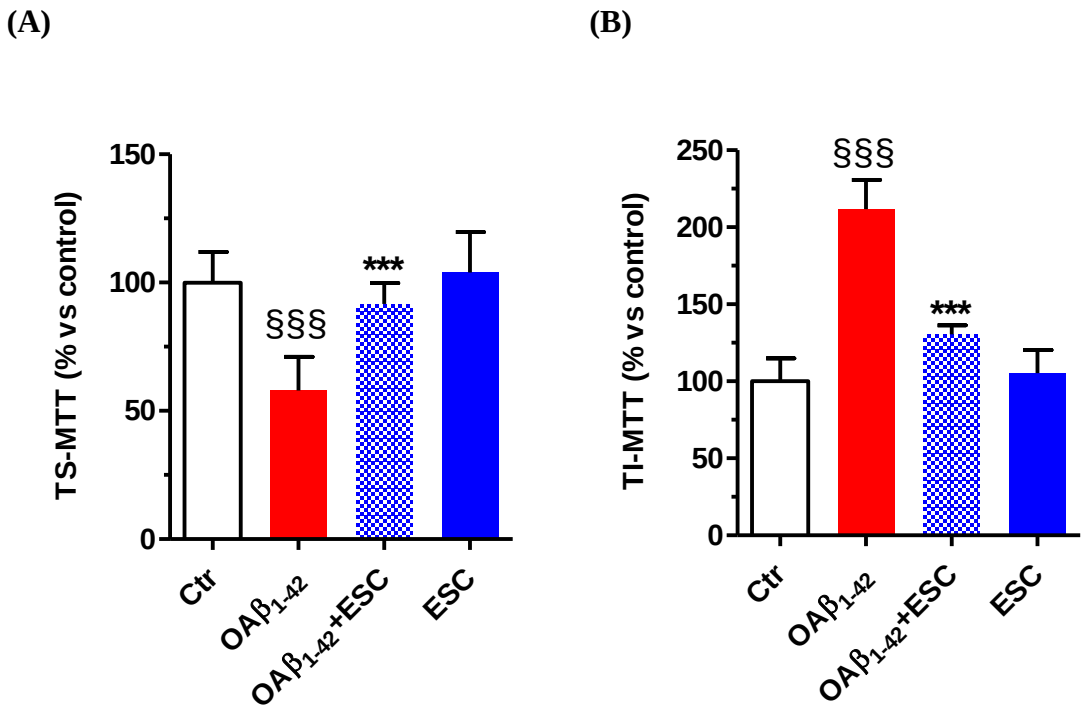

Figure 16. ESC counteracts the early neurotoxic events induced by $OA\beta_{1-42}$ in SH-SY5Y cells. Cells were incubated with ESC [20 µM] and $OA\beta_{1-42}$ [10 µM] for 4 hours. At the end of incubation, intracellular Tween 20-soluble MTT (TS-MTT) (A) and extracellular Tween 20-insoluble MTT (TI-MTT) (B) were measured by using MTT

formazan exocytosis assay as previously described in the materials and methods section. The levels of TS- and TI-MTT are expressed as percentages with control (untreated cells) set at 100 %. Data are reported as mean ± SD of at least three independent experiments ($^{§§§}p<0.001$ versus untreated cells; ***$p<0.001$ versus cells treated with $OA\beta_{1-42}$ at one-way ANOVA with Bonferroni post hoc test).

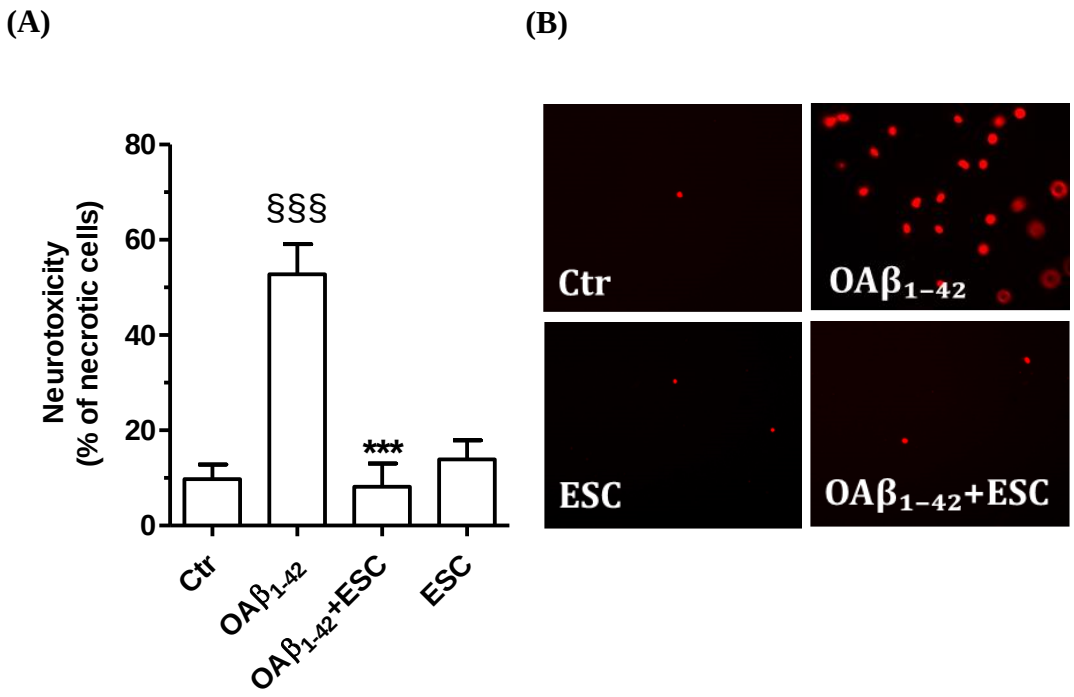

Figure 17. ESC counteracts the late neurotoxic events induced by $OA\beta_{1-42}$ in SH-SY5Y cells. (A) Cells were incubated with ESC [20 µM] and $OA\beta_{1-42}$ [10 µM] for 24 hours. At the end of incubation, the necrosis was determined using the fluorescent probe PI as previously described in the materials and methods section. (B) Representative images of necrosis. Neurotoxicity values are expressed as percentages of necrotic cells. Data are reported as mean ± SD of at least three independent experiments ($^{§§§}p<0.001$ versus untreated cells; ***$p<0.001$ versus cells treated with $OA\beta_{1-42}$ at one-way ANOVA with Bonferroni post hoc test).

Finally, we investigated the ability of ESC to prevent both the oxidative stress and the necrosis elicited by OAβ_{1-42}. SH-SY5Y cells were incubated for 24 hours with ESC [20 µM] and then treated with OAβ_{1-42} [10 µM] for 3 hours. At the end of incubation, the ROS formation was determined using the fluorescent probe DHE. The pre-treatment with ESC showed to decrease significantly the ROS formation induced by OAβ_{1-42} (Fig. 18). In parallel SH-SY5Y cells were incubated for 24 hours with ESC [20 µM] and then 24 hours with OAβ_{1-42} [10 µM]. At the end of incubation, the necrosis was measured using the fluorescent probe PI. The treatment with ESC prevented significantly the necrosis induced by OAβ_{1-42} in SH-SY5Y cells (Fig. 19).

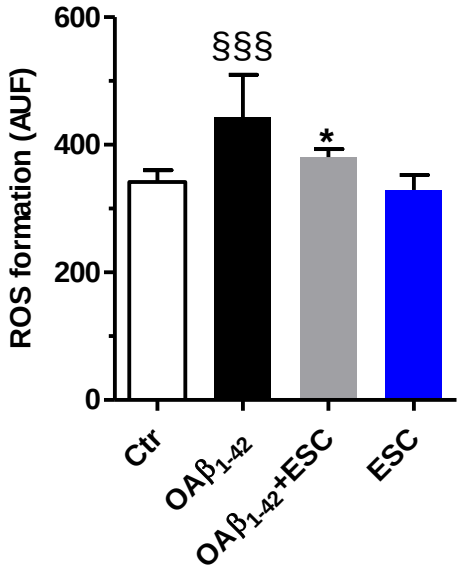

Figure 18. ESC prevents the ROS formation induced by OAβ_{1-42} in SH-SY5Y cells. Cells were incubated with ESC [20 µM] for 24 hours and then treated with OAβ_{1-42} [10 µM] for 3 hours. At the end of incubation, the ROS formation was determined using the fluorescent probe DHE as previously described in the materials and methods section. Values are expressed as arbitrary units of fluorescence (AUF). Data are reported as

mean ± SD of at least three independent experiments ($^{§§§}p<0.001$ versus untreated cells; $*p<0.05$ versus cells treated with $OA\beta_{1-42}$ at one-way ANOVA with Bonferroni post hoc test).

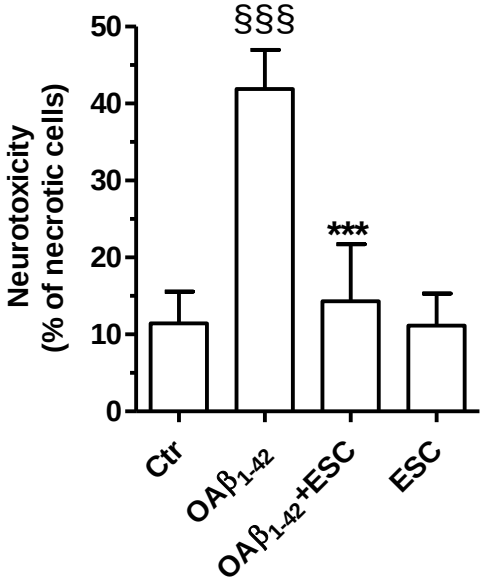

Figure 19. ESC prevents the late neurotoxic events induced by $OA\beta_{1-42}$ in SH-SY5Y. Cells were incubated with ESC [20 µM] for 24 hours and then treated with $OA\beta_{1-42}$ [10 µM] for 24 hours. At the end of incubation, the necrosis was determined using the fluorescent probe PI as previously described in the materials and methods section. Neurotoxicity values are expressed as percentages of necrotic cells. Data are reported as mean ± SD of at least three independent experiments ($^{§§§}p<0.001$ versus untreated cells; $***p<0.001$ versus cells treated with $OA\beta_{1-42}$ at one-way ANOVA with Bonferroni post hoc test).

To understand if the neuroprotective effects of ESC were mediated by the activation of Erk and Akt pathways we used PD98059 and LY294002, two neuronal specific inhibitors of Erk and Akt phosphorylation respectively. We also evaluated the neuroprotective effects of ESC in the presence of BSO, an inhibitor of GSH synthesis.

SH-SY5Y cells were treated with ESC [20 µM] and the specific inhibitors PD98059 [5 µM], LY294002 [10 µM] and BSO [400 µM] for 24 hours. Then cells were incubated for 24 hours with $OA\beta_{1-42}$ [10 µM]. At the end of incubation, the neurotoxicity was measured using the fluorescent probe PI. We observed that the neuroprotective effects of ESC were abrogated in SH-SY5Y cells by using these specific inhibitors (Fig. 20).

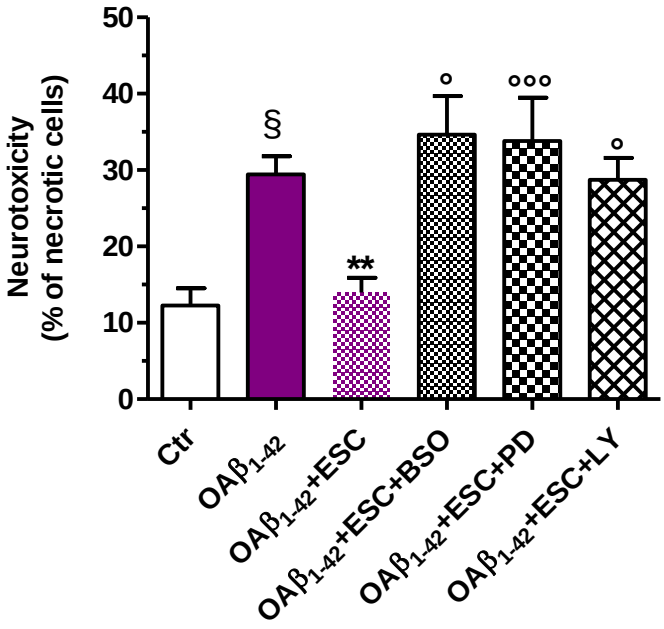

Figure 20. Neuroprotective effects of ESC are abrogated by the specific inhibitors BSO, PD98059 and LY294002 in SH-SY5Y. Cells were incubated for 24 hours with ESC [20 µM] and with the specific inhibitors. Then cells were treated for 24 hours with $OA\beta_{1-42}$ [10 µM] and at the end of incubation, the necrosis was determined using the fluorescent probe PI as previously described in the materials and methods section. Neurotoxicity values are expressed as percentages of necrotic cells. Data are reported as mean ± SD of at least three independent experiments ($^{\S}p<0.05$ versus untreated cells; $^{**}p<0.01$ versus cells treated with $OA\beta_{1-42}$; $^{\circ}p<0.05$ and $^{\circ\circ\circ}p<0.001$ versus cells treated with $OA\beta_{1-42}$ + ESC at one-way ANOVA with Bonferroni post hoc test).

4. Discussion

Alzheimer's disease (AD) is characterized by a progressive decline in cognitive functions with memory loss, language deficit, disorientation and inability to perform everyday activities. The pathogenesis of AD involves a progressive neuronal loss particularly in hippocampus and cortex, associated with abnormal accumulation of extracellular amyloid-beta peptide and intracellular tau tangles. Although its causes are still unknown it is clear that AD develops through a multifactorial process and several factors were identified as responsible for increasing the risk of developing AD. Among the most significant risk factors, it is well known that oxidative stress due to generation of reactive oxygen species (ROS) is involved in the crucial events leading to the neural death and contributing to the pathogenesis of neurodegenerative disorders including AD. The involvement of oxidative stress in the incidence and progression of neurodegenerative diseases has led to investigate into the potential for using antioxidant molecules as therapeutic treatment. In our study, we focused on the natural phenolic coumarins that are known to show an extensive range of biological activities including antioxidant activity. Initially, we evaluated the intrinsic antioxidant activities of coumarins against DPPH and ABTS radicals. ESC showed the strongest quenching capacities against both the radicals, followed by DAPH. FRAX was less active in DPPH and ABTS radicals scavenging while SCOP was not effective [54–56]. Further ESC, FRAX and DAPH counteracted significantly the ROS formation induced by *t*-BuOOH in SH-SY5Y cells. These results indicated that the catechol (*orto*-dihydroxyl) group markedly contributed to the direct antioxidant activities of these coumarins. The coumarins ESC, FRAX and DAPH having a catechol group can act like classic phenol or quinone based antioxidants. Several studies reported that the phenolic coumarins

such as ESC, FRAX and DAPH are excellent antioxidant and radical scavengers thanks to its *orto*-dihydroxyl group [57,58]. Lin *et al*. suggest that the number of hydroxyl groups on the ring structure of coumarins is correlated with their antioxidant effects. Further, the catechol group connected to aromatic ring can carry free radical reactions suggesting also the importance of the α-pyrone ring to the antioxidant activities of these coumarins [59].

Subsequently, we investigated the indirect antioxidant activity of the studied coumarins against the ROS formation induced by *t*-BuOOH. Among the coumarins, ESC and DAPH registered the ability to prevent the ROS formation induced by *t*-BuOOH in SH-SY5Y cells showing to possess indirect antioxidant activities. Bilgin *et al*. underline the antioxidant property of coumarins including ESC in the prevention of oxidative stress induced by carbon tetrachloride in rats [60]. Lin *et al*. showed that pre-treatment with ESC significantly decreased the oxidative damage in primary cultured rat hepatocytes induces by *t*-BuOOH [61]. Kim *et al*. recorded the ability of ESC to prevent the oxidative stress evoked by hydrogen peroxide in hamster fibroblasts [62]. Further, ESC and DAPH increased significantly the cytosolic TAA in SH-SY5Y cells suggesting their ability to pass through the cell membrane and reach the cytoplasm. These results suggest that both the coumarins ESC and DAPH possess a good lipophilicity to enter the cells. ESC also showed the interesting ability to cross the intestinal and blood–brain barrier in different animal models. In particular, ESC was able to prevent the dopaminergic neuronal death in a mouse model of Parkinson's disease [63,64].

Recent studies have demonstrated that GSH depletion and GSH-related enzyme deficit are involved in the onset and progression of neurodegenerative disorders including AD. Decreased GSH levels have been reported in the blood and brain samples of AD [65,66]. For this reason, we decided to examine the ability of the antioxidant coumarins ESC and DAPH to enhance the intracellular GSH levels in neuronal SH-SY5Y cells. We found that only ESC was able to increase intracellular GSH levels while DAPH did not have effects. Among the endogenous antioxidant, we also focused on the transcription factor Nrf2 that is considered a critical regulator of the cellular antioxidant response to protect against oxidative stress [67]. Nrf2 activation mitigates multiple pathogenesis processes involved in AD through upregulation of antioxidant defences, inhibition of inflammation, improvement of mitochondrial function and maintenance of protein homeostasis. Several inducers of Nrf2 have shown protective effects in numerous human cell and animal models of neurodegenerative diseases [68]. Interestingly, ESC activated Nrf2 translocation to nucleus after 1 hour of treatment while DAPH did not show activity in SH-SY5Y cells. Han *et al*. reported that treatment with ESC inhibited H_2O_2 – induced ROS generation in C2C12 myoblasts and increased phosphorylation of Nrf2 in a time dependent manner [69]. To investigate whether the translocation of Nrf2 induced by ESC in SH-SY5Y cells involved Erk and Akt/GSK3β signalling pathways, we assessed the phosphorylation forms of Erk, Akt and GSK3β. Immunoblotting data indicated that phosphorylation of Erk, Akt and GSK3β occurred after 120 minutes of treatment with ESC. These results suggest that Erk and Akt/GSK3β signalling pathways are involved in the ESC-mediated activation of Nrf2. In particular, the phosphorylation of GSK3β at ser9 leads to the formation of its inactive form and seems to play a central role in AD pathogenesis. Evidence from different studies

supports that GSK3β is intimately involved in the hyper-phosphorylation of tau, memory and learning impairments, the increased production of Aβ from APP (via β and γ secretase-mediated cleavage) and in microglial-mediated inflammatory responses in the local vicinity of Aβ plaques. GSK3 also reduces acetylcholine synthesis, which is in accordance with the cholinergic deficit present in AD. Moreover, GSK3 is a key mediator of apoptosis and thereby might directly contribute to neuronal loss in AD. GSK3β suppression in a mouse model of AD was found to increase nuclear Nrf2 and total glutathione-S transferase, a Nrf2 transcriptional target, in cortex. Several studies suggest the possible association between GSK3 inhibition and Nrf2 activation [70–72]. ESC exerts dual antioxidant effects: direct protective properties and indirect antioxidant ability inducing antioxidant enzymes via Nrf2/ARE activation.

Amyloid-β (Aβ) peptide neurotoxicity has been identified as one of the major features in AD pathology. The inhibition of MTT reduction by Aβ peptide is an early indication of the Aβ-induced impairment in the cellular redox activity. Recent studies reported that Aβ peptite inhibits cellular MTT reduction by enhancing MTT formazan exocytosis [73–75]. In this study, we recorded that the early MTT formazan exocytosis elicited by $A\beta_{1\text{-}42}$ oligomers ($OA\beta_{1\text{-}42}$) was inhibited by 4 hours of treatment with ESC. On microscope examination, SH-SY5Y cells treated with $OA\beta_{1\text{-}42}$ and incubated with MTT showed marked appearance of needle like exocytosed formazan crystals on the cell surface compared with the intracellular formazan granules observed in the untreated control cells. While, cells treated with $OA\beta_{1\text{-}42}$ plus ESC or ESC showed intracellular unexcytosed MTT granules indicating the neuroprotective effects of ESC on MTT exocytosis. Interestingly, ESC counteracted also the necrosis induced by 24 hours of

treatment with $OA\beta_{1-42}$ in SH-SY5Y cells. These findings suggest that ESC is able to counteract both the early and late neurotoxic events evoked by $OA\beta_{1-42}$ in terms of MTT formazan exocytosis and necrosis. We could hypothesize a direct interaction of ESC with $OA\beta_{1-42}$ as a result of neuroprotection.

Finally, we investigated the ability of ESC to prevent the oxidative damage and the neurotoxicity induced by 24 hours of treatment with $OA\beta_{1-42}$ in SH-SY5Y cells. ESC prevented significantly both the ROS formation and necrosis induced by $OA\beta_{1-42}$. Recent studies reported that ESC is a potent agent in protecting cells from ROS-mediated Aβ-damage [76,77]. In addition, the protective effects of ESC against the necrosis induced by $OA\beta_{1-42}$ were abrogated in SH-SY5Y cells pre-treated with BSO, PD98059 and LY294002 suggesting the implication of survival signalling pathway as well as endogenous antioxidant defence in the neuroprotective effects of ESC against $OA\beta_{1-42}$ - induced toxicity.

Taken together, these results showed the ability of ESC to prevent both the oxidative stress and necrosis induced by $OA\beta_{1-42}$. At this regard, recent studies reported that ESC exhibited potent inhibitory activity against AChE, BChE and BACE1 thanks to the presence of the catechol group [33]. Thus, ESC with its substantial inhibitory activity against BACE1 may represent a potential novel candidate for AD treatment by targeting Aβ formation and deposition. Our results encourage further research in Alzheimer's disease animal models to explore the potential profile of ESC as novel neuroprotective agent and to further elucidate the molecular mechanisms involved in the neuroprotective effects of ESC.

Chapter II

1. Introduction

1.1 Huntington's disease

Huntington's disease (HD) is an autosomal dominant inherited neurodegenerative disorder that affects approximately 5-10 individuals per 100,000. HD is caused by an abnormal CAG trinucleotide repeat expansion within the exon 1 of the gene encoding for the huntingtin (HTT) protein. Individuals typically suffer from involuntary movements including chorea, dyskinesia and dystonia, psychiatric disturbances, depression and cognitive deficits. With the progression of the disease, motor rigidity and dementia predominate. The most striking neuropathological hallmark of this disorder is the atrophy of the striatum as seen in post mortem brain tissue. The disease preferentially affects the GABAergic medium size spiny neurons in the striatum and in other regions such as the cerebral cortex. Cortical atrophy and early degeneration of the hypothalamus are also important aspects of HD pathogenesis. Currently, treatment is limited to suppress chorea, the involuntary and irregular movements that accompanies HD. In affected individuals, the number of CAG repeats expands from 37 to more than 120 repeats. This leads to an elongated polyglutamine tract at the amino terminus of the translated HTT protein that is associated with protein aggregation. The formation of cytoplasmic aggregates and nuclear inclusions throughout the brain is considered a hallmark of HD. Despite its monogenic nature, HD pathogenesis is very complex and involves multiple cellular mechanisms (Fig. 1) [78,79].

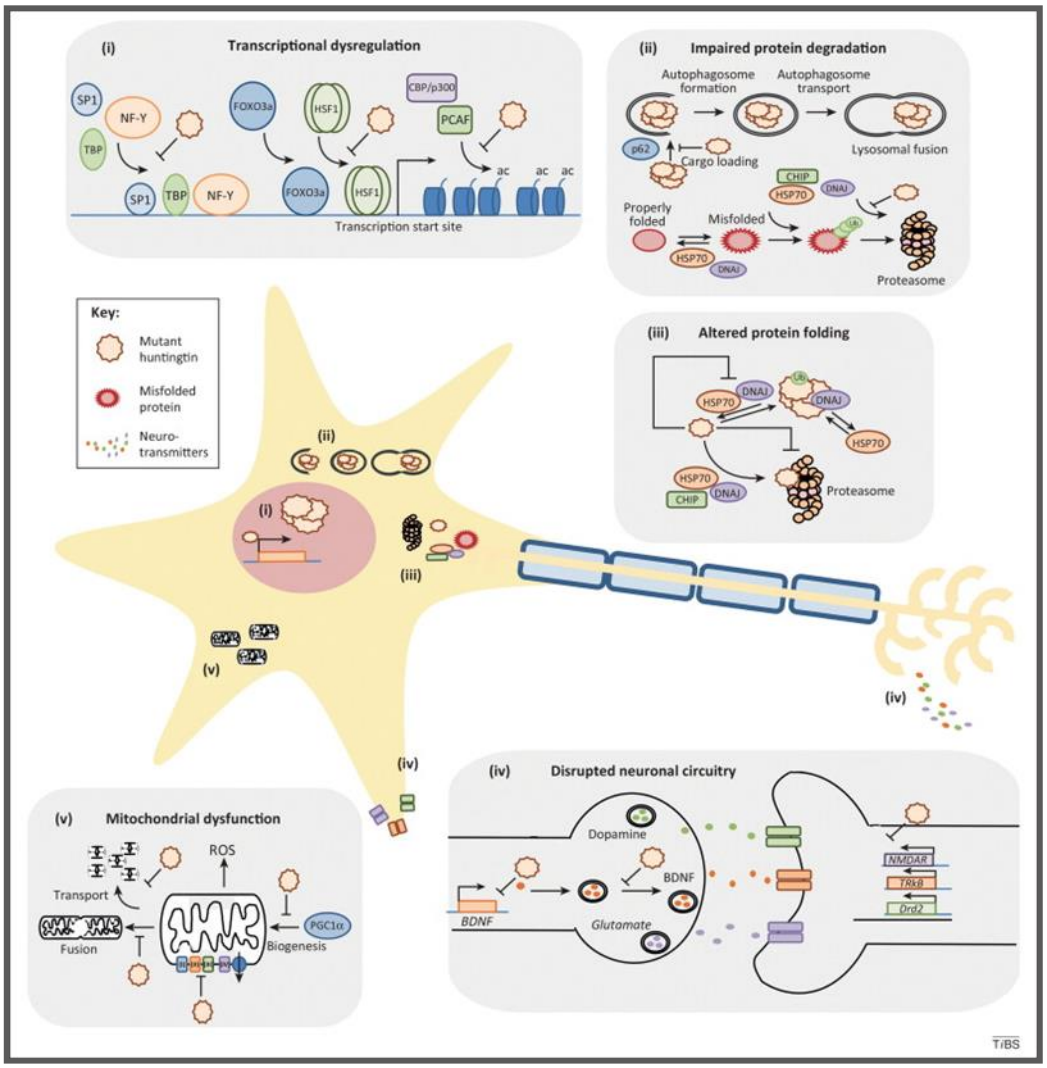

Figure 1. Major cellular pathways disrupted in HD. (i) Transcriptional dysregulation of basal and inducible gene expression, (ii) impaired protein degradation, (iii) altered protein folding, (iv) disrupted synaptic signalling and (v) perturbed energy metabolism through altered mitochondrial maintenance and localization (from Labbadia and Morimoto, *Huntington's disease: underlying molecular mechanisms and emerging concepts*, Trends Biochem. Sci. 38 (2013) 378-385).

1.2 Transcriptional dysregulation

The expression of mutant HTT protein affects the transcriptome suggesting that transcriptional dysregulation represents a key feature of HD pathogenesis. Mutant HTT protein interacts with the major components of the global transcriptional machinery disrupting both general promoter accessibility and recruitment of RNA polymerase II [80]. Several studies demonstrated that mutant HTT protein impairs the functions of some important mediators of general promoter accessibility and transcription initiation such as TATA box binding protein (TBP) and CAAT box transcription factor NF-γ [81–85]. The expression of mutant HTT protein also disrupts the activity of histone acetyl transferases that results in histone hypoacetylation and increased heterochromatin formation [86].

1.3 Impaired proteostasis

Under normal conditions, proteome integrity is maintained by the proteostasis network that involves molecular chaperons and clearance machineries as main effectors. Chronic expression of expanded polyglutamine peptides results in an age-dependent collapse of proteostasis with an increased aggregation and mislocalization of metastable proteins. Restoration of protein-folding capacity through chaperone overexpression or enhancement of chaperone gene regulation pathways suppresses mutant HTT protein toxicity in multiple models of HD [87]. Recent studies conducted in *C. elegans* identified a new gene *moag-4*, that influences polyglutamine aggregation independently of the proteasome or autophagy and without activation of stress response pathways or upregulation of molecular chaperons [88]. The ubiquitin proteasome system (UPS)

represents an important target since mutant HTT protein inclusions were identified ubiquitin-positive. The mechanism by which mutant HTT protein causes dysfunction of the UPS is still unclear. Brain tissue from HD patients and HD mice present an accumulation of ubiquitin chains. Recent findings suggest that the accumulation of ubiquitin chains in HD is not the result of direct proteasome inhibition by mutant HTT oligomers. But it seems that mutant HTT protein aggregates interfere with the proteostasis network leading to increased levels of polyubiquitylated proteins within the cell. This abundance of polyubiquitylated proteins overloads the proteasome. In addition, autophagosome formation and lysosomal fusion appear to be affected by the expression of mutant HTT protein. Thus, UPS impairments and defects in autophagy are thought to contribute to neurodegeneration in HD [89–91].

1.4 Disrupted neuronal circuitry

Perturbed neuronal activity underlines the cognitive and physical decline observed in HD patients. The expression of genes important for calcium homeostasis, neuronal differentiation, neuronal survival and neurotransmission are reduced in the early stage of HD. In addition, mutant HTT protein dramatically impairs neurotransmitter release at pre-synaptic junctions by physically impeding axonal transport and by reducing the efficiency of synaptic cargos transport onto microtubules. Medium spiny neurons of the striatum exhibit major vulnerability to the presence of mutant HTT protein aggregates. This observation has been attributed to several factors including reduced neurotrophin availability and glutamate receptor mediated excitotoxicity cell death. Glutamatergic excitotoxicity of medium spiny neurons through aberrant NMDA receptors activity is considered an important component in HD pathogenesis. NMDA receptors activity can

be modified by neuroactive metabolites of the tryptophan degradation pathway, particularly kynurenic acid (an NMDA antagonist) and quinolinic acid (an NMDA agonist). Perturbations in the kynurenine pathway of tryptophan degradation have been linked to the pathogenesis of neurodegenerative disorders including HD. Several studies reported that the inhibition of the enzyme kynurenine-3-monoxoygenase (KMO) improved neurodegeneration in diverse models of HD. The novel KMO inhibitor JM6 successfully suppresses disease in rodent models of HD without entering the brain but modifying metabolites in the blood. Excitotoxicity can be also directly suppressed by small molecules NMDA receptors antagonists. Treatment with memantine showed to counteract neurodegenerative effects in HD mice [92–95].

1.5 Mitochondrial dysfunction

Numerous studies support a role for mitochondrial dysregulation in HD pathogenesis. Mutant HTT protein leads to an impairment of electron transport chain complexes II and III with depletion of intracellular ATP levels and increased reactive oxygen species (ROS). Specifically, it appears that mutant HTT protein inhibits the activity of succinate dehydrogenase enzyme of complex II of mitochondria leading to the bioenergetic deficit observed in HD. The mitochondrial dysfunction in HD involves also the mitochondrial trafficking. Retrograde and anterograde mitochondrial trafficking along axons is impeded by mutant HTT protein aggregates causing disruption of mitochondrial maintenance and reduced deposition of mitochondria at sites with high energy demand. Moreover, mutant HTT protein directly impairs the ability of PGC-1α to activate downstream target genes involved in mitochondrial biogenesis, thermogenesis and oxidative phosphorylation. Further amplifying the damage, mutant HTT is able to

promote calcium-dependent mitochondrial depolarization and mitochondrial swelling. Mutant HTT protein interacts also with GTPase dynamin related protein-1 (DRP-1) leading to an increase of its activity. This increase of DRP-1 GTPase activity is related to aberrant mitochondrial fission and impaired mitochondrial transport. Interestingly, treatment of HD transgenic mice with an inhibitor of DRP-1 restores normal mitochondrial fission and transport improving HD mice phenotypes [96,97].

In this context, the aim of our research was to investigate the potential neuroprotective effects of the natural coumarin esculetin in different Huntington's disease models. We used a stable inducible cell line (PC12 HD-Q74) and a transgenic *Drosophila melanogaster* model (HTT93Q, pan-neuronal expression), both of which express mutant huntingtin (HTT) exon 1 fragments, a typical feature of HD. Several parameters including oxidative damage, mitochondrial dysfunction and neuronal death elicited by mutant HTT, were assessed in order to evaluate the neuroprotective activities of esculetin.

2. Materials and methods

2.1 Cell culture

The stable inducible rat pheochromocytoma cell line (PC12) expressing GFP-tagged exon 1 of the Huntington gene with 74 glutamine repeats (HD-Q74) was kindly obtained by Dr. David C. Rubinsztein at the University of Cambridge (United Kingdom). The cells were cultured in Dulbecco's modified Eagle's Medium (DMEM) supplemented with 10% horse serum, 5% fetal bovine serum (FBS), 2 mM L-glutamine, 100 U/mL penicillin, 100 µg/mL streptomycin, 50 µg/mL G418 and 70 µg/mL hygromycin B at 37°C in a humidified incubator with 5% CO_2. The expression of huntingtin (HTT) exon 1 fragment containing 74 glutamines fused to the green fluorescent protein (GFP) is driven by a minimal cytomegalovirus promoter under the control of a tetracycline responsive element. The expression of HTT exon 1 fragment with 74 glutamines was induced by 72 hours of incubation with doxycycline 1 µg/mL (Sigma Aldrich).

2.2 Determination of cell proliferation and necrosis

PC12 HD-Q74 cells were seeded in 100 mm dishes at 2×10^6 cells/dish and incubated for 72 hours with doxycycline (DOX) at 37°C in 5% CO_2 to obtain the expression of HTT exon 1 fragment. ESC [5 µM] was added during the last 24 hours of incubation with DOX. At the end of incubation, cell proliferation and necrosis were both evaluated by using the dye eosin (Sigma Aldrich). Briefly, the cell suspensions were simply mixed with eosin (1:5) and then visually examined to determine viable and dead cells. Further,

cells were counted to measure their proliferation activity. Cell proliferation and necrosis values are expressed as number of total cells and percentages of necrosis, respectively.

2.3 Determination of mutant HTT protein aggregation

PC12 HD-Q74 cells were seeded in 100 mm dishes at 2×10^6 cells/dish and incubated for 72 hours with DOX at 37°C in 5% CO_2 to obtain the expression of HTT exon 1 fragment. ESC [5 µM] was added during the last 24 hours of incubation with DOX. At the end of incubation, cells were counted to obtain 5×10^5 cells/mL suspension from each dish. Then 100 µL of the cell suspension were added to a black 96 well plate. Mutant HTT protein aggregation was detected (excitation at 485 nm and emission at 535 nm) using a VICTOR™ X3 multilabel plate reader. Values are expressed as arbitrary unit of fluorescence (AUF).

2.4 Determination of neurotoxicity

PC12 HD-Q74 cells were seeded in 100 mm dishes at 2×10^6 cells/dish and incubated for 24 hours with different concentrations of ESC [2.5 - 10 µM] at 37°C in 5% CO_2. At the end of incubation, cells were counted to obtain 5×10^5 cells/mL suspension from each dish. Then, stock solution MTT [5mg/mL] was added to each cell suspension (1:10 dilution). After 1 hour of incubation at 37°C in 5% CO_2, the cell suspensions were centrifugated at 6000 rpm for 10 minutes and the obtained pellet containing formazan crystals were dissolved in isopropanol. The amount of formazan was measured (570 nm, reference filter 690 nm) using a VICTOR™ X3 multilabel plate reader. The neurotoxicity is expressed as percentages of neuronal viability.

2.5 Morphological analysis of mitochondria

PC12 HD-Q74 cells were seeded in 100 mm dishes at 2×10^6 cells/dish and incubated for 72 hours with DOX at 37°C in 5% CO_2 to obtain the expression of HTT exon 1 fragment. ESC [5 µM] was added during the last 24 hours of incubation with DOX. At the end of incubation, cells were counted to obtain 1×10^6 cells suspension from each dish. Subsequently, cells were fixed with a solution containing 2.5% (v/v) glutaraldehyde in 0.1 M sodium cacodylate (pH = 7.4) for 1 hour at room temperature, then quickly washed and post-fixed with 1% OsO_4 in 0.1 M phosphate buffer for 1 h. After dehydration in a graded series of ethanol, the samples were embedded in Epon resin (Sigma Aldrich). Ultrathin sections were counterstained with uranyl acetate and lead citrate and observed under a Philips CM10 (FEI Company, Eindhoven, the Netherlands). The images were digitally captured by SIS Megaview III CCD camera (FEI Company). Mitochondria were individually traced, and size parameters were obtaining using ImageJ software. Mitochondrial size in terms of mitochondrial area was reported in squared micrometres (μm^2). Further, the number of mitochondria per viable cell was reported. The same procedure was adopted to analyse cell necrosis.

2.6 Determination of mitochondrial activity

The mitochondrial activity was indirectly measured by using the CellTiter-Glo® Luminescent Cell Viability Assay (Promega, Madison, WI, USA), a homogeneous method based on quantitation of adenosine triphosphate (ATP). PC12 HD-Q74 cells were seeded in 100 mm dishes at 2×10^6 cells/dish and incubated for 72 hours with DOX at 37°C in 5% CO_2 to obtain the expression of HTT exon 1 fragment. ESC [5 µM] was added during the last 24 hours of incubation with DOX. At the end of incubation, cells were counted to obtain 2×10^5 cells/mL suspension from each dish. Then 100 µL per well of the cell suspension were added to an opaque-walled 96-well plate while control wells containing medium without cells were prepared to obtain a value for background luminescence. The plate and its contents were equilibrated at room temperature for approximately 30 min. Subsequently, 100 µL of CellTiter-Glo® Reagent was added to each well and contents were mixed for 2 min on an orbital shaker to induce cell lysis. The plate was incubated at room temperature for 10 min to stabilize luminescent signal. The luminescence was recorded using a VICTOR™ X3 luminometer (PerkinElmer). The luminescent signal is proportional to the amount of ATP present in cells. The CellTiter-Glo® Assay relies on the properties of a thermostable luciferase (Ultra-Glo™ Recombinant Luciferase), which generates a stable luminescent signal in the presence of ATP. The luciferase reaction is shown in figure 2. Values are expressed as ATP levels (nM) per viable cell.

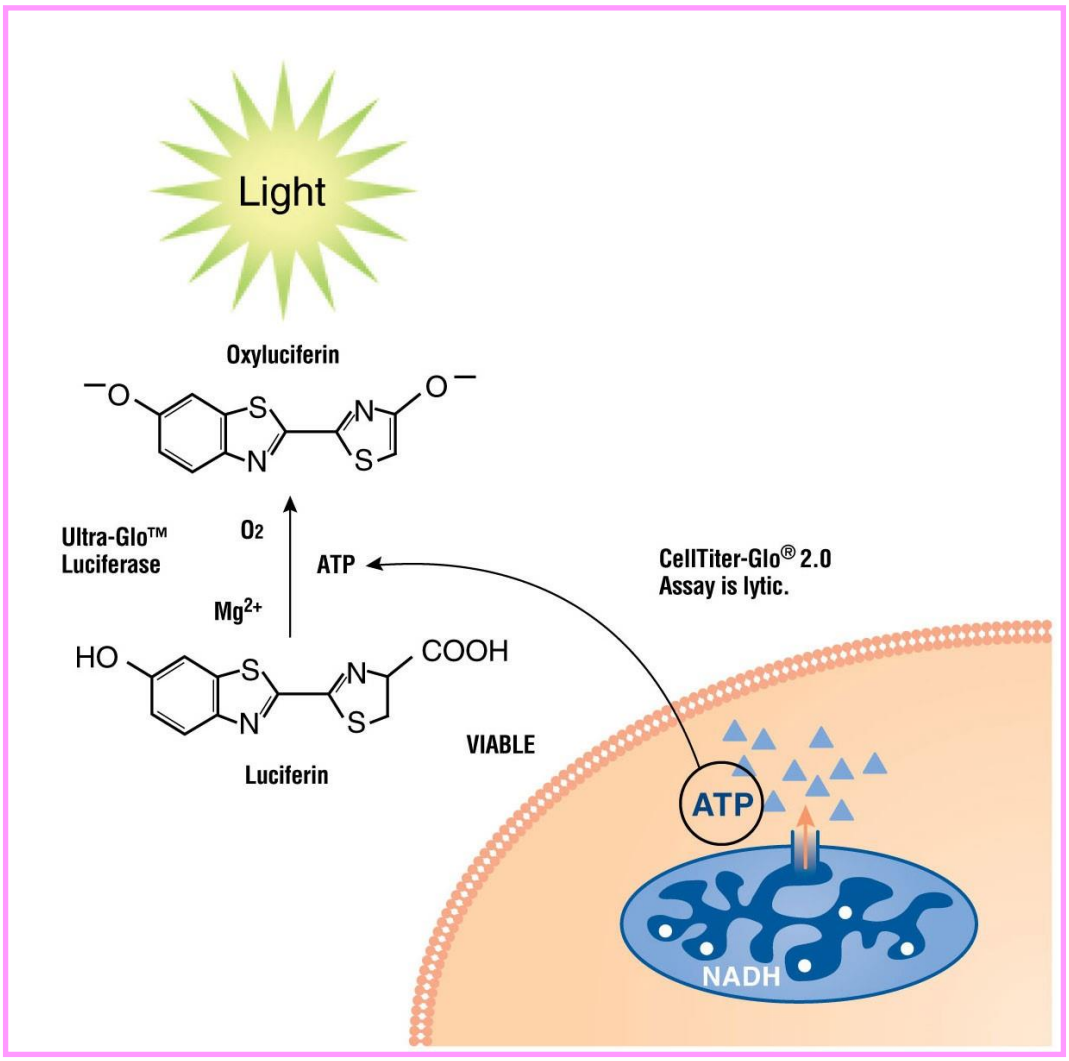

Figure 2. Mono-oxygenation of luciferin is catalysed by luciferase in the presence of Mg^{2+}, ATP and molecular oxygen.

2.7 Determination of antioxidant activity

PC12 HD-Q74 cells were seeded in 100 mm dishes at 2×10^6 cells/dish and incubated for 72 hours with DOX at 37°C in 5% CO_2 to obtain the expression of HTT exon 1 fragment. ESC [5 µM] was added during the last 24 hours of incubation with DOX. At the end of incubation, cells were counted to obtain 5×10^5 cells/mL suspension from each dish. Then 100 µL of the cell suspension and 100 µL of DCFH-DA [20 µg/mL]

were added to a black 96 well plate. After 30 min of incubation at room temperature, the reactive oxygen species (ROS) formation was measured (excitation at 485 nm and emission at 535 nm) using a VICTOR™ X3 multilabel plate reader. The values are expressed as arbitrary units of fluorescence (AUF).

2.8 Determination of intracellular glutathione levels

PC12 HD-Q74 cells were seeded in 100 mm dishes at 2×10^6 cells/dish and incubated for 72 hours with DOX at 37°C in 5% CO_2 to obtain the expression of HTT exon 1 fragment. ESC [5 µM] was added during the last 24 hours of incubation with DOX. At the end of incubation, cells were counted to obtain 5×10^5 cells/mL suspension from each dish. Then 100 µL of the cell suspension and 100 µL of MCB [100 µM] were added to a black 96 well plate. After 30 min of incubation at 37°C, GSH levels were measured (excitation at 355 nm and emission at 460 nm) using a VICTOR™ X3 multilabel plate reader. Values are expressed as arbitrary units of fluorescence (AUF).

2.9 Determination of nuclear Nrf2 levels

PC12 HD-Q74 cells were seeded in 100 mm dishes at 2×10^6 cells/dish and incubated for 72 hours with DOX at 37°C in 5% CO_2 to obtain the expression of HTT exon 1 fragment. ESC [5 µM] was added during the last 24 hours of incubation with DOX. At the end of incubation, nuclear extraction and determination of Nrf2 nuclear levels were performed using the Nuclear Extract Kit (Active Motif, Carlsbad, CA, USA) and the TransAM® Nrf2 Transcription Factor ELISA Kit (Active Motif), respectively.

The TransAM® Nrf2 Kit is composed of a 96 wells plate in which oligonucleotides containing ARE sequences (Nrf2 binding sites) are immobilized at the bottom of the wells. Active Nrf2 contained in the nuclear extracts binds specifically the ARE sequences. A specific antibody directed against Nrf2 and a secondary antibody conjugated to horseradish peroxidase (HRP) provides a sensitive colorimetric reaction that is easily quantified by spectrophotometry (Fig. 3).

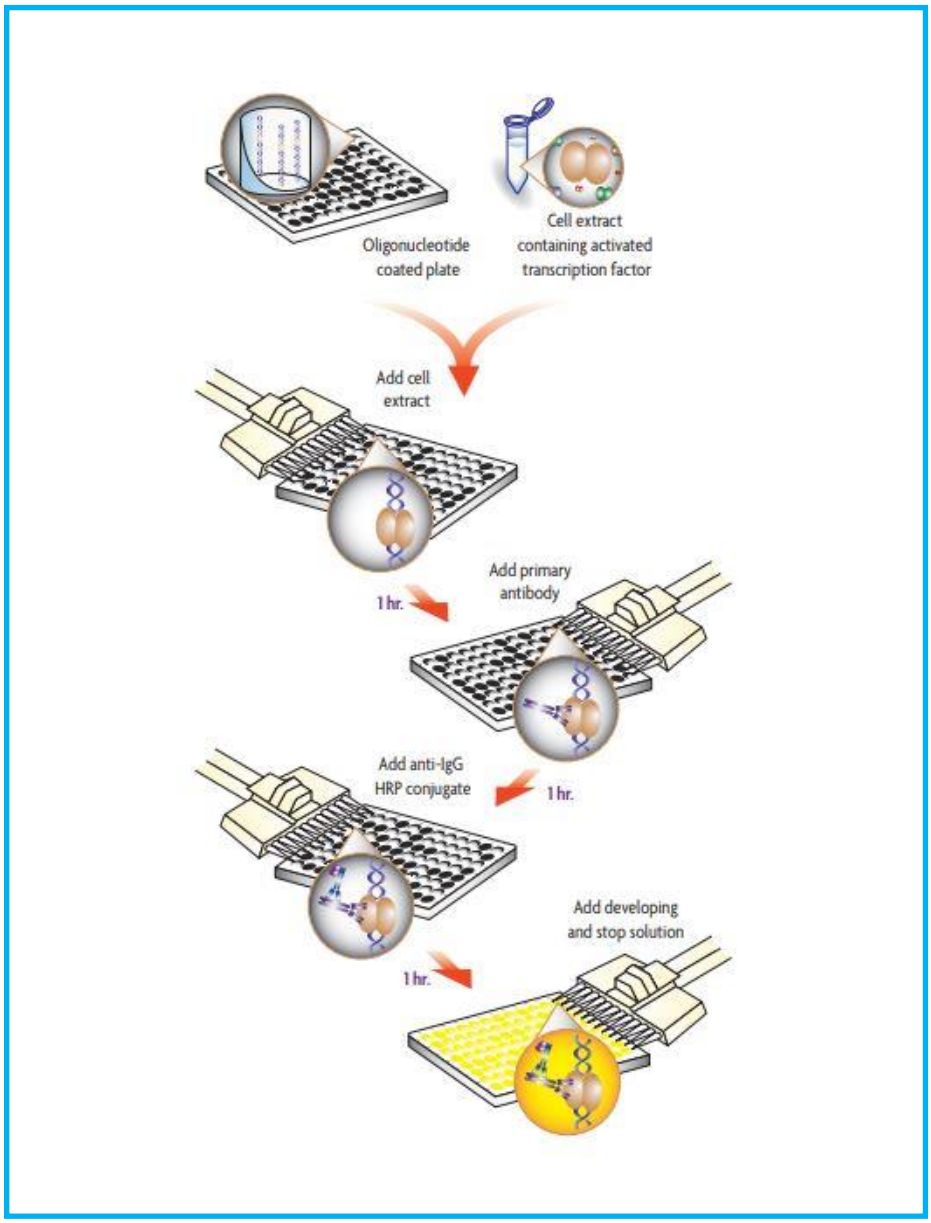

Figure 3. TransAM® Nrf2 ELISA-based assay.

2.10 RNA isolation and quantitative Real Time-PCR

PC12 HD-Q74 cells were seeded in 100 mm dishes at 2×10^6 cells/dish and incubated for 72 hours with DOX at 37°C in 5% CO_2 to obtain the expression of HTT exon 1 fragment. ESC [5 µM] was added during the last 24 hours of incubation with DOX. At the end of incubation, cells were centrifugated at 6000 rpm for 5 min at 4°C to obtain a pellet. RNA was isolated from the obtained pellet by using the PureLink® RNA Mini Kit (Life technologies, Carlsbad, CA, USA) (Fig. 4). Samples were lysed and homogenized in the presence of guanidinium isothiocyanate, a chaotropic salt capable of protecting the RNA from endogenous RNases. After homogenization, ethanol was added to the sample. The sample was then processed through a Spin Cartridge containing a clear silica-based membrane to which the RNA binds. The purified total RNA was eluted in RNase-free water and then quantified spectrometrically with the NanoVue Plus spectrophotometer (GE Healthcare, Chicago, Illinois, USA) for quantitative Real-Time PCR (qRT-PCR). Reverse transcription of RNA was performed using the SuperScript® VILO MasterMix (Invitrogen, Carlsbad, CA, USA). First-strand cDNA synthesis was performed with 1 µg of total RNA. The CFX Connect™ Real Time System (Bio-Rad, Hercules, CA, USA) was used for amplification and real time quantification. PCR reactions of each sample were performed in triplicate in a final volume of 20 µL in a 96-well plate. The PCR mixture contained 2 µL of cDNA [10 ng/µL], 10 µL of SYBR™ Select Master Mix (Invitrogen) and primers at a final concentration of 300 nM was amplified with the following conditions: initial denaturation at 95°C for 3 min, followed by 40 amplification cycles at 95°C for 3 sec

and 60°C for 30 sec. After the amplification reaction, melting curve analysis was performed starting at 65°C and increasing to 95°C with 5 acquisitions/°C. Relative normalized expression were calculated according to the $2^{-\Delta\Delta Cq}$ method with β-Actin and Ywhaz (Life technologies) as reference genes and uninduced cells (- DOX) as control. Primer sequences used in this study are listed in Table 1.

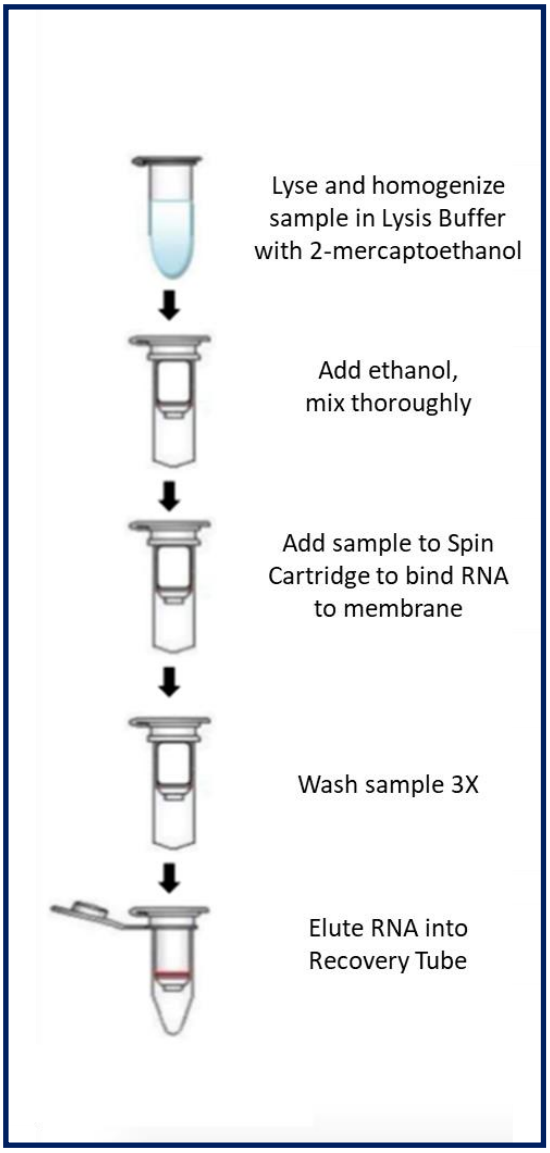

Figure 4. Illustration of the steps for isolating total RNA using the PureLink® RNA Mini Kit.

Gene name	**Forward/Reverse**	**5' to 3' Sequence**
β-Actin	For	CTGGCTCCTAGCACCATGA
	Rev	TAGAGCCACCAATCCACACA
Ywhaz	For	AAATGAGCTGGTGCAGAAGG
	Rev	GGCTGCCATGTCATCGTAT
NF-E2 related factor 2	For	TTCCTAGCAGAGCCCAGTG
	Rev	TCAGAGAGCGACTGACTAATGG
NAD(P)H dehydrogenase quinone 1	For	TCAGCGCTTGACACTACGAT
	Rev	CGTGGGCCAATACAATCAG
Glutathione S-transferase pi2	For	TGCTGGTCCACCAAGTCC
	Rev	GAGCCACATAGGCAGAGAGC
Catalase	For	AGCTTCAGCGCACCAGAG
	Rev	CATCTGCAGAGCACTGGCTA
Glutamate-cysteine ligase, catalytic subunit	For	AAGCCTCCTCCTCCAAACTC
	Rev	TACCTCCATTGGTCGGAACT
Heme oxygenase 1	For	TCAAGCACAGGGTGACAGAA
	Rev	CAGCTCCTCAAACAGCTCAA
Glutathione peroxidase 1	For	TCTGAATTCCCTCAAGTATGTCC
	Rev	CATTCACCTCGCACTTCTCA
Superoxide dismutase 1	For	GAGAGGCATGTTGGAGACCT
	Rev	ATGGACACATTGGCCACAC
Metallothionein 3	For	ATGCACGAACTGCAAGAAGA
	Rev	TTGGCACACTTCTCACATCC

Table 1. Primer sequences for quantitative RT-PCR.

2.11 *Drosophila melanogaster*

Flies were maintained in standard maize food at 25 °C in light/dark cycle of 12:12. The *elav*GAL4 [c155] fly stocks were obtained from the Bloomington Stock Center (Bloomington, IN, USA). The transgenic line expressing mutant HTT exon 1 fragment (HTT93Q) was kindly provided by prof. Flaviano Giorgini at the University of Leicester (United Kingdom). Crosses were set up between male flies carrying *elav*GAL4 driver and virgin females carrying the HTT93Q transgene. In the F1 generation only females expressed the HTT93Q, while males were used as controls (Fig. 5).

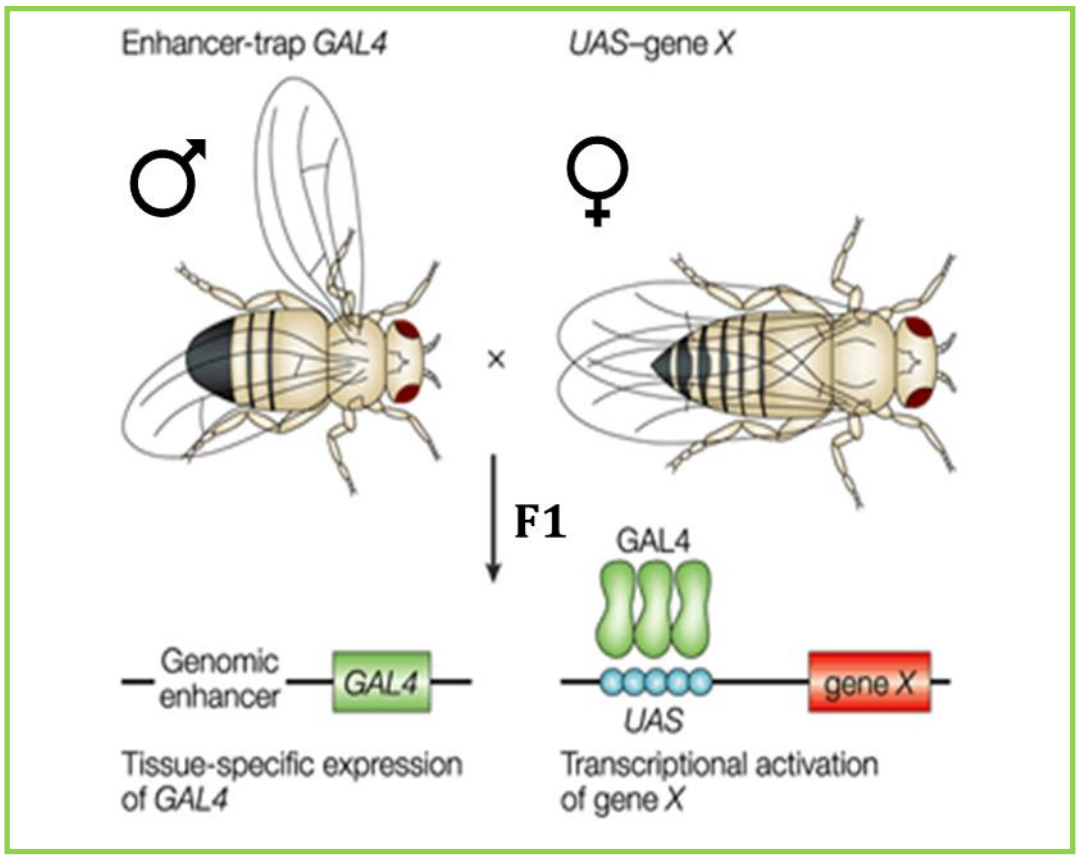

Figure 5. Binary *elav*GAL4/UAS system.

2.12 *Drosophila* compound feeding

For compound feeding experiments, maize food was heated until liquid and distributed into vials. ESC (Sigma Aldrich) was freshly prepared in DMSO as 1000 X stock and added to the food at 10 and 100 µM for growing experimental larvae or flies.

2.13 Pseudopupil analysis

This assay allows rapid visualization of rhabdomere arrangement in the ommatidia of the compound eye which is a direct measurement of the number of surviving photoreceptor neurons (Fig. 6). Appropriate crosses were carried out in order to obtain the desired genotype. Newly emerged HTT93Q exon 1 flies were transferred to vials containing normal or treated food, which was changed daily for 7 days. At day 7, flies were anaesthetized with CO_2, their heads removed and mounted face-up on microscope slides. A Nikon Optiphot-2 microscope at 50 X magnification was used for counting rhabdomeres from approximately 100 ommatidia per fly and 12 flies per treatment. Pseudopupil assay was performed also at day 0. Appropriate crosses were carried out directly into vials containing normal and treated food. At the day of emergence from pupal case, HTT93Q exon 1 flies were anaesthetized with CO_2 and their heads removed. The decapitated head was mounted on a microscope slide and the eyes analysed under Nikon Optiphot-2 microscope with 50 X oil objective.

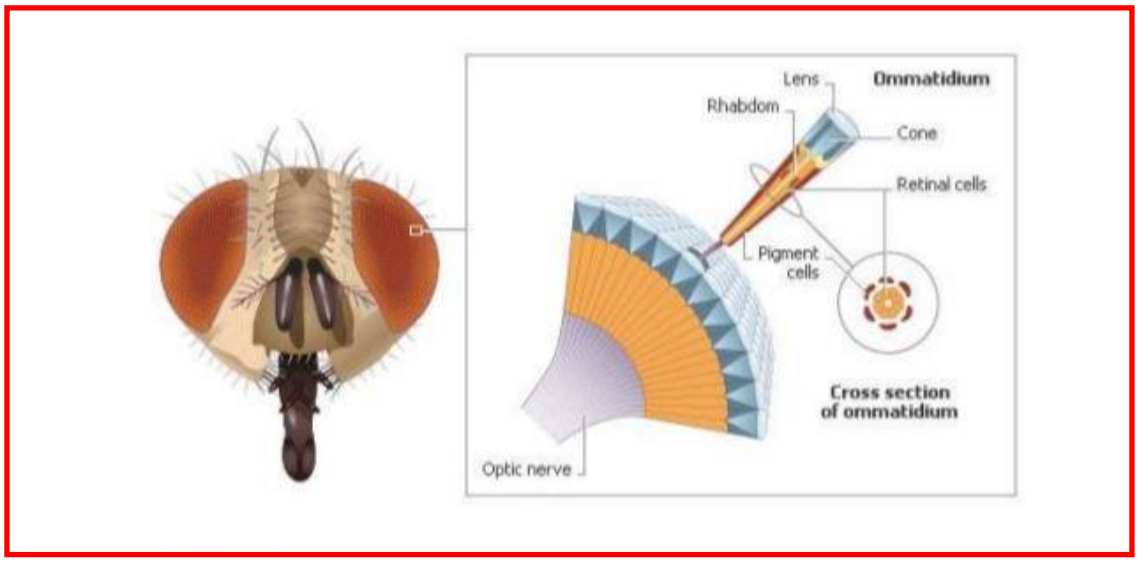

Figure 6. Structure of the *Drosophila* compound eye.

2.14 Eclosion analysis

Males carrying the sex-linked *elav*GAL4 driver were crossed to virgin females homozygous for the UAS-HTT93Q transgene generating experimental females and control males in the F1 generation. Parental flies were removed 5 days after mating. Flies were allowed to lay eggs on vials containing normal or treated food. The number of adult females and males emerging from the pupal case in each vial was counted every day for 10 days (Fig. 7). Eclosion percent was determined by the following calculation: (number of female flies / number of male flies) × 100.

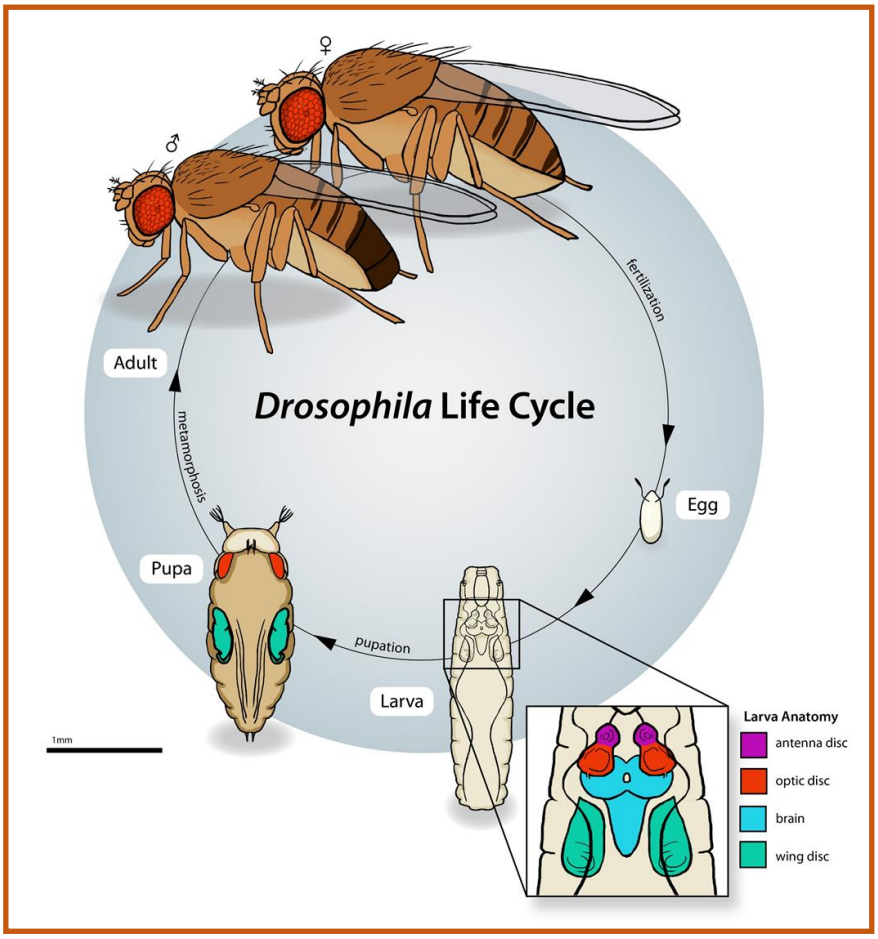

Figure 7. *Drosophila* life cycle

2.15 Longevity analysis

Virgin females of the desired genotype were collected and kept in groups of 10 in separate vials containing normal or treated food. Vials were inspected and changed every day. The number of flies remaining alive was scored. Data are expressed as percent survival.

2.16 Statistical analysis

Data are reported as mean ± SEM. Statistical analysis was performed using one-way ANOVA with Dunnett or Bonferroni or Newman-Keuls post hoc test. Differences were considered significant at $p < 0.05$. Analyses were performed using PRISM 5 software (GraphPad Software, La Jolla, CA, USA).

3. Results

3.1 Neurotoxicity induced by HTT exon 1 expression in PC12 HD-Q74 cells

It has been shown that the PC12 HD-Q74 cell line with 74 glutamine repeats exhibits many of the features of HD including the formation of aggregates with an EM structure similar to those observed *in vivo*, reduced neurite outgrowth and moderate caspase dependent cell death. In particular, we observed that the expression of expanded repeats (Q74) leads to a time-dependent reduction of cell proliferation, an increase of necrosis and aggregation of insoluble mutant HTT protein. After 72 hours of induction with DOX, cell proliferation in terms of cytostatic effect and necrosis were assessed using the dye eosin. The treatment with DOX decreased significantly the number of total cells and increased the necrosis at 72 hours (Fig. 8A-B). Further, after 72 hours of induction we observed insoluble aggregates produced by HD-Q74 cells that were localized both in the cytoplasm and nucleus. The amount of insoluble aggregates of mutant HTT protein was detected by using a VICTOR™ X3 multilabel plate reader (Fig. 8C). Aggregates appeared as bright enhanced green fluorescent protein (EGFP) signals when analysed by fluorescence microscopy. Uninduced HD-Q74 cells showed a uniformly distributed EGFP with a lower fluorescence intensity (Fig. 8D).

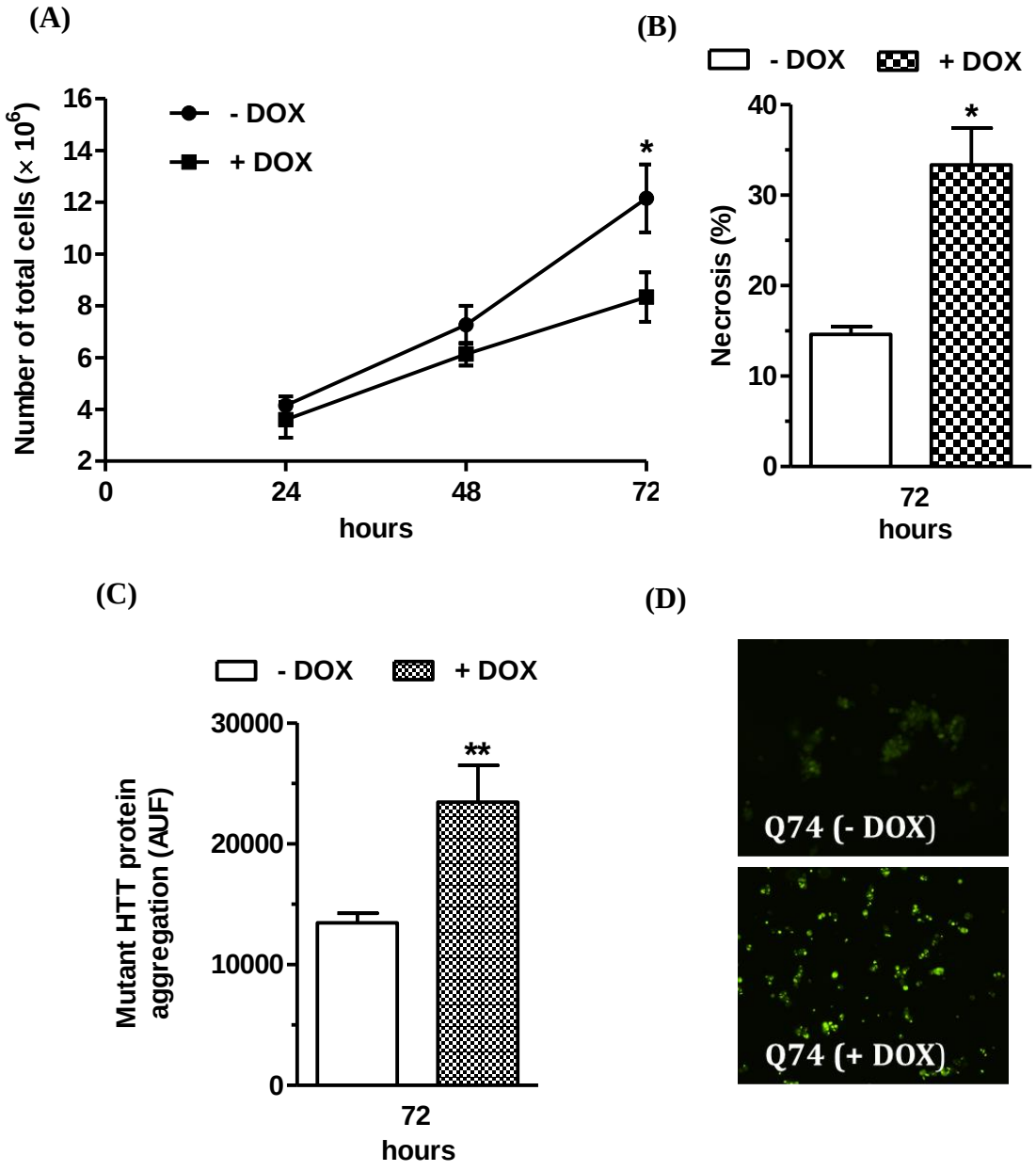

Figure 8. Expression of HTT exon 1 fragment containing 74 glutamines leads to time-dependent neurotoxicity in PC12 HD-Q74 cells. (A) Cells were treated with DOX [1 µg/mL] for different times (24, 48 and 72 hours) and cell proliferation was assessed by using eosin as described in the materials and methods section. Values are expressed as number of total cells. (B) Cells were treated with DOX [1 µg/mL] for 72 hours and the necrosis was evaluated by using eosin as described in the materials and methods section. Values are expressed as percentages of necrosis. (C) Cells were treated with DOX [1 µg/mL] for 72 hours and mutant HTT protein aggregation was assessed as described in the materials and methods section. Values are expressed as arbitrary units

of fluorescence (AUF). (D) Representative images of visible Q74 aggregates fused to EGFP. Data are reported as mean ± SEM of at least three independent experiments (*p<0.05 and **p<0.01 versus - DOX at one-way ANOVA with Dunnett post hoc test).

3.2 Neurotoxicity of ESC in PC12 HD-Q74 cells

In the first part of the experiments, we determined the neurotoxicity of ESC in PC12 HD-Q74 cell line by using the MTT assay. After 24 hours of treatment with different concentrations of ESC [2.5 - 10 µM] we observed that concentrations up to 5 µM did not affect neuronal viability (Fig. 9). Therefore, we selected the concentration of 5 µM for all the following experiments.

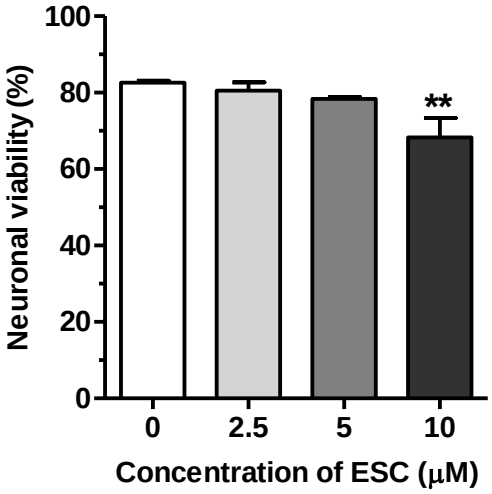

Figure 9. Neurotoxicity of ESC in PC12 HD-Q74 cells. Cells were incubated for 24 hours with different concentrations of ESC [2.5 – 10 µM]. At the end of incubation, the neuronal viability was measured using MTT assay as described in the materials and methods section. MTT values are expressed as percentages of neuronal viability. Data are reported as mean ± SEM of at least three independent experiments (**p<0.01 versus untreated cells at one-way ANOVA with Dunnett post hoc test).

3.3 Effects of ESC on mutant HTT protein aggregation

Mutant HTT protein aggregation is an important early and upstream process in the development of HD. Therefore, we decided to investigate whether ESC could modulate mutant HTT protein aggregation in HD-Q74 cells. ESC [5 µM] was added to the last 24 hours of treatment with DOX and at the end of incubation the fluorescence of EGFP-tagged HTT74Q aggregates in PC12 cell line model was quantified by using a VICTOR™ X3 multilabel plate reader. The measure based upon EGFP signal recorded the capacity of ESC to partially modulate mutant HTT protein aggregates formation (Fig. 10).

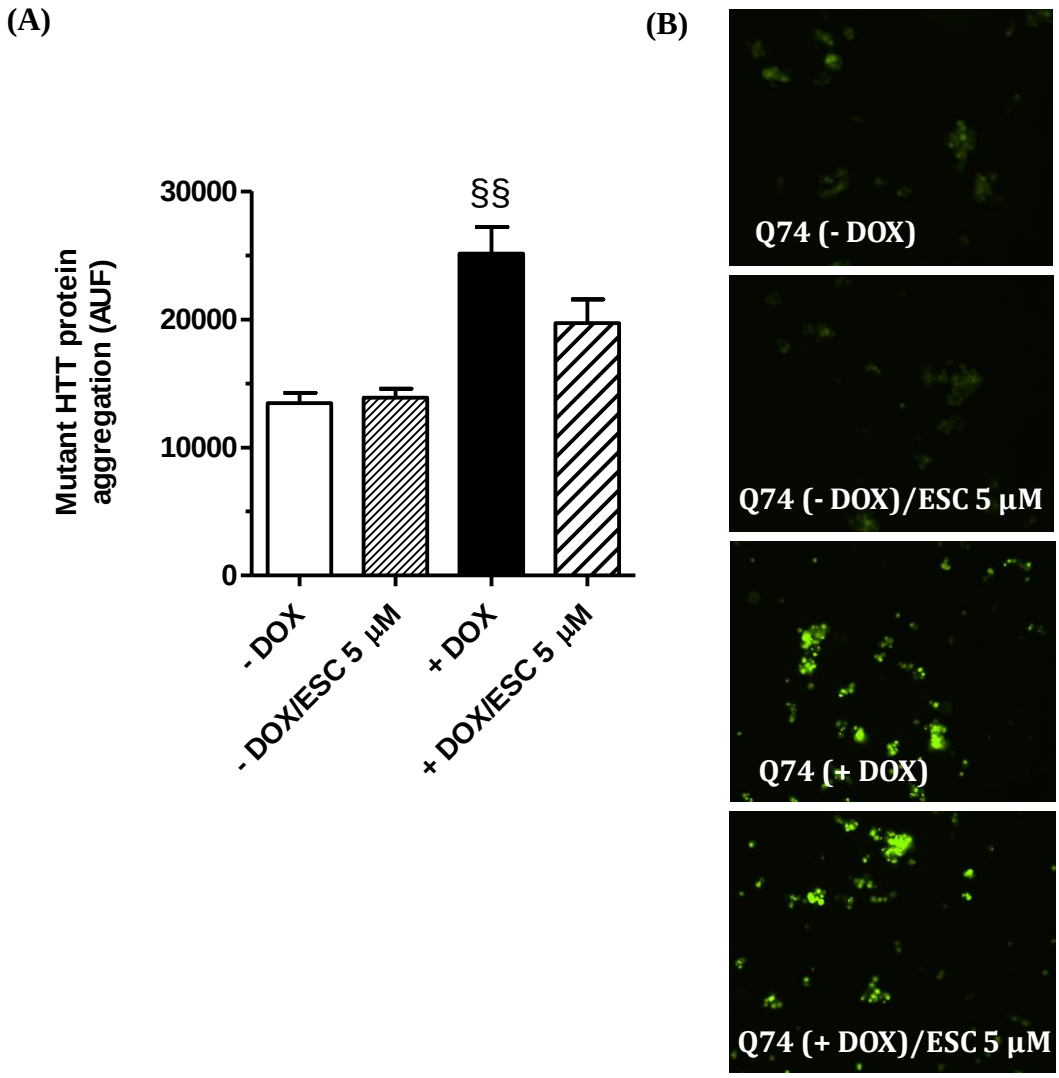

Figure 10. ESC partially modulates HTT74Q aggregation in PC12 HD-Q74 cell line. (A) Cells were incubated with DOX [1 µg/mL] for 72 hours and treated for 24 hours with ESC [5 µM]. The fluorescence of EGFP-tagged HTT74Q aggregates was measured by using a multilabel plate reader as described in the materials and methods section. (B) Representative images of HTT74Q aggregates in induced and uninduced PC12 HD-Q74 cells. Values are expressed as arbitrary units of fluorescence (AUF). Data are reported as mean ± SEM of at least three independent experiments ($^{§§}p<0.01$ versus - DOX at one-way ANOVA with Bonferroni post hoc test).

3.4 Neuroprotective effects of ESC in PC12 HD-Q74 cells

Further, we investigated the ability of ESC to counteract the reduced cell proliferation in terms of cytostatic effects and the necrosis induced by the expression of mutant HTT exon 1 fragment with 74 glutamines. PC12 HD-Q74 cells were induced by 72 hours of treatment with DOX [1 µg/mL] and ESC [5 µM] was added to the last 24 hours of incubation with DOX. The treatment with ESC showed to counteract significantly both the cytostatic effect and the necrosis induced by HTT74Q expression (Fig. 11A-B). Further, low magnification TEM images of uninduced PC12 HD-Q74 cells showed the presence of a few necrotic cells characterized by a pyknotic nuclear chromatin and highly degraded cytoplasm. After the induction with DOX, the number of PC12 HD-Q74 necrotic cells clearly increased, while it decreased in PC12 HD-Q74 cells treated with both DOX and ESC (Fig. 11C).

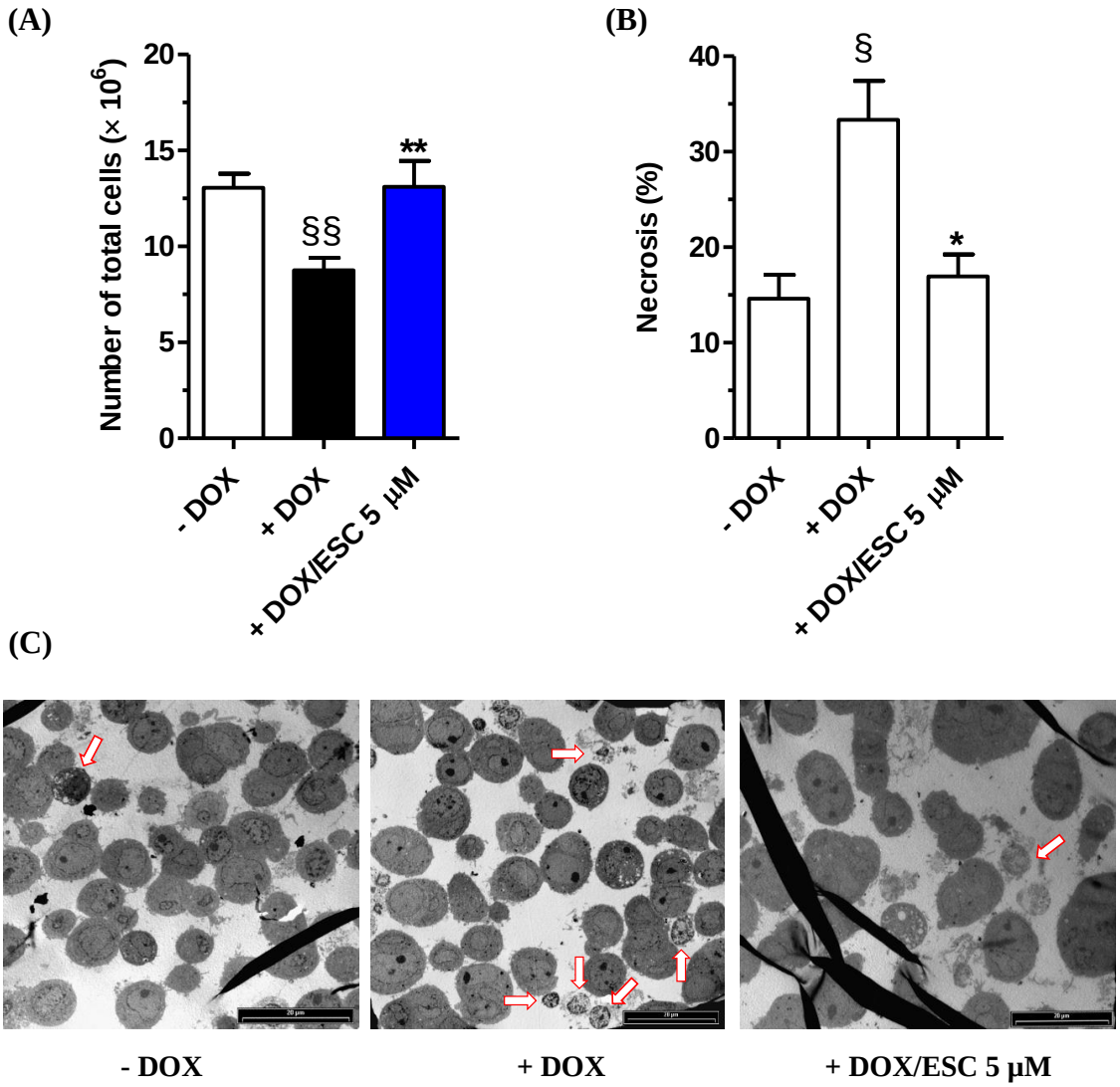

Figure 11. ESC counteracts the cytostatic effect and the necrosis induced by HTT74Q expression in PC12 HD-Q74 cells. Cells were incubated with DOX [1 µg/mL] for 72 hours and treated with ESC [5 µM] for 24 hours. Cell proliferation in terms of cytostatic effect (A) and necrosis (B) were assessed by using the dye eosin as described in the materials and methods section. Values are expressed as number of total cells and percent necrosis. (C) Representative low magnification TEM images showing the presence of necrotic (arrow) and living cells in uninduced PC12 HD-Q74 cells, in induced PC12 HD-Q74 cells and in induced PC12 HD-Q74 cells treated with ESC (scale bar: 20 µm). Data are reported as mean ± SEM of at least three independent experiments ($^{\S}p<0.05$ and $^{\S\S}p<0.01$ versus - DOX; *$p<0.05$ and **$p<0.01$ versus + DOX at one-way ANOVA with Bonferroni post hoc test).

3.5 Antioxidant effects of ESC in PC12 HD-Q74 cells

Oxidative stress due to imbalance in oxidant and antioxidant species has been known to play a crucial role in the pathophysiology of neurodegenerative diseases, including HD. The ability of ESC to counteract the oxidative damage elicited by HTT74Q expression was evaluated by using the fluorescent probe DCFH-DA. After 24 hours of treatment with ESC [5 µM] we recorded a significant reduction of ROS formation in induced PC12 HD-Q74 cells (Fig. 12A). In parallel, the same treatment with ESC showed to increase intracellular GSH levels and restore nuclear Nrf2 basal levels as the result of a protective mechanism in PC12 HD-Q74 cells expressing EGFP-tagged HTT74Q (Fig. 12B-C). Recent combined micro array studies provide ample evidence for the induction of a protective oxidative stress response in cells expressing mutant HTT. Strikingly, ESC showed the ability to strengthen this protective response in induced PC12 HD-Q74 cells through activation of the Nrf2/ARE pathway.

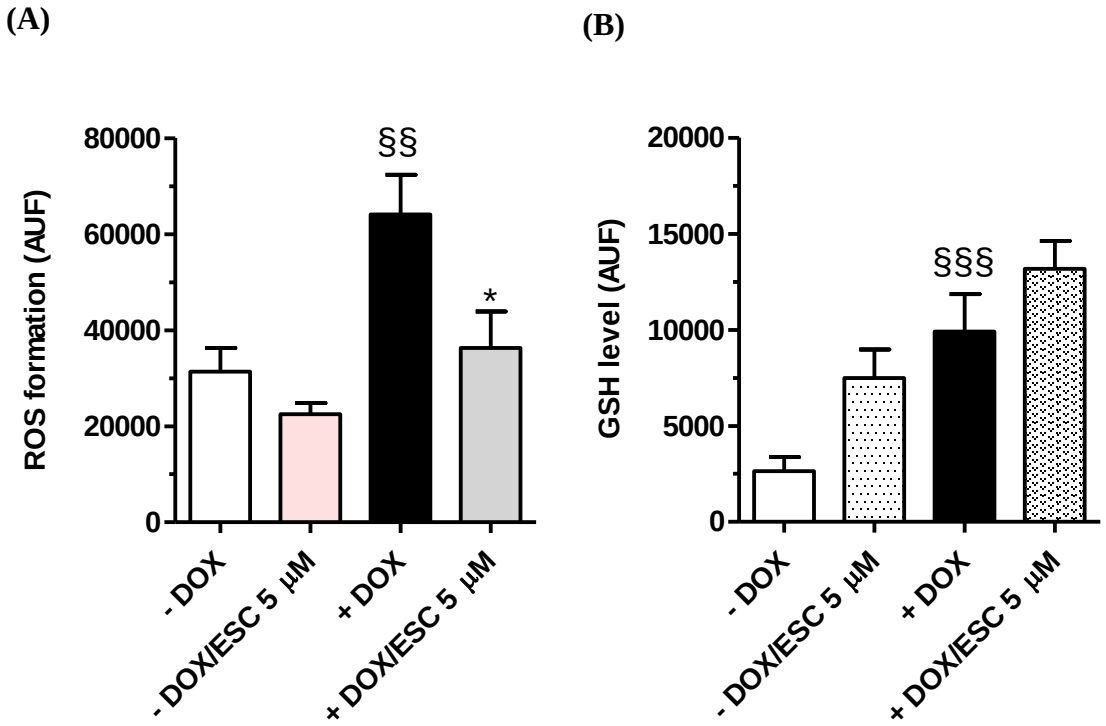

(C)

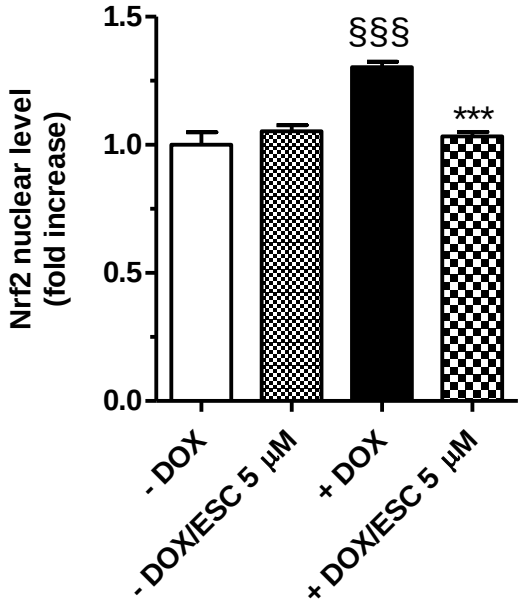

Figure 12. ESC decreases the oxidative stress elicited by HTT74Q expression in PC12 HD-Q74 cells. Cells were induced with DOX [1 µg/mL] for 72 hours and treated with ESC [5 µM] for 24 hours. At the end of incubation, the ROS formation (A), the intracellular GSH levels (B) and the nuclear Nrf2 levels (C) were evaluated as described in the materials and methods section. Values are expressed as arbitrary units of fluorescence (AUF) and fold increases, respectively. Data are reported as mean ± SEM of at least three independent experiments ($^{§§}p<0.01$ and $^{§§§}p<0.001$ versus - DOX; *p<0.05 and ***p<0.001 versus + DOX at one-way ANOVA with Bonferroni post hoc test).

3.6 Effects of ESC on mitochondrial activity in PC12 HD-Q74 cells

Disruption of mitochondrial homeostasis and subsequent mitochondrial dysfunction play a key role in the pathophysiology of HD. The potential cytoprotective effects of ESC against the mitochondrial dysfunction evoked by HTT74Q expression were

investigated. The induction with DOX did not modify the mitochondrial number per viable cell (Fig. 13A) while it increased the mitochondrial size in terms of area occupied by each mitochondrion in the cytoplasm (Fig. 13B) as well as the amount of ATP per viable cell (Fig. 13C). The expansion of mitochondrial area and the increase of ATP levels could be associated with the mitochondrial dysfunction observed in HD. The treatment with ESC did not change the number of mitochondria per cell in induced PC12 HD-Q74 cells (Fig. 13A), but it decreased significantly the mitochondrial size as well as the amount of ATP (Fig. 13B-C). To better characterize these results, PC12 HD-Q74 cells were analysed by TEM. TEM images of uninduced PC12 cells showed well preserved round shape morphology, both in nuclear and cytoplasmic components (Fig. 14A). At higher magnification, several tubular mitochondria were detected with dense cristae clearly observed (Fig. 14A, insert). In induced PC12 cells a preserved cell morphology was observed in low magnification images (Fig. 14B). On the contrary, the cytoplasm showed several, small and round shape mitochondria, with less dense matrix and swollen cristae (Fig. 14B, insert). Induced PC12 cells treated with ESC [5 µM] for 24 hours showed a regular round shape morphology (Fig. 14C) and tubular mitochondria with dense matrix and regular cristae (Fig. 14C, insert).

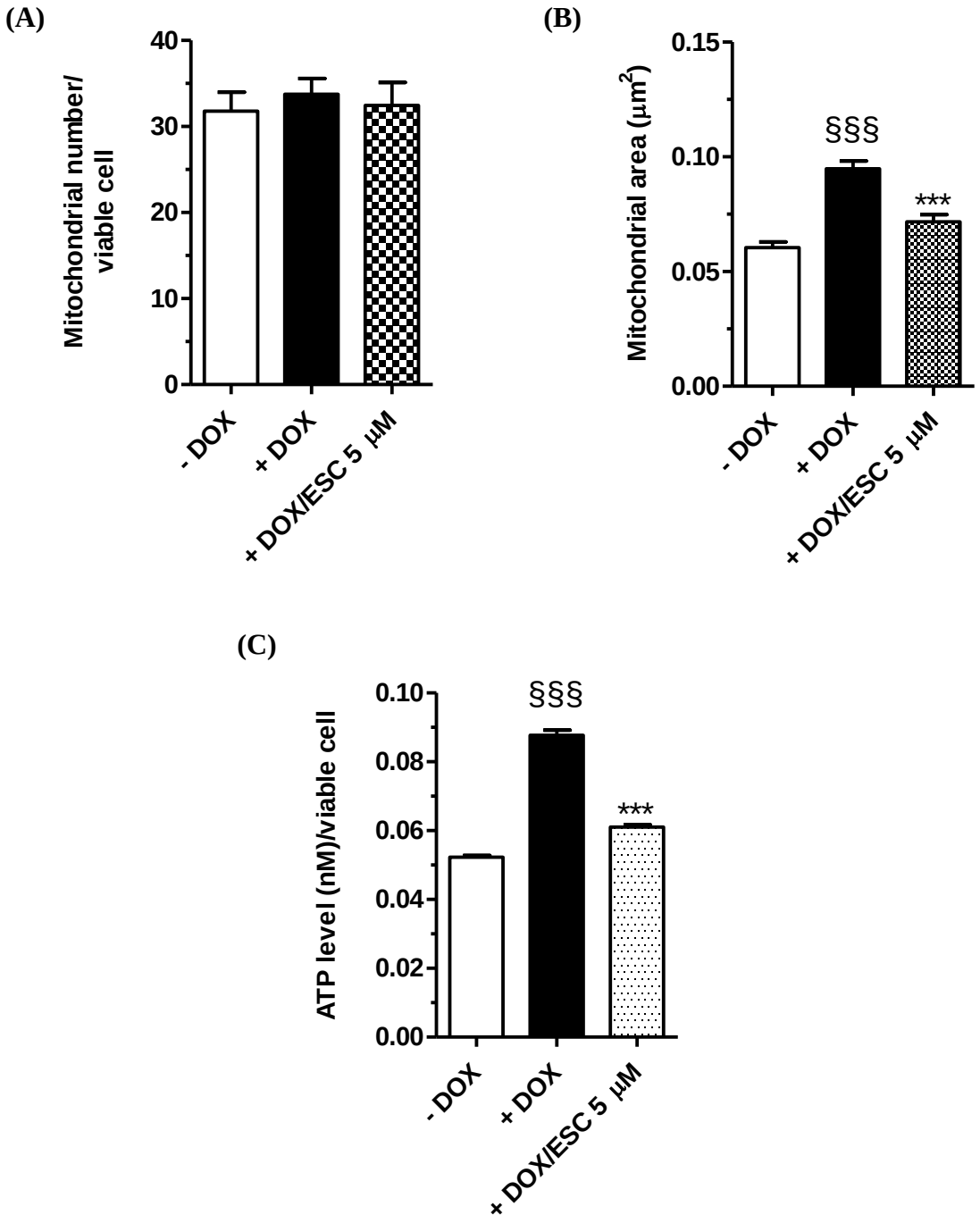

Figure 13. Effects of ESC on mitochondrial activity in PC12 HD-Q74 cells. Cells were induced with DOX [1 µg/mL] for 72 hours and treated with ESC [5 µM] for 24 hours. At the end of incubation, the number of mitochondria per viable cell (A), the mitochondrial area (B) and ATP levels per viable cell (C) were assessed as described in the materials and methods section. Values are expressed as mitochondrial number per viable cell, mitochondrial area measured in μm^2 and ATP levels expressed in nM per

viable cell, respectively. Data are reported as mean ± SEM of at least three independent experiments ($^{§§§}p<0.001$ versus - DOX; ***$p<0.001$ versus + DOX at one-way ANOVA with Bonferroni post hoc test).

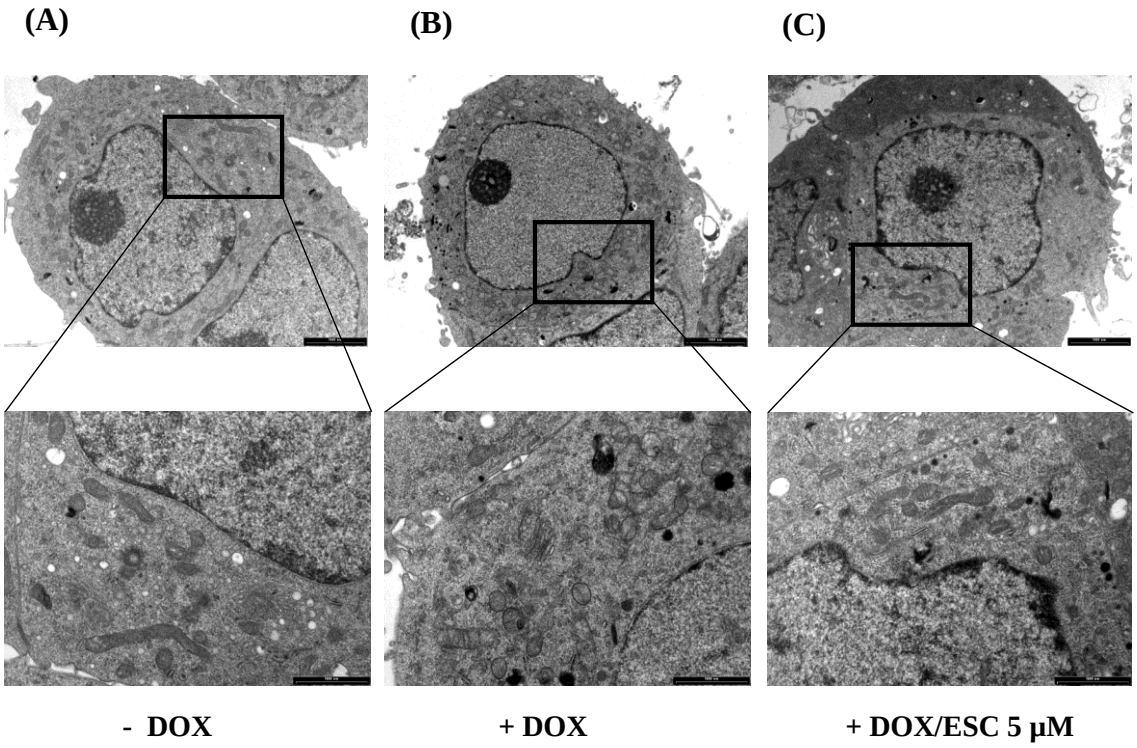

Figure 14. Morphological analysis of mitochondria in PC12 HD-Q74 cells. (A) Ultrastructural TEM images of uninduced PC12 HD-Q74 cells (scale bar: 2000 nm). Detail of mitochondria showing a tubular shape with dense matrix and regular cristae (insert; scale bar: 1000 nm). (B) Ultrastructural TEM image of induced PC12 HD-Q74 cells (scale bar: 2000 nm). Several mitochondria with round shape morphology, extracted matrix and swollen cristae are observed (insert; scale bar: 1000 nm). (C) Ultrastructural TEM image of induced PC12 HD-Q74 cells treated with ESC [5 µM] (scale bar: 2000 nm). Mitochondria show a tubular shape, with dense matrix and regular cristae (insert; scale bar: 1000 nm).

3.7 Effects of ESC on Nrf2-responsive genes and oxidative stress related genes in PC12 HD-Q74 cells

At the transcriptional level, ESC did not show the ability to modify the protective response induced by HTT74Q expression in PC12 HD-Q74 (Fig. 15).

(A)

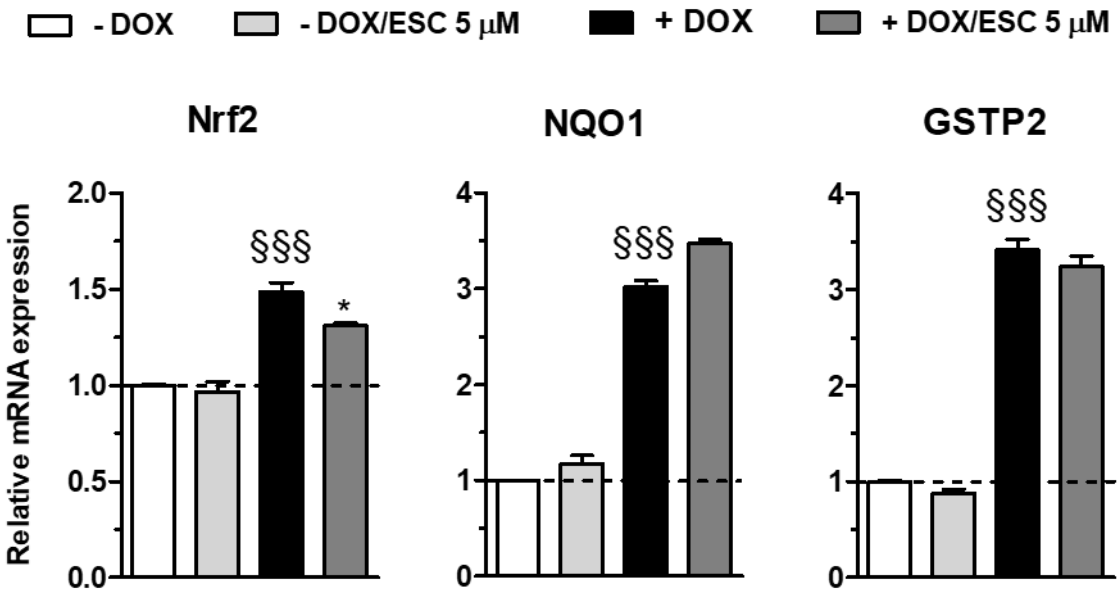

(B)

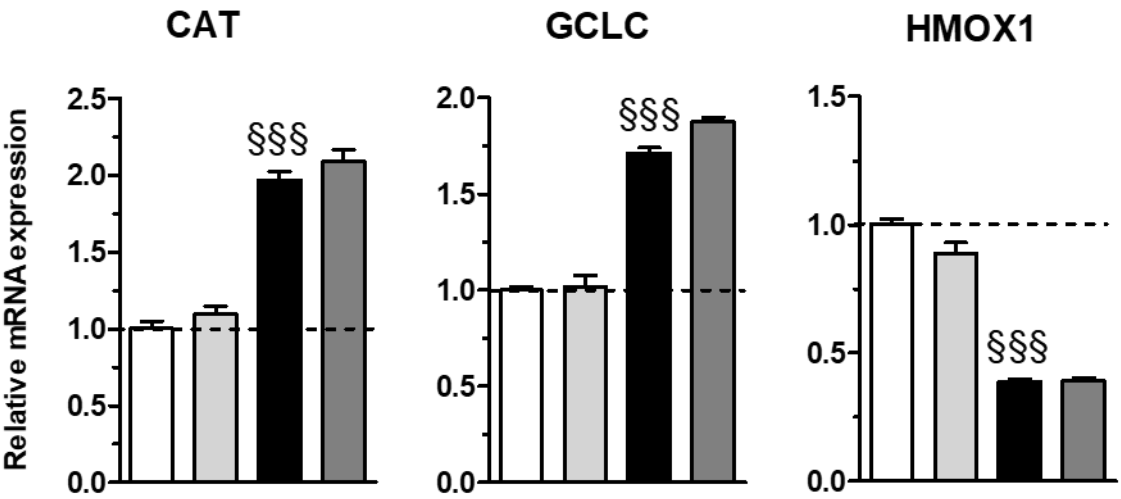

(C)

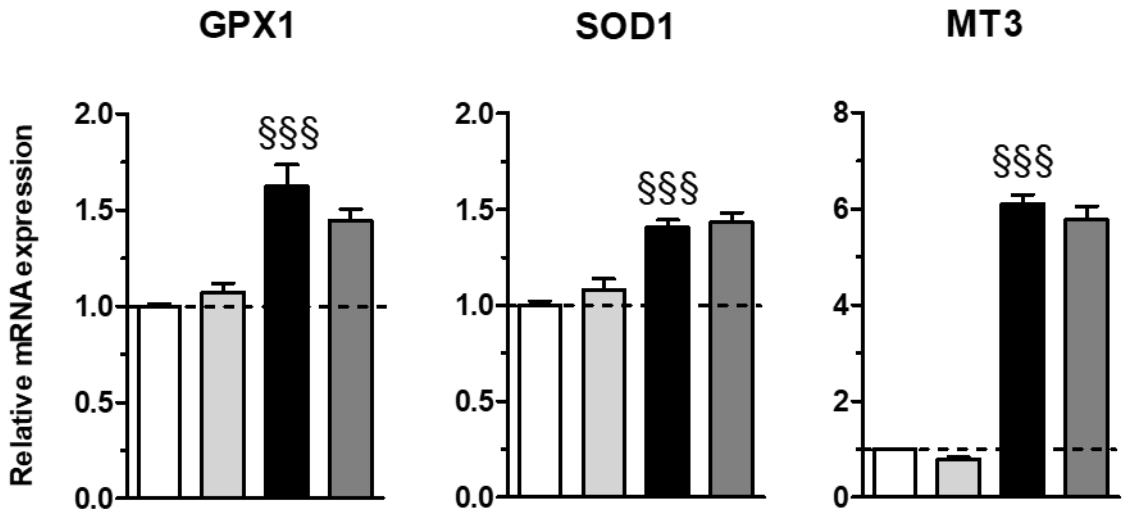

Figure 15. ESC doesn't modulate the protective response induced by HTT74Q expression in PC12 HD-Q74 cells. Cells were induced with DOX [1 µg/mL] for 72 hours and treated with ESC [5 µM] for 24 hours. Nrf2-responsive genes and oxidative stress related genes were examined by quantitative real time PCR as described in the materials and methods section. Values are expressed as relative mRNA levels compared to expression levels of uninduced cells (- DOX) with β-Actin and Ywhaz as reference genes. **(A)** Nrf2 and Nrf2-responsive genes involved in detoxification. Nrf2: NF-E2 related factor 2, NQO1: NAD(P)H dehydrogenase quinone 1, GSTP2: glutathione S-transferase pi2. **(B)** Nrf2-responsive genes involved in antioxidant/reducing potential. CAT: catalase, GCLC: the catalytic subunit of glutamate – cysteine ligase, HMOX1: heme oxygenase 1. **(C)** Non-Nrf2 responsive genes involved in protection against oxidative stress. GPX1: glutathione peroxidase 1, SOD1: superoxide dismutase 1, MT3: metallothionein 3. Data are expressed as relative mRNA expression and reported as mean ± SEM of at least three independent experiments ($^{§§§}p<0.001$ versus - DOX; *$p<0.05$ versus + DOX at one-way ANOVA with Bonferroni post hoc test).

3.8 ESC ameliorates photoreceptor neurodegeneration in mutant HTT expressing fruit fly

Driven by these interesting results, we decided to further explore the neuroprotective effects of ESC using fruit flies expressing a mutant HTT fragment. We employed a widely studied fruit fly model of mutant HTT toxicity, in which the human mutant HTT exon 1 fragment (HTT93Q) is expressed under control of the *elav*GAL4 pan-neuronal driver using the binary GAL4/UAS system. These flies exhibit several phenotypes that recapitulate HD symptoms, including neurodegeneration, locomotor impairments, and reduced lifespan. Neurodegeneration can be easily assessed by scoring the number of photoreceptor neurons, known as rhabdomeres, present in the fly eye. The compound eyes of *Drosophila* contain repeating units of ommatidia. Each ommatidia contains eight rhabdomeres, seven of which are visible by using the pseudopupil assay. At day 7 post-eclosion, wild type (WT) flies exhibit an average of 7 rhabdomeres while HTT93Q-expressing flies present an average of 5 rhabdomeres (Fig. 16A). Rhabdomere quantification was assessed during development (day 0) and after disease progression (day 7 post-eclosion). ESC significantly ameliorates rhabdomere neurodegeneration in pathogenetic HTT93Q flies, when administered during larval stage (at the time of the disease onset) or during adult period (when the disease has progressed). In particular, ESC reduces significantly the neurodegeneration in HTT93Q exon 1 flies at 100 μM when administered during larval instar and ameliorates degeneration at all concentrations tested when administered only during adult period (Fig. 16B). These results indicate that ESC confers neuroprotection in HTT93Q exon 1 fruit flies and provide support for our findings in *in vitro* cell line HD model.

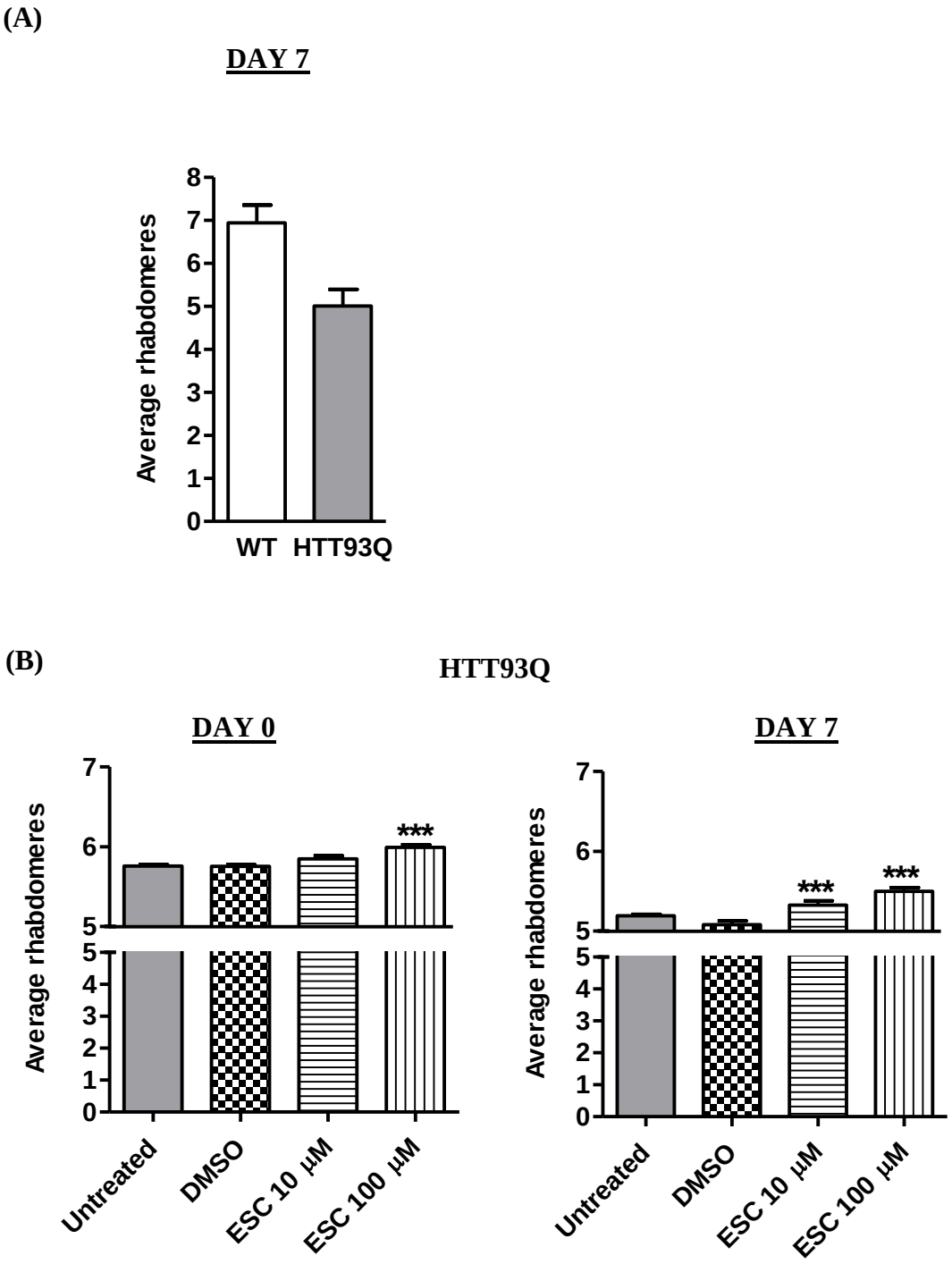

Figure 16. ESC ameliorates rhabdomere neurodegeneration in pathogenetic HTT93Q flies. (A) Rhabdomeres in WT and HTT93Q flies at day 7 post eclosion. (B) *Drosophila* expressing HTT93Q exon 1 pan-neuronally were exposed to ESC in their food at different concentrations during development and adult period. Rhabdomeres were scored via the pseudopupil assay at day 0 and at day 7 post eclosion as described

in the materials and methods section. Data are expressed as mean rhabdomere count per ommatidium ± SEM (n = 12 per condition) (***$p < 0.001$ versus HTT93Q flies treated with DMSO at one-way ANOVA with Newman-Keuls post hoc test).

3.9 ESC feeding rescues HTT93Q-dependent eclosion defects

HTT93Q flies exhibit a variety of HD-relevant phenotypes including impaired emergence of the adult fly from the pupal case (eclosion). HTT93Q flies show a progressive degenerative phenotype characterized by a 70% of larvae lethality. WT flies did not present defects in eclosion (Fig. 17A). Male flies carrying the *elav*GAL4 driver were crossed to virgin females carrying the UAS-HTT93Q transgene in order to generate females expressing HTT93Q and control males in the F1 generation. 10–35 crosses were set up in separate vials for each condition and parental flies were removed 5 days after mating. The number of female or male progeny emerging was scored over 10 days post-eclosion. We observed that the low level of emergence of adult HD flies from the pupal case was enhanced by feeding of ESC in a dose dependent manner (Fig. 17B). These data suggest that ESC exerts neuroprotective effects ameliorating HTT93Q-dependent eclosion defects.

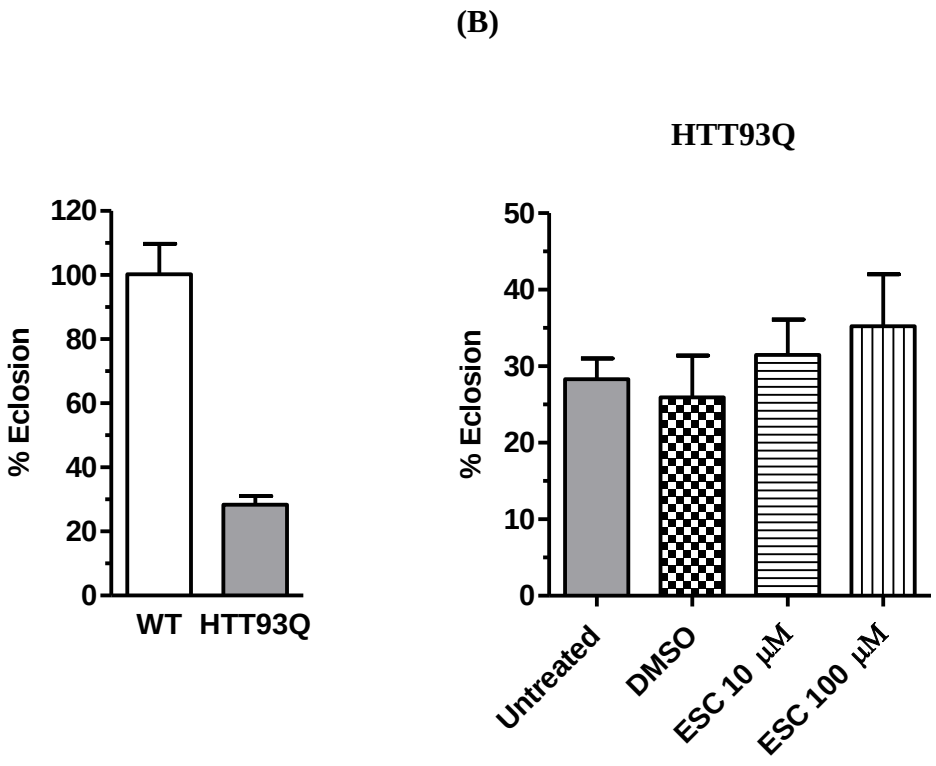

Figure 17. ESC rescues HTT93Q-dependent eclosion impairments. (A) Eclosion in WT and HTT93Q flies. (B) Crosses were set up in food containing 10 and 100 μM ESC. The number of adult females and males emerging from the pupal case was scored by using eclosion analysis as described in the materials and methods section. Data are expressed as mean ± SEM (n = 100 per condition).

3.10 ESC enhances the reduced longevity in HTT93Q flies

Further we decided to investigate the ability of ESC to ameliorate the reduced survival time in HTT93Q adult flies. The expression of the human mutant HTT exon 1 fragment 93Q leads to a reduced life span compared with control flies, whose maximum longevity is 3 months (Fig. 18A). For longevity assay, newly emerged female flies of the desired genotype were collected and kept in groups of 10 in separate vials. Flies were moved to fresh food every day and the number of dead individuals scored daily.

We observed a small but interesting improvement in the shortening of median life span in HD flies fed with 10 µM ESC (Fig. 18B).

(A)

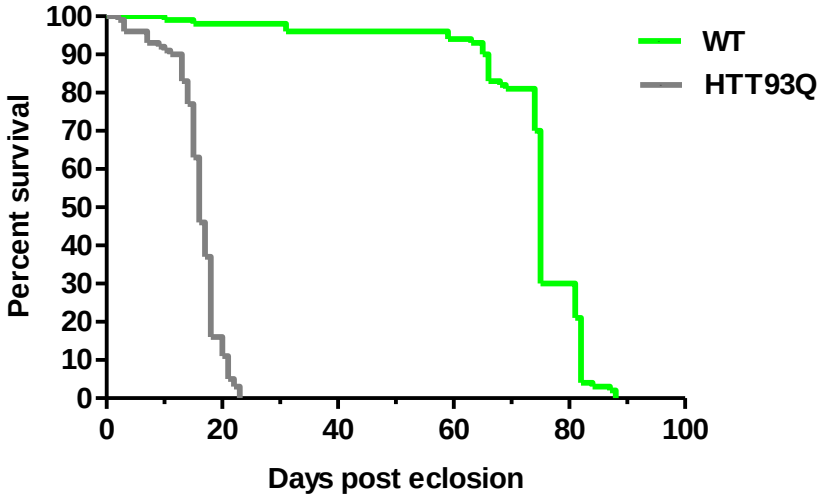

(B)

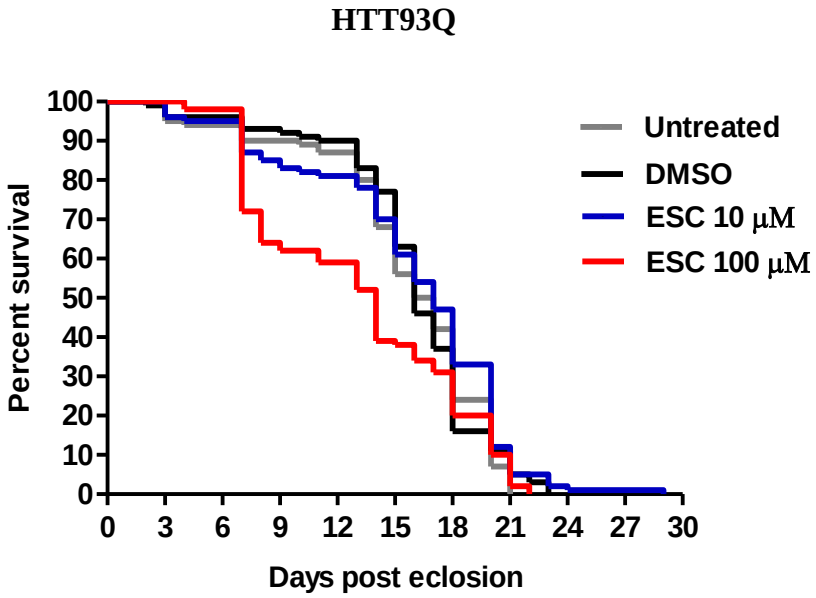

Figure 18. ESC enhances average life span of HD flies. (A) Longevity in WT and HTT93Q flies. (B) Appropriate crosses were carried out to obtain the desired genotype and ESC was mixed in fly food at different concentrations for growing adult flies as described in the materials and methods section. Data are expressed as mean ± SEM (n = 100 per condition).

4. Discussion

Huntington's disease (HD) is a progressive autosomal dominant neurodegenerative disorder characterized by a CAG trinucleotide repeat expansion in the coding region of the HTT gene. The neuropathology of HD involves a selective dysfunction and death of specific neuronal subpopulation within the central nervous system. The most striking neuropathological change in HD is the early atrophy of the striatum. While disease progresses, other brain structures also degenerate, including the cerebral cortex. The HTT gene provides instruction for making a protein called huntingtin. Although the function of this protein is not clear, it seems to play an important role in neuronal cell survival by controlling apoptosis pathways, regulating intracellular transport machinery, vesicle trafficking and secretion. In healthy individuals, the CAG segment is repeated 4 to 36 times within the gene. In individuals affected by HD, the CAG segment is repeated 37 to more than 120 times. An increase in the size of the CAG segment leads to the production of an abnormally expanded version of the HTT protein. The mutant protein is cut into smaller toxic fragments that bind together and accumulate into cytoplasmic and nuclear aggregates in neurons, disrupting the normal functions of these cells. The formation of aggregates is considered a hallmark of HD. Currently there are no therapies that meaningfully control or prevent the development of HD. Various therapeutic targets are being focused to develop potential therapeutic drugs or treatments which can slow down disease progression or delay disease onset. Cytotoxicity and biochemical dysfunctions observed in HD models and patients are attributed to the expansion of HTT gene. Several studies have demonstrated that aberrant forms of HTT protein lead to significant impairment of the proteostasis network, dysregulated transcription, mitochondrial toxicity, cellular energy imbalance,

synaptic dysfunction and axonal transport impairment. A complete understanding of the molecular pathways and how they may be altered in HD patients and disease models can illuminate possible new pharmacological strategies for the treatment of HD. Numerous *in vivo* and *in vitro* studies have documented the protective role of various natural products including phenolic compounds with multiple cellular targets in the prevention of neurodegenerative diseases, including HD [98]. In our research work, we evaluated the potential neuroprotective effects of the phenolic coumarin esculetin (ESC) against the toxic events occurring in HD pathogenesis using different HD models. We used a stable inducible neuronal PC12 cell line that express HTT exon 1 fragment with 74 glutamines under doxycycline control [99]. In the first part of the experiments, we reported a basic characterization of this cell line model investigating specifically the mitochondrial activity in terms of cell proliferation, cell death and mutant HTT aggregation. After 72 hours of induction with DOX, we recorded a significant reduction of cell proliferation and a strong increase of cell necrosis. Further, we observed the presence of mutant HTT aggregates fused to EGFP in the cytoplasm and nucleus. The treatment with ESC for 24 hours partially interfered with the aggregation of mutant HTT protein and it showed to ameliorate the cell proliferation as well as to counteract the necrosis. The same treatment with ESC counteracted significantly the ROS formation induced by the expression of mutant HTT exon 1 fragment and it increased the intracellular GSH levels. Further, we recorded the ability of ESC to restore nuclear Nfr2 basal levels in induced PC12 HD-Q74 cells. It has been seen that elevated oxidative stress due to accumulation of HTT protein, imbalance in oxidant-antioxidant status and impairment in electron transport chain, plays a critical role in the late stage of

HD pathogenesis. A recent study reports that the expression of oxidative stress related genes is altered in cells expressing mutant HTT [100].

Finally, ESC showed to ameliorate the mitochondrial activity in induced PC12 HD-Q74 cells. Mitochondrial dysfunction play an important role in neurodegenerative disorders especially in HD. Several studies reported that mitochondrial morphological changes in terms of abnormal dynamics and unbalanced fusion/fission mechanisms result in dysfunction. Mitochondrial fusion and fission are significantly perturbed and imbalanced in HD leading to accumulation of fragmented and damage mitochondria and increased levels of oxidative stress in cell. Based on TEM analysis we saw that mitochondria in induced PC12 HD-Q74 cells appeared smaller, shorter and more round shaped compare to uninduced and induced PC12 HD-Q74 cells exposed to ESC. These results display in induced PC12 HD-Q74 cells an imbalance in fusion/fission dynamics with an excessive mitochondrial fission. The excessive mitochondrial fission could be ascribed to dysfunction [101,102]. ESC is able to counteract this imbalance.

Esculetin-supplemented diet improved different neurodegenerative phenotypes in HTT93Q transgenic *Drosophila*. In our present study, we demonstrated that ESC administered since larval stage or only during adult period ameliorated rhabdomeres neurodegeneration in pathogenetic HTT93Q flies. Further, we observed that ESC feeding rescued HTT93Q-dependent eclosion defects in a dose dependent manner. We also registered a small but interesting improvement in the shortening of median life span in HTT93Q flies fed with 10 µM ESC. Our results show that ESC ameliorates several disease-related neurodegenerative dysfunctions in both PC12 HD-Q74 cells and

Drosophila HTT93Q, suggesting its potential development as a novel neuroprotective agent for the treatment of HD.

Bibliography

[1] H.J. Kim, Y.G. Yu, H. Park, Y.S. Lee, HIV gp41 binding phenolic components from Fraxinus sieboldiana var. angustata, Planta Med. 68 (2002) 1034–1036.

[2] K.N. Venugopala, V. Rashmi, B. Odhav, Review on natural coumarin lead compounds for their pharmacological activity, Biomed Res. Int. 2013 (2013) 1–14.

[3] P.T. Thuong, T.M. Hung, T.M. Ngoc, D.T. Ha, B.S. Min, S.J. Kwack, T.S. Kang, J.S. Choi, K. Bae, Antioxidant activities of coumarins from Korean medicinal plants and their structure-activity relationships, Phyther. Res. 24 (2010) 101–106.

[4] L. Wu, X. Wang, W. Xu, F. Farzaneh, R. Xu, The structure and pharmacological functions of coumarins and their derivatives, Curr. Med. Chem. 16 (2009) 4236–4260.

[5] E. Jameel, T. Umar, N. Hoda, Coumarin: a privileged scaffold for the design and development of antineurodegenerative agents, Chem. Biol. Drug Des. 87 (2016) 21–38.

[6] R. Planells-Cases, J. Lerma, A. Ferrer-Montiel, Pharmacological intervention at ionotropic glutamate receptor complexes, Curr. Pharm. Des. 12 (2006) 3583–3596.

[7] S.Y. Kang, K.Y. Lee, S.H. Sung, Y.C. Kim, Four new neuroprotective dihydropyranocoumarins from Angelica gigas, J. Nat. Prod. 68 (2005) 56–59.

[8] K. Chen, D.P. Holschneider, W. Wu, I. Rebrin, J.C. Shih, A spontaneous point mutation produces monoamine oxidase A/B knock-out mice with greatly elevated monoamines and anxiety-like behavior, J. Biol. Chem. 279 (2004) 39645–39652.

[9] D.T. Huong, H.C. Choi, T.C. Rho, H.S. Lee, M.K. Lee, Y.H. Kim, Inhibitory activity of monoamine oxidase by coumarins from Peucedanum japonicum, Arch. Pharm. Res. 22 (1999) 324–326.

[10] M.W. Irvine, B.M. Costa, A. Volianskis, G. Fang, L. Ceolin, G.L. Collingridge, D.T. Monaghan, D.E. Jane, Coumarin-3-carboxylic acid derivatives as potentiators and inhibitors of recombinant and native N-methyl-D-aspartate receptors, Neurochem. Int. 61 (2012) 593–600.

[11] H. Zhai, M. Nakatsukasa, Y. Mitsumoto, Y. Fukuyama, Neurotrophic effects of talaumidin, a neolignan from Aristolochia arcuata, in primary cultured rat cortical neurons, Planta Med. 70 (2004) 598–602.

[12] C. Zuccato, E. Cattaneo, Brain-derived neurotrophic factor in neurodegenerative diseases, Nat. Rev. Neurol. 5 (2009) 311–322.

[13] R.D. Price, S.A. Milne, J. Sharkey, N. Matsuoka, Advances in small molecules promoting neurotrophic function, Pharmacol. Ther. 115 (2007) 292–306.

[14] L. Yan, X. Zhou, X. Zhou, Z. Zhang, H.M. Luo, Neurotrophic effects of 7,8-dihydroxycoumarin in primary cultured rat cortical neurons, Neurosci. Bull. 28 (2012) 493–498.

[15] S. Amor, F. Puentes, D. Baker, P. van der Valk, Inflammation in neurodegenerative diseases, Immunology. 129 (2010) 154–169.

[16] S.T. Dheen, C. Kaur, E.A. Ling, Microglial activation and its implications in the brain diseases, Curr. Med. Chem. 14 (2007) 1189–1197.

[17] N.B. Piller, A comparison of the effectiveness of some anti-inflammatory drugs on thermal oedema, Br. J. Exp. Pathol. 56 (1975) 554–559.

[18] R. Jakob-Roetne, H. Jacobsen, Alzheimer's disease: from pathology to therapeutic approaches, Angew. Chemie Int. Ed. 48 (2009) 3030–3059.
[19] A. Castro, A. Martinez, Peripheral and dual binding site acetylcholinesterase inhibitors: implications in treatment of Alzheimer's disease, Mini Rev. Med. Chem. 1 (2001) 267–272.
[20] R. Hoerr, M. Noeldner, Ensaculin (KA-672 HCl): a multitransmitter approach to dementia treatment, CNS Drug Rev. 8 (2002) 143–158.
[21] P.J. Houghton, Y. Ren, M.J. Howes, Acetylcholinesterase inhibitors from plants and fungi, Nat. Prod. Rep. 23 (2006) 181.
[22] V. Tumiatti, M.L. Bolognesi, A. Minarini, M. Rosini, A. Milelli, R. Matera, C. Melchiorre, Progress in acetylcholinesterase inhibitors for Alzheimer's disease: an update, Expert Opin. Ther. Pat. 18 (2008) 387–401.
[23] M.J. Howes, P.J. Houghton, Acetylcholinesterase inhibitors of natural origin, Int. J. Biomed. Pharm. Sci. 3 (2009) 67–86.
[24] A. Hornick, A. Lieb, N.P. Vo, J.M. Rollinger, H. Stuppner, H. Prast, The coumarin scopoletin potentiates acetylcholine release from synaptosomes, amplifies hippocampal long-term potentiation and ameliorates anticholinergic- and age-impaired memory, Neuroscience. 197 (2011) 280–292.
[25] J.B. Calixto, M.F. Otuki, A.R. Santos, Anti-inflammatory compounds of plant origin. Part I. Action on arachidonic acid pathway, nitric oxide and nuclear factor κB (NF-κB), Planta Med. 69 (2003) 973–983.
[26] G. Le Bras, C. Radanyi, J.F. Peyrat, J.D. Brion, M. Alami, V. Marsaud, B. Stella, J.M. Renoir, New novobiocin analogues as antiproliferative agents in breast cancer cells and potential inhibitors of heat shock protein 90, J. Med. Chem. 50 (2007) 6189–6200.
[27] S. Toda, Inhibitory effects of phenylpropanoid metabolites on copper-induced protein oxidative modification of mice brain homogenate, in vitro, Biol. Trace Elem. Res. 85 (2002) 183–188.
[28] C.Y. Shaw, C.H. Chen, C.C. Hsu, C.C. Chen, Y.C. Tsai, Antioxidant properties of scopoletin isolated from Sinomonium acutum, Phyther. Res. 17 (2003) 823–825.
[29] C. Patterson, C. Lynch, A. Bliss, M. Lefevre, W. Weidner, World Alzheimer Report 2018 The state of the art of dementia research: new frontiers, 2018.
[30] A. Kumar, J.W. Tsao, Alzheimer Disease, 2018.
[31] X. Du, X. Wang, M. Geng, Alzheimer's disease hypothesis and related therapies, Transl. Neurodegener. 7 (2018) 1–7.
[32] J. Cummings, P.S. Aisen, B. Dubois, L. Frölich, C.R. Jack, R.W. Jones, J.C. Morris, J. Raskin, S.A. Dowsett, P. Scheltens, Drug development in Alzheimer's disease: the path to 2025, Alzheimer's Res. Ther. 8 (2016) 1–12.
[33] Y. Ali, S. Jannat, H.A. Jung, R.J. Choi, A. Roy, J.S. Choi, Anti-Alzheimer's disease potential of coumarins from Angelica decursiva and Artemisia capillaris and structure-activity analysis, Asian Pac. J. Trop. Med. 9 (2016) 103–111.
[34] R. Vassar, M. Citron, Abeta-generating enzymes: recent advances in beta- and gamma-secretase research, Neuron. 27 (2000) 419–422.
[35] M.R. Brier, B. Gordon, K. Friedrichsen, J. Mccarthy, A. Stern, C. Owen, P. Aldea, Y. Su, J. Hassenstab, J. Nigel, D.M. Holtzman, A.M. Fagan, J.C. Morris, T.L. Benzinger, B.M. Ances, Tau and Aβ imaging, CSF measures, and cognition in Alzheimer's disease, Sci. Transl. Med. 8 (2016) 1–19.

[36] A.A. Podtelezhnikov, C. Zhang, T. Xie, L. Tran, C. Suver, H. Shah, M. Mahajan, T. Gillis, J. Mysore, V. Gudnason, A.J. Myers, E.E. Schadt, H. Neumann, Integrated systems approach identifies genetic nodes and networks in late-onset Alzheimer's disease, Cell. 153 (2014) 707–720.

[37] R. Guerreiro, A. Wojtas, J. Bras, M. Carrasquillo, E. Rogaeva, E. Majounie, C. Cruchaga, C. Sassi, J.S. Kauwe, S. Younkin, L. Hazrati, J. Collinge, J. Pocock, T. Lashley, J. Williams, J.C. Lambert, P. Amouyel, A. Goate, R. Rademakers, K. Morgan, J. Powell, A. Singleton, J. Hardy, TREM-2 variants in Alzheimer's disease, N. Engl. J. Med. 368 (2013) 117–127.

[38] W. Song, B. Hooli, K. Mullin, S.C. Jin, M. Cella, T.K. Ulland, Y. Wang, R.E. Tanzi, M. Colonna, Alzheimer's disease-associated TREM2 variants exhibit either decreased or increased ligand-dependent activation, Alzheimer's Dement. J. Alzheimer's Assoc. 13 (2017) 381–387.

[39] M. Colonna, Y. Wang, TREM2 variants: new keys to decipher Alzheimer disease pathogenesis, Nat. Rev. Neurosci. 17 (2016) 201–207.

[40] M. Bolós, J.R. Perea, J. Avila, Alzheimer's disease as an inflammatory disease, Biomol. Concepts. 8 (2017) 37–43.

[41] P.L. McGeer, E.G. McGeer, Targeting microglia for the treatment of Alzheimer's disease, Expert Opin. Ther. Targets. 19 (2015) 497–506.

[42] R. Schliebs, T. Arendt, The cholinergic system in aging and neuronal degeneration, Behav. Brain Res. 221 (2011) 555–563.

[43] C. Geula, S. Darvesh, Butyrylcholinesterase, cholinergic neurotransmission and the pathology of Alzheimer's disease, Drugs of Today. 40 (2004) 711–721.

[44] M. Bélanger, I. Allaman, P.J. Magistretti, Brain energy metabolism: focus on astrocyte-neuron metabolic cooperation, Cell Metab. 14 (2011) 724–738.

[45] J.T. Coyle, P. Puttfarcken, Oxidative stress, glutamate, and neurodegenerative disorders, Science. 262 (1993) 689–695.

[46] S. Manoharan, G.J. Guillemin, R.S. Abiramasundari, M.M. Essa, M. Akbar, M.D. Akbar, The role of reactive oxygen species in the pathogenesis of Alzheimer's disease, Parkinson's disease, and Huntington's disease: a mini review, Oxid. Med. Cell. Longev. 2016 (2016) 1–15.

[47] J. Wojsiat, K.M. Zoltowska, K. Laskowska-Kaszub, U. Wojda, Oxidant/antioxidant imbalance in Alzheimer's disease: therapeutic and diagnostic prospects, Oxid. Med. Cell. Longev. 2018 (2018) 1–16.

[48] M.A. Lovell, C. Xie, S.P. Gabbita, W.R. Markesbery, Decreased thioredoxin and increased thioredoxin reductase levels in Alzheimer's disease brain, Free Radic. Biol. Med. 28 (2000) 418–427.

[49] J.M. Lee, J.A. Johnson, An important role of Nrf2-ARE pathway in the cellular defense mechanism, J. Biochem. Mol. Biol. 37 (2004) 139–143.

[50] C.P. Ramsey, C.A. Glass, M.B. Montgomery, K.A. Lindl, G.P. Ritson, L.A. Chia, R.L. Hamilton, C.T. Chu, K.L. Jordan-Sciutto, Expression of Nrf2 in neurodegenerative diseases, J. Neuropathol. Exp. Neurol. 66 (2007) 75–85.

[51] C. Cheignon, M. Tomas, D. Bonnefont-Rousselot, P. Faller, C. Hureau, F. Collin, Oxidative stress and the amyloid beta peptide in Alzheimer's disease, Redox Biol. 14 (2018) 450–464.

[52] R. Castellani, K. Hirai, G. Aliev, K.L. Drew, A. Nunomura, A. Takeda, A.D. Cash, M.E. Obrenovich, G. Perry, M.A. Smith, Role of mitochondrial dysfunction in Alzheimer's disease, J. Neurosci. Res. 70 (2002) 357–360.

[53] G.E. Gibson, K.F. Sheu, J.P. Blass, Abnormalities of mitochondrial enzymes in Alzheimer disease, J. Neural Transm. 105 (1998) 855–870.
[54] C. Liang, W. Ju, S. Pei, Y. Tang, Y. Xiao, Pharmacological activities and synthesis of esculetin: a mini review, Molecules. 22 (2017) 1–13.
[55] B.C. Lee, S.Y. Lee, H.J. Lee, G.S. Sim, J.H. Kim, J.H. Kim, Y.H. Cho, D.H. Lee, H.B. Pyo, T.B. Choe, D.C. Moon, Y.P. Yun, J.T. Hong, Anti-oxidative and photo-protective effects of coumarins isolated from Fraxinus chinensis, Arch. Pharm. Res. 30 (2007) 1293–1301.
[56] R.S. Razo-Hernández, K. Pineda-Urbina, M.A. Velazco-Medel, M. Villanueva-García, M.T. Sumaya-Martínez, F.J. Martínez-Martínez, Z. Gómez-Sandoval, QSAR study of the DPPH• radical scavenging activity of coumarin derivatives and xanthine oxidase inhibition by molecular docking, Cent. Eur. J. Chem. 12 (2014) 1067–1080.
[57] C.R. Wu, M.Y. Huang, Y.T. Lin, H.Y. Ju, H. Ching, Antioxidant properties of Cortex Fraxini and its simple coumarins, Food Chem. 104 (2007) 1464–1471.
[58] T. Kaneko, N. Baba, M. Matsuo, Protection of coumarins against linoleic acid hydroperoxide-induced cytotoxicity, Chem. Biol. Interact. 142 (2003) 239–254.
[59] J.B. Veselinović, A.M. Veselinović, Ž.J. Vitnik, V.D. Vitnik, G.M. Nikolić, Antioxidant properties of selected 4-phenyl hydroxycoumarins: Integrated in vitro and computational studies, Chem. Biol. Interact. 214 (2014) 49–56.
[60] H. Murat Bilgin, M. Atmaca, B. Deniz Obay, S. Özekinci, E. Taşdemir, A. Ketani, Protective effects of coumarin and coumarin derivatives against carbon tetrachloride-induced acute hepatotoxicity in rats, Exp. Toxicol. Pathol. 63 (2011) 325–330.
[61] W.L. Lin, C.J. Wang, Y.Y. Tsai, C.L. Liu, J.M. Hwang, T.H. Tseng, Inhibitory effect of esculetin on oxidative damage induced by t-butyl hydroperoxide in rat liver, Arch. Toxicol. 74 (2000) 467–472.
[62] S.H. Kim, K.A. Kang, R. Zhang, M.J. Piao, D.O. Ko, Z.H. Wang, S.S. Kang, K.H. Lee, H.K. Kang, H.W. Kang, J.W. Hyun, Protective effect of esculetin against oxidative stress-induced cell damage via scavenging reactive oxygen species, Acta Pharmacol. Sin. 29 (2008) 1319–1326.
[63] S.R. Subramaniam, E.M. Ellis, Neuroprotective effects of umbelliferone and esculetin in a mouse model of Parkinson's disease, J. Neurosci. Res. 91 (2013) 453–461.
[64] Y.Y. Li, Y.Y. Song, C.H. Liu, X.T. Huang, X. Zheng, N. Li, M.L. Xu, S.Q. Mi, N.S. Wang, Simultaneous determination of esculin and its metabolite esculetin in rat plasma by LC-ESI-MS/MS and its application in pharmacokinetic study, J. Chromatogr. B. 907 (2012) 27–33.
[65] S. Saharan, P.K. Mandal, The emerging role of glutathione in Alzheimer's disease, J. Alzheimer's Dis. 40 (2014) 519–529.
[66] F. Gu, V. Chauhan, A. Chauhan, Glutathione redox imbalance in brain disorders, Curr. Opin. Clin. Nutr. Metab. Care. 18 (2015) 89–95.
[67] S.R. Subramaniam, E.M. Ellis, Esculetin-induced protection of human hepatoma HepG2 cells against hydrogen peroxide is associated with the Nrf2-dependent induction of the NAD(P)H: Quinone oxidoreductase 1 gene, Toxicol. Appl. Pharmacol. 250 (2011) 130–136.
[68] A.T. Dinkova-Kostova, R. V. Kostov, A.G. Kazantsev, The role of Nrf2 signaling in counteracting neurodegenerative diseases, FEBS J. 285 (2018) 3576–

3590.
[69] M.H. Han, C. Park, D.S. Lee, S.H. Hong, I.W. Choi, G.Y. Kim, S.H. Choi, J.H. Shim, J.I. Chae, Y.H. Yoo, Y.H. Choi, Cytoprotective effects of esculetin against oxidative stress are associated with the upregulation of Nrf2-mediated NQO1 expression via the activation of the ERK pathway, Int. J. Mol. Med. 39 (2017) 380–386.
[70] M. Culbreth, M. Aschner, GSK-3β , a double-edged sword in Nrf2 regulation: implications for neurological dysfunction and disease, F1000Research. 7 (2018) 6–11.
[71] B. DaRocha-Souto, M. Coma, B.G. Pérez-Nievas, T.C. Scotton, M. Siao, P. Sánchez-Ferrer, T. Hashimoto, Z. Fan, E. Hudry, I. Barroeta, L. Serenó, M. Rodríguez, M.B. Sánchez, B.T. Hyman, T. Gómez-Isla, Activation of glycogen synthase kinase-3 beta mediates β-amyloid induced neuritic damage in Alzheimer's disease, Neurobiol. Dis. 45 (2012) 425–437.
[72] C. Hooper, R. Killick, S. Lovestone, The GSK3 hypothesis of Alzheimer's disease, J. Neurochem. 104 (2008) 1433–1439.
[73] M.L. Liu, S.T. Hong, Early phase of amyloid beta42-induced cytotoxicity in neuronal cells is associated with vacuole formation and enhancement of exocytosis, Exp. Mol. Med. 37 (2005) 559–566.
[74] Y. Liu, D. Schubert, Cytotoxic amyloid peptides inhibit cellular 3-(4,5-dimethylthiazol-2-yl)-2,5-diphenyltetrazolium bromide (MTT) reduction by enhancing MTT formazan exocytosis, J. Neurochem. 69 (1997) 2285–2293.
[75] H.S. Hong, I. Maezawa, N. Yao, B. Xu, R. Diaz-Avalos, S. Rana, D.H. Hua, R.H. Cheng, K.S. Lam, L.W. Jin, Combining the rapid MTT formazan exocytosis assay and the MC65 protection assay led to the discovery of carbazole analogs as small molecule inhibitors of Aβ oligomer-induced cytotoxicity, Brain Res. 1130 (2007) 223–234.
[76] T. Kaneko, S. Tahara, F. Takabayashi, Suppression of lipid hydroperoxide-induced oxidative damage to cellular DNA by esculetin, Biol. Pharm. Bull. 26 (2003) 840–844.
[77] H.C. Lin, S.H. Tsai, C.S. Chen, Y.C. Chang, C.M. Lee, Z.Y. Lai, C.M. Lin, Structure-activity relationship of coumarin derivatives on xanthine oxidase-inhibiting and free radical-scavenging activities, Biochem. Pharmacol. 75 (2008) 1416–1425.
[78] J. Labbadia, R.I. Morimoto, Huntington's disease: underlying molecular mechanisms and emerging concepts, Trends Biochem. Sci. 38 (2013) 378–385.
[79] K. Kieburtz, R. Reilmann, C.W. Olanow, Huntington's disease: current and future therapeutic prospects, Mov. Disord. 33 (2018) 1033–1041.
[80] T. Seredenina, R. Luthi-Carter, What have we learned from gene expression profiles in Huntington's disease?, Neurobiol. Dis. 45 (2012) 83–98.
[81] A.W. Dunah, H. Jeong, A. Griffin, Y.M. Kim, D.G. Standaert, S.M. Hersch, M.M. Mouradian, A.B. Young, N. Tanese, D. Krainc, Sp1 and TAFII130 transcriptional activity disrupted in early Huntington's disease, Science. 296 (2002) 2238–2243.
[82] G. Schaffar, P. Breuer, R. Boteva, C. Behrends, N. Tzvetkov, N. Strippel, H. Sakahira, K. Siegers, M. Hayer-Hartl, F.U. Hartl, Cellular toxicity of polyglutamine expansion proteins: mechanism of transcription factor deactivation, Mol. Cell. 15 (2004) 95–105.

[83] W. Zhai, H. Jeong, L. Cui, D. Krainc, R. Tjian, In vitro analysis of huntingtin-mediated transcriptional repression reveals multiple transcription factor targets, Cell. 123 (2005) 1241–1253.

[84] S. Huang, J.J. Ling, S. Yang, X.J. Li, S. Li, Neuronal expression of TATA box-binding protein containing expanded polyglutamine in knock-in mice reduces chaperone protein response by impairing the function of nuclear factor-Y transcription factor, Brain. 134 (2011) 1943–1958.

[85] T. Yamanaka, H. Miyazaki, F. Oyama, M. Kurosawa, C. Washizu, H. Doi, N. Nukina, Mutant Huntingtin reduces HSP70 expression through the sequestration of NF-Y transcription factor, EMBO J. 27 (2008) 827–839.

[86] J.S. Steffan, L. Bodai, J. Pallos, M. Poelman, A. McCampbell, B.L. Apostol, A. Kazantsev, E. Schmidt, Y.Z. Zhu, M. Greenwald, R. Kurokawa, D.E. Housman, G.R. Jackson, J.L. Marsh, L.M. Thompson, Histone deacetylase inhibitors arrest polyglutamine-dependent neurodegeneration in Drosophila, Nature. 413 (2001) 739–743.

[87] P.J. Muchowski, J.L. Wacker, Modulation of neurodegeneration by molecular chaperones, Nat. Rev. Neurosci. 6 (2005) 11–22.

[88] T.J. van Ham, M.A. Holmberg, A.T. van der Goot, E. Teuling, M. Garcia-Arencibia, H.E. Kim, D. Du, K.L. Thijssen, M. Wiersma, R. Burggraaff, P. van Bergeijk, J. van Rheenen, G. Jerre van Veluw, R.M. Hofstra, D.C. Rubinsztein, E.A. Nollen, Identification of MOAG-4/SERF as a regulator of age-related proteotoxicity, Cell. 142 (2010) 601–612.

[89] X.J. Li, S. Li, Proteasomal dysfunction in aging and Huntington disease, Neurobiol. Dis. 43 (2011) 4–8.

[90] E.J. Bennett, T.A. Shaler, B. Woodman, K.Y. Ryu, T.S. Zaitseva, C.H. Becker, G.P. Bates, H. Schulman, R.R. Kopito, Global changes to the ubiquitin system in Huntington's disease, Nature. 448 (2007) 704–708.

[91] M.S. Hipp, C.N. Patel, K. Bersuker, B.E. Riley, S.E. Kaiser, T.A. Shaler, M. Brandeis, R.R. Kopito, Indirect inhibition of 26S proteasome activity in a cellular model of Huntington's disease, J. Cell Biol. 196 (2012) 573–587.

[92] S. Okamoto, M.A. Pouladi, M. Talantova, D. Yao, D.E. Ehrnhoefer, R. Zaidi, A. Clemente, M. Kaul, K. Rona, D. Zhang, H.V. Chen, G. Tong, M.R. Hayden, S.A. Lipton, Balance between synaptic versus extrasynaptic NMDA receptor activity influences inclusions and neurotoxicity of mutant huntingtin, Nat. Med. 15 (2010) 1407–1413.

[93] D. Zwilling, S.Y. Huang, K. V. Sathyasaikumar, F.M. Notarangelo, P. Guidetti, H.Q. Wu, J. Lee, J. Truong, Y. Andrews-Zwilling, E.W. Hsieh, J.Y. Louie, T. Wu, K. Scearce-Levie, C. Patrick, A. Adame, F. Giorgini, S. Moussaoui, G. Laue, A. Rassoulpour, G. Flik, Y. Huang, J.M. Muchowski, E. Masliah, R. Schwarcz, P.J. Muchowski, Kynurenine 3-monooxygenase inhibition in blood ameliorates neurodegeneration, Cell. 145 (2011) 863–874.

[94] S. Campesan, E.W. Green, C. Breda, K. V Sathyasaikumar, P.J. Muchowski, R. Schwarcz, C.P. Kyriacou, F. Giorgini, The kynurenine pathway modulates neurodegeneration in a Drosophila model of Huntington's disease, Curr. Biol. 21 (2011) 961–966.

[95] A.T. van der Goot, W. Zhu, R.P. Vazquez-Manrique, R.I. Seinstra, K. Dettmer, H. Michels, F. Farina, J. Krijnen, R. Melki, R.C. Buijsman, M. Ruiz Silva, K.L. Thijssen, I.P. Kema, C. Neri, P.J. Oefner, E.A. Nollen, Delaying aging and the

aging-associated decline in protein homeostasis by inhibition of tryptophan degradation, Proc. Natl. Acad. Sci. 109 (2012) 14912–14917.

[96] G. Liot, J. Valette, J. Pépin, J. Flament, E. Brouillet, Energy defects in Huntington's disease: why "in vivo" evidence matters, Biochem. Biophys. Res. Commun. 483 (2017) 1084–1095.

[97] S. Franco-Iborra, M. Vila, C. Perier, Mitochondrial quality control in neurodegenerative diseases: focus on Parkinson's disease and Huntington's disease, Front. Neurosci. 12 (2018) 1–25.

[98] A. Chongtham, N. Agrawal, Curcumin modulates cell death and is protective in Huntington's disease model, Sci. Rep. 6 (2016) 1–10.

[99] A. Wyttenbach, J. Swartz, H. Kita, T. Thykjaer, J. Carmichael, J. Bradley, R. Brown, M. Maxwell, A. Schapira, T.F. Orntoft, K. Kato, D.C. Rubinsztein, Polyglutamine expansions cause decreased CRE-mediated transcription and early gene expression changes prior to cell death in an inducible cell model of Huntington's disease., Hum. Mol. Genet. 10 (2001) 1829–1845.

[100] W.M. van Roon-Mom, B.A. Pepers, P.A. 't Hoen, C.A. Verwijmeren, J.T. den Dunnen, J.C. Dorsman, G.B. van Ommen, Mutant huntingtin activates Nrf2-responsive genes and impairs dopamine synthesis in a PC12 model of Huntington's disease, BMC Mol. Biol. 9 (2008) 1–13.

[101] S. Hwang, M.H. Disatnik, D. Mochly-Rosen, Impaired GAPDH-induced mitophagy contributes to the pathology of Huntington's disease, EMBO Mol. Med. 7 (2015) 1307–1326.

[102] R.J. Youle, A.M. van der Bliek, Mitochondrial fission, fusion, and stress, Science. 337 (2012) 1062–1065.